Dynamic Simulations of Earthquake Cycles in Strike-Slip Fault Zones

by

Prithvi Thakur

A dissertation submitted in partial fulfillment
of the requirements for the degree of
Doctor of Philosophy
(Earth and Environmental Sciences)
in the University of Michigan
2022

Doctoral Committee:

      Associate Professor Yihe Huang, Chair
      Professor August Evrard
      Associate Professor Eric Hetland
      Professor Jeroen Ritsema

Prithvi Thakur

prith@umich.edu

ORCID ID: 0000-0001-6687-0787

ACKNOWLEDGMENTS

I owe my greatest debt to my doctoral thesis advisor, Dr. Yihe Huang, for giving me the opportunity to work in her lab as one of her first graduate students, and for providing me with such an interesting problem to work on. Without her constant support, mentoring, insights, encouragement, and patience this project would not have been possible. I also extend my thanks to Dr. Yoshihiro Kaneko for his collaboration and guidance on the specifics of earthquake cycle modeling, which greatly expedited my growth as an earthquake modeler.

I am also thankful to the following people:

TABLE OF CONTENTS

LIST OF FIGURES

LIST OF TABLES

ABSTRACT

Earthquakes are a complex phenomena occurring over a variety of spatial and temporal scales. The fault zones hosting such earthquakes are also structurally complex networks of fractures that evolve through time. This thesis presents novel numerical simulations of the spatial and temporal complexities of fault zones over multiple earthquake sequences, to uncover the physics of long-term earthquake cycles that include earthquakes and aseismic events. We use seismic, geological, and geodetic observations as well as laboratory experiments to constrain the dynamics of earthquake wave propagation and quasi-static strain accumulation in strike-slip fault systems.

In chapter 2, we examine the behavior of earthquake nucleation and rupture dynamics on a fault surrounded by a damage zone over a thousand-year timescale. Our simulations reveal that the reflection of seismic waves from the fault damage zone boundaries leads to complexity in earthquake sequences, such as variability in earthquake locations and sizes. We also show that a shallow fault damage zone produces shallower earthquakes with earthquake depths centered around two locations (i.e., bimodal depth distribution), as opposed to a deep fault damage zone with the earthquake depths centered around a single location (i.e., unimodal depth distribution). Our study suggests that imaging the geometry and physical properties of fault damage zones could affect the depths of future earthquakes with implications for earthquake probabilistic hazard assessment.

In chapter 3, we simulate the evolution of fault damage zones by prescribing coseismic damage accumulation and interseismic healing as constrained by seismic and geodetic observations. Depending on the compliance (i.e., the ability to accommodate deformation) of the damage zone with respect to the surrounding host rock, the maturity of fault zone can vary, with higher compliance corresponding to a more mature fault zone. We find that our

models with immature fault zone tends to produce smaller earthquakes whose slip does not reach the surface of the earth, and the duration between earthquakes is irregular. As fault zones become more mature in the models, earthquakes can rupture to the surface and occur more regularly. Our results highlight a link between regional seismic hazard and fault structural maturity.

Finally, chapter 4 investigates the predictive behavior of precursory seismic signals by simulating earthquake sequences with prescribed seismic velocity changes as precursors, under different homogeneous and heterogeneous stress conditions. We find that such precursory velocity changes can affect how fast and how early the earthquakes nucleate, with earlier onset of precursors leading to earlier earthquake nucleation. The slow-slip events seen in the earthquake cycle simulations with fault zones grow into dynamic earthquakes in the presence of velocity precursors. Precursory velocity changes also amplify the shear stress heterogeneities along the fault, which may result from fault damage zones or self-similar background stresses.

CHAPTER 1

Introduction

Earthquakes are among the deadliest and costliest natural hazards, cumulatively accounting for nearly 3% of human population affected in the past twenty years (*Tschoegl et al.*, 2006). Globally, these earthquakes are not completely random in space, but they preferentially occur along major planes of weaknesses in the earth's crust, i.e., along tectonic plate boundaries and along fault systems. Despite having known this for several decades, we are not any closer to understanding and forecasting future earthquake sequences. Earthquake rupture forecast and ground motion prediction are limited to the most well instrumented regions of the world (*Field et al.*, 2014). We, however, do know that larger earthquakes are less frequent than smaller ones. The magnitude-frequency of earthquakes usually follow a power-law relationship, best described by the Gutenberg-Richter (G-R) distribution: $logN = a - bM$. Here, N is the number of earthquakes having magnitude greater than or equal to M, and a and b are constants. Most observations of global and regional seismicity agree with the G-R distribution (*Rundle*, 1989; *Page and Felzer*, 2015). However, certain observations of magnitude-frequency distributions along more planar faults (e.g., the San Andreas Fault) have shown a "characteristic earthquake" distribution, wherein the largest earthquake of a characteristic size recurs with an approximately regular interval. The duration between two such characteristic earthquakes is generally quiescent except for low-level seismic activity (*Schwartz and Coppersmith*, 1984; *Wesnousky*, 1994).

Mechanically, earthquakes are shear cracks propagating in the earth's crust along some interface of weakness, i.e., fault zones. Large strike-slip earthquakes tend to create a zone of geometrically complex networks of fractures surrounding the main fault. This zone, referred to as a fault damage zone, becomes highly localized as the fault matures, with an off-fault width of few hundred meters. The fault damage zone also evolves through time as more earthquakes generate damage in the vicinity of the slip surfaces. Observations of the complete shear-crack system at seismogenic depths, including the surrounding network of damage and the stress conditions are, however, limited. Additionally, modern seismic and geodetic observations are limited to the past 50 years, and the infrequent occurrences of

large earthquakes along such fault systems poses another significant limitation in studying them. How the earthquakes start, propagate, and stop are among the most fundamental questions in seismology. Furthermore, the influence of this evolving fault damage zone on earthquake source physics remains elusive. Therefore, a self-consistent view of the long-term fault zone evolution is imperative to understand the potential for future earthquakes.

One approach towards understanding earthquake physics is mechanics based numerical modeling of fault slip over long timescales. The driving force behind such models is a constant-rate tectonic plate motion, whereas the shear resistance on the fault interface is provided by a constitutive friction law. Numerous earlier studies focused on discrete modeling of fault slip using single degree of freedom spring-block slider, wherein the spring constant represents the elastic stiffness in the earth's crust and the block attached to the spring is moving across an interface, i.e., a fault (e.g., *Burridge and Knopoff*, 1967; *Ben-David et al.*, 2010). Despite such approximations, these models were able to reproduce the chaotic behavior of fault slip, as well as the log-linear relationship between event sizes and the frequency of their occurrence (*Carlson and Langer*, 1989; *Shaw*, 1995). Around the same time, experimental rock deformation studies showed that the shear resistance along an interface depends not only on the amount of deformation but also on the rate of deformation and some state variables describing the contact interface (*Dieterich*, 1979; *Ruina*, 1983; *Blanpied et al.*, 1991; *Scholz*, 1998). *Rice* (1993) developed a formulation for continuum modeling of earthquake cycles, which approximated the inertial effects due to the dynamic earthquake rupture using a damping term in the elastostatic formulation, known as quasidynamic model. Subsequently, numerous discrete (*Olami et al.*, 1992) and continuum (*Rice and Ben-Zion*, 1996; *Lapusta and Rice*, 2003a) models were used to study the long-term fault slip history. Fully dynamic earthquake cycle models are at a relatively nascent stage owing to the huge computational costs associated with them. The most successful ones are able to model multiple earthquakes and interseismic deformation along fault interfaces with complex nonlinear friction laws in two- and three- dimensions (*Lapusta et al.*, 2000; *Jiang and Lapusta*, 2016; *Thomas et al.*, 2014), with the caveat of being unable to incorporate bulk heterogeneities. Fully dynamic models based on volume-discretization are few in literature and typically limited to two-dimensions (*Kaneko et al.*, 2011; *Herrendörfer et al.*, 2018), and consequently the effects of off-fault heterogeneities (e.g., fault damage zones) have not been explored in great detail outside of single rupture events (*Huang and Ampuero*, 2011; *Huang et al.*, 2014a).

To address these issues, we develop fully dynamic earthquake cycle models based on *Kaneko et al.* (2011)'s algorithm with improved computational efficiency and multithread parellelization to simulate earthquake cycles on a two-dimensional, mode-III fault system

2

with an off-fault elastic damage zone. Chapters 2 and 3 address the effects of fault damage zone structure on earthquake sequences along strike-slip faults. In Chapter 2, we model earthquake sequences with full inertial effects on a two-dimensional vertical strike-slip fault surrounded by a fault damage zone. This fully dynamic modeling approach can simulate interseismic slip, earthquake nucleation, rupture propagation, and postseismic deformation during multiple seismic cycles in a single computational framework. We investigate how seismic wave reflections from fault damage zone influences the long-term stress evolution and contribute to the variability in earthquake magnitudes and hypocenter locations. We show that the variability in earthquake hypocenters is significant only in the cases where the damage zone truncates close to the nucleation site or extends beyond the nucleation zone, suggesting that frictional and rheological effects may be a dominant mechanism for hypocenter variability when the damaged structure is very shallow. Our results also provide a possible explanation for the bimodal depth distribution of seismicity observed along mature strike-slip faults with shallow fault damage zone structures. In chapter 3, we model the fault zone structure evolution as changes in the shear-wave velocity of an elastic layer surrounding a strike-slip fault. We show that an immature fault zone tends to produce more slow-slip events and irregular earthquake sequences with predominantly subsurface events. In contrast, a more mature fault damage zone tends to produce a more regular sequence of earthquakes with a combination of surface-reaching and subsurface events.

Another key question in earthquake physics is the short- and long-term predictability of future earthquakes based on past and current observations. Earthquake recurrence models (*Shimazaki and Nakata*, 1980) are generally used in regional seismic hazard assessment and ground motion prediction. In more recent times, a variety of preseismic signals have been observed in the form of b-value reduction, slow-slip events (*Nanjo et al.*, 2012; *Ito et al.*, 2015), and seismic wave velocity changes (*Scuderi et al.*, 2016). In chapter 4, we investigate the effects of seismic velocity precursors on earthquake sequences by imposing shear wave velocity changes in the fault damage zones. We discuss these effects in the presence of both homogeneous and self-similar heterogeneous initial stresses. Our results show that precursory velocity drop causes an earlier nucleation of earthquakes, therefore causing a reduction in recurrence intervals over the seismic cycle.

The overall contribution of this work is to understand the long-term fault slip dynamics of spatiotemporally complex fault zone structures. We demonstrate how such material heterogeneities can cause periodic earthquake ruptures to become variable in space and time, and introduce a spectrum of slow-slip events and variable creep. Our results highlight the importance of short- and long-term monitoring of fault zone structures for better assessment of regional seismic hazard.

CHAPTER 2

Effects of Low-Velocity Fault Damage Zones on Long-Term Earthquake Behaviors on Mature Strike-Slip Faults [*]

Abstract

Mature strike-slip faults are usually surrounded by a narrow zone of damaged rocks characterized by low seismic wave velocities. Observations of earthquakes along such faults indicate that seismicity is highly concentrated within this fault damage zone. However, the long-term influence of the fault damage zone on complete earthquake cycles, i.e., years to centuries, is not well understood. We simulate aseismic slip and dynamic earthquake rupture on a vertical strike-slip fault surrounded by a fault damage zone for a thousand-year timescale using fault zone material properties and geometries motivated by observations along major strike-slip faults. The fault damage zone is approximated as an elastic layer with lower shear wave velocity than the surrounding rock. We find that dynamic wave reflections, whose characteristics are strongly dependent on the width and the rigidity contrast of the fault damage zone, have a prominent effect on the stressing history of the fault. The presence of elastic damage can partially explain the variability in the earthquake sizes and hypocenter locations along a single fault, which vary with fault damage zone depth, width and rigidity contrast from the host rock. The depth extent of the fault damage zone has a pronounced effect on the earthquake hypocenter locations, and shallower fault damage zones favor shallower hypocenters with a bimodal distribution of seismicity along depth. Our findings also suggest significant effects on the hypocenter distribution when the fault damage zone penetrates to the nucleation sites of earthquakes, likely being influenced by

both lithological (material) and rheological (frictional) boundaries.

2.1   Introduction

Natural faults are often approximated as a single plane of intense deformation, macroscopically seen as a principal slip surface. However, geological (e.g., *Chester and Logan*, 1986; *Chester et al.*, 1993; *Lockner et al.*, 2011), geophysical (e.g., *Li and Leary*, 1990; *Unsworth et al.*, 1997; *Lewis and Ben-Zion*, 2010), and geodetic (e.g., *Fialko et al.*, 2002) observations delineate faults as a geometrically complex network of multiple slip surfaces and fractures, with a nested hierarchy of increasing deformation towards the principal slip surface (Fig. 2.1). These damaged rocks exhibit a dense network of fractures which can be macroscopically approximated as an elastic zone with reduced shear modulus and seismic velocities (*Chester et al.*, 1993; *Harris and Day*, 1997). Elastic deformation models have explored the effect of fault damage zones in two-dimensions on coseismic slip (*Barbot et al.*, 2008), three-dimensional crustal deformation (*Barbot et al.*, 2009), and on patterns of interseismic strain accumulation (*Lindsey et al.*, 2014). The damage zones may exhibit sharp contrast in seismic velocities with respect to the host rock, being capable of trapping seismic waves within the fault zone. The fault damage zone can potentially promote complex stress distribution along faults due to its pronounced dynamic effect on earthquake rupture nucleation and propagation (e.g., *Harris and Day*, 1997; *Huang and Ampuero*, 2011; *Huang et al.*, 2014b; *Ma and Elbanna*, 2015a; *Albertini and Kammer*, 2017; *Weng et al.*, 2016; *Huang*, 2018). We aim to understand the effects of low-velocity damage zones on dynamic rupture propagation and sequence of earthquakes, which include interseismic slip, earthquake nucleation, rupture propagation, and postseismic slip, and study its influence on the variability in earthquake sizes, recurrence intervals and stressing history of the fault.

Previous numerical models in homogeneous medium (*Rundle and Jackson*, 1977; *Rundle*, 1989) and experiments (*Mogi*, 1962; *Scholz*, 1968) showed that both mechanical properties of fault rocks and fault stresses can greatly contribute to the variability in earthquake magnitudes and the power-law behavior of the magnitude-frequency distribution. Dynamic models of multiple spring-block sliders (*Carlson and Langer*, 1989; *Shaw*, 1995) and discrete models of fault slip (*Olami et al.*, 1992) have been successful in reproducing the Gutenberg-Richter distribution and non-uniform recurrence times. Quasi-dynamic continuum models in homogeneous medium have previously used extreme frictional parameters to reproduce observed complexity of earthquakes (*Cochard and Madariaga*, 1996; *Hillers et al.*, 2006). Recently, *Barbot* (2019a); *Cattania* (2019) have shown that many complexi-

ties of fault dynamics, including Gutenberg-Richter distribution of earthquake sizes, can be modeled under quasi-dynamic approximation if the ratio of the fault dimension to the earthquake nucleation dimension is large enough. These models do not assume any structural or material heterogeneities, thus implying that such complexities are a sole manifestation of fault friction. *Erickson and Dunham* (2014) incorporated a heterogeneous medium in quasi-dynamic earthquake cycle simulations in the form of a sedimentary basin and showed the emergence of sub-surface events in addition to surface breaking events. *Abdelmeguid et al.* (2019) have shown the generation of subsurface events and multi-period sequences in a low-velocity layered fault damage zone under the quasi-dynamic approximation. *Thomas et al.* (2014) showed that incorporating inertia in earthquake cycle simulations, i.e., fully dynamic simulations, can exhibit significant differences from the quasi-dynamic approximation, especially under enhanced dynamic weakening frictional behavior. Here we consider fully dynamic models with fault damage zone surrounding mature strike-slip faults. Using fully dynamic earthquake cycle simulations, *Kaneko et al.* (2011) showed that a fault-parallel, narrow damage zone causes a reduction in the nucleation size of the earthquakes and amplification of slip rates during dynamic earthquake events. Despite a multitude of studies documenting the effects of fault damage zones on single rupture (*Harris and Day*, 1997; *Huang and Ampuero*, 2011; *Huang et al.*, 2014b), their long-term effects on earthquake sequences are not well understood, partially owing to a lack of seismological records over centuries.

We model earthquake sequences with full inertial effects on a two-dimensional vertical strike-slip fault surrounded by a fault damage zone. The constitutive response of the fault is governed by laboratory derived rate-and-state friction laws (*Dieterich*, 1979; *Ruina*, 1983). This fully dynamic modeling approach can simulate interseismic slip, earthquake nucleation, rupture propagation and postseismic deformation during multiple seismic cycles in a single computational framework (e.g., *Lapusta et al.*, 2000; *Kaneko et al.*, 2011; *Barbot et al.*, 2012; *Jiang and Lapusta*, 2016). The fault damage zone is modeled as an elastic layer with a lower seismic wave velocities compared to the surrounding host rock. Other important features of fault damage zones such as off-fault damage generation during the rupture (*Okubo et al.*, 2019; *Ma and Elbanna*, 2015b) and plastic deformation (*Huang et al.*, 2014b) have been modeled previously for single earthquake ruptures. We investigate how the wave reflections from fault damage zone modeled as a low-velocity layer influences the long-term stress evolution and contribute to the variability in earthquake magnitudes and hypocenter locations. We show that the variability in earthquake hypocenter is significant only in the cases where the damage zone truncates close to the nucleation site or extends beyond the nucleation zone, suggesting that frictional and rheological effects may

6

be a dominant mechanism for hypocenter variability when the damaged structure is very shallow. Our results also provide a possible explanation for the bimodal depth distribution of seismicity observed along mature strike-slip faults with shallow fault damage zone structures. We describe the observed geometry and material properties of the fault damage zone along the San Andreas Fault that inspire the design of our simulations in section 2.2. The two-dimensional model setup, model assumptions, friction laws, and simulation methodology are presented in section 2.3. We demonstrate the effects of the fault damage zone with varying widths and rigidity contrasts on the variability of earthquake magnitudes and hypocenters in section 2.4.

2.2 Observed Dimension and Material Properties of Fault Damage Zones

Fault damage zones can be delineated using potential field methods and seismic observations based on trapped waves within the damaged zone. Seismic reflections, magnetotelluric and resistivity surveys along the Parkfield segment of San Andreas Fault reveal a $500\,\mathrm{m}$ wide and $4\,\mathrm{km}$ deep fault damage zone (*Unsworth et al.*, 1997). This study also suggests a presence of a deeper fault zone whose properties are not well resolved, and a shallow $5\,\mathrm{km}$ wider damage zone surrounding the $\sim 500\,\mathrm{m}$ wide damage zone, representing a flower structure. Other studies along San Jacinto Fault Zone and San Andreas Fault Zone (e.g., *Li and Vernon*, 2001; *Wu et al.*, 2010) also indicate that the low-velocity zone may extend to seismogenic depths. *Cochran et al.* (2009) have combined seismology and geodesy to infer a wide and deep damage zone along Calico fault in southern California. Fault zone trapped wave studies along the Parkfield segment *Lewis and Ben-Zion* (2010) indicate a $3\,\mathrm{km}$ to $5\,\mathrm{km}$ deep, $150\,\mathrm{m}$ to $300\,\mathrm{m}$ wide fault damage zone, with a potentially nested fault zone extending up to $7\,\mathrm{km}$ to $10\,\mathrm{km}$. Geologic interpretations on the same region from the SAFOD cores *Lockner et al.* (2011) delineate a $\sim 200\,\mathrm{m}$ wide fault damage zone at $2.7\,\mathrm{km}$ depth. A detailed 3-D seismic wave velocity map *Thurber et al.* (2003a) also reveals a several hundred meters wide fault zone structure at about $5\,\mathrm{km}$ to $8\,\mathrm{km}$ depth. The shear wave velocity contrast between the host rock and the fault damage zone is found to be around $10\,\%$ to $60\,\%$ (table 1 in *Huang et al.* (2014b) and references therein). Most of these studies report variations in fault damage zone structure along fault strike. We summarize the observed damage zone geometry along the Parkfield segment in Table 2.1. Fault damage zones have been observed in other regions as well, including the North Anatolian fault in Turkey, the Nojima fault in Japan, and the Kunlun fault in Tibetian plateau (*Ben-*

Zion et al., 2003; *Lockner et al.*, 2000; *Bhat et al.*, 2007). Based on this short review, it is clear that the fault damage zone width spans several hundred meters, whereas the depth extent is more debatable since the narrow damage zone is more difficult to resolve at depth. We use these observations to guide our model setup as described in the following section.

2.3 Methodology

2.3.1 Model Description

We consider a two-dimensional strike-slip fault embedded in an elastic medium with mode III rupture (Fig. 2.2). This implies that the fault motion is out of the plane and only the depth variations of parameters are considered. The top boundary is stress-free and represents Earth's free surface. The other three boundaries are absorbing boundaries that allow the waves to pass through. Since our model is symmetric across fault, we restrict the computational domain to only one side of the fault. Our domain extends to $48\,\mathrm{km}$ depth, where the top $24\,\mathrm{km}$ of the fault is bordered at the bottom by a region constantly slipping at $35\,\mathrm{mm\,yr^{-1}}$. This represents the tectonic plate motion that loads the fault and accumulates stresses. The seismogenic zone extends from $2\,\mathrm{km}$ to $15\,\mathrm{km}$, which is locked during the interseismic period and capable of hosting earthquakes. The rest of the fault creeps aseismically. Earthquakes are captured in our simulations when the maximum slip velocity on the fault exceeds the threshold of $0.001\,\mathrm{m\,s^{-1}}$. This model is inspired by the San Andreas fault, and is similar in setup to *Lapusta et al.* (2000) and *Kaneko et al.* (2011).

We model the fault damage zone as an elastic layer with lower seismic wave velocities compared to the host rock. We will focus on how the geometry, spatial extent, and damage intensity of this fault damage zone influence the earthquake sequence behavior. We consider four different scenarios: (I) a homogeneous elastic medium as a reference model, (II, III) a medium with a sharp, narrow fault damage zone with various depths, widths and velocity contrasts that extends throughout the seismogenic depth in model II and truncates at a shallow depth in model III, and (IV) a flower structure in which a narrow fault damage zone extending through the domain surrounded by a wider, trapezium-shaped fault damage zone truncated at a shallow depth (Fig. 2.2). In natural settings, the outer trapezium-shaped fault damage zone may not have a sharp boundary at depth but may show a smooth transition because its structure is more diffused than the inner fault damage zone. We use a sharp boundary at a depth of $8\,\mathrm{km}$ as an approximation of the flower structure in order to highlight the effects of dynamic wave reflections. These four sets of models are described in Fig. 2.2. We vary the width (H) and shear wave velocity (c_s) contrast of the fault damage

zone in the Model (II) and the depth (D) in model III to study their effects on earthquake sizes and hypocenters (Fig. 2.2a). The choices of 'H' and 'c_s' are shown in Fig. 2.3. We choose four different values of 'D' including two depths ($6\,\text{km}$ and $8\,\text{km}$) shallower than the nucleation site in the homogeneous medium, one depth intersecting the nucleation zone ($10\,\text{km}$) and one depth extending beyond the nucleation zone ($12\,\text{km}$). In the Model (IV), the outer, wider fault damage zone has a shear wave velocity reduction of $20\,\%$ compared to the host rock, while the inner one has a $40\,\%$ reduction. The second and third models are inspired by the geological and geophysical observations of the San Andreas fault zone as discussed in section 2.2, and the fourth model is inspired by the classic flower structure of fault damage zones (*Sibson*, 1977; *Unsworth et al.*, 1997; *Caine et al.*, 1996; *Pelties et al.*, 2015; *Perrin et al.*, 2016).

2.3.2 Friction Laws

The laboratory-derived rate- and state-dependent friction laws relate the shear strength on the fault to the fault slip rate (*Dieterich*, 1979; *Ruina*, 1983; *Scholz*, 1998). We use the regularized form for the shear strength interpreted as a thermally activated creep model (*Rice and Ben-Zion*, 1996; *Lapusta et al.*, 2000), which relates the shear strength (T) to the slip rate ($\dot{\delta}$) as follows:

$$T = a\bar{\sigma} \operatorname{arcsinh}\left[\frac{\dot{\delta}}{2\dot{\delta}_o} e^{\frac{f_o + b\ln(\dot{\delta}\theta/L_c)}{a}} \right] \tag{2.1}$$

where $\bar{\sigma}$ is the effective normal stress (the difference between lithostatic stress and the pore fluid pressure), f_o is a reference friction coefficient corresponding to a reference slip rate $\dot{\delta}_o$, and a and b are empirical constants dependent on the mechanical and thermal properties of the contact surface. The parameter θ is a state variable interpreted as the average lifetime of the contact asperity, and L_c is the characteristic distance over which most of the evolution in shear resistance occurs, as measured in the laboratory during velocity steps. *Barbot* (2019b) has also shown that the state variable θ is the age of contact strengthening. In our models, the evolution of the state variable is governed by the aging law:

$$\frac{d\theta}{dt} = 1 - \frac{\dot{\delta}\theta}{L_c} \tag{2.2}$$

The frictional stability of faults is determined by the frictional parameters, L_c, $(a - b)$, and the ratio $\frac{a}{b}$. Depending on the value of $(a - b)$, we can have an unstable slip for a steady state velocity weakening frictional regime $(a - b) < 0$, or a stable sliding for a

9

steady state velocity strengthening frictional regime $(a - b) > 0$. Earthquakes occur when the velocity-weakening region of the fault exceeds a critical nucleation size that depends on the shear moduli of near-fault rocks, effective normal stress and frictional parameters (*Rice*, 1993; *Rubin and Ampuero*, 2005). More generally, the fault dynamics is controlled by R_u, the ratio of the velocity-weakening patch size to the nucleation size, and the ratio $\frac{b-a}{a}$ that controls the relative importance of strengthening and weakening effects and the ratio of static to dynamic stress drops. For higher values of R_u, we can obtain more chaotic rupture styles such as partial and full ruptures, aftershock sequence, and a wide range of events. For our simulations, the theoretical nucleation size is $\sim 2\,\mathrm{km}$, and the width of velocity weakening region is $\sim 10\,\mathrm{km}$, implying the value of $R_u \sim 5$, which predicts single-period full ruptures (*Barbot*, 2019a).

We use a depth dependent profile for $(a - b)$ as inferred from granite samples in laboratory experiments (*Blanpied et al.*, 1991, 1995). The seismogenic zone is the velocity weakening region extending from a depth of $2\,\mathrm{km}$ to $15\,\mathrm{km}$. The rest of the fault is velocity strengthening and accommodates aseismic creep. The velocity strengthening region at the top $2\,\mathrm{km}$ of the fault is suggested by laboratory observations under low stresses (*Blanpied et al.*, 1991). The effective normal stress is assumed constant below the depth of $2\,\mathrm{km}$, since the increase in the lithostatic stress is accommodated by the pore fluid pressure at depth (*Rice*, 1993). The seismogenic zone is overstressed initially (Fig. 2.2b). *Blanpied et al.* (1991) also shows the temperature weakening behavior of the friction for higher temperatures, but we only use the velocity dependence of the friction in this study. *Barbot* (2019b) derived an alternative formulation that incorporates thermal dependence of fault strength and and provides an explicit relationship between frictional parameters and micromechanical properties. We have chosen a relatively standard model of the regularized rate- and state-dependent friction described by *Rice and Ben-Zion* (1996); *Lapusta et al.* (2000) so that it is easier to compare the results with previous studies.

2.3.3 Numerical Simulation of Fully Dynamic Earthquake Sequences

We use a spectral element method to simulate dynamic ruptures and aseismic creep on the fault (*Kaneko et al.*, 2011). Full inertial effects are considered during earthquake rupture and an adaptive time stepping technique is used to switch from interseismic to seismic events based on a threshold maximum slip velocity of $0.5\,\mathrm{mm\,s^{-1}}$ on the fault. This method is able to capture all four phases of the earthquake cycle including nucleation, rupture propagation, post seismic deformation, and interseismic creep. We implement *Kaneko et al.* (2011)'s algorithm in Julia (*Bezanson et al.*, 2017) using a more efficient linear solver

based on the Algebraic Multigrid scheme (*Ruge and Stüben*, 1987) for the elliptic (interseismic) part of the earthquake sequence. We use the Algebraic Multigrid as a preconditioner while solving the sparse linear system using the conjugate gradient method. This combines the superior convergence properties of the Algebraic Multigrid with the stability of Krylov methods and is very well suited for symmetric, positive definite matrices. This iterative technique uses a fixed number of iterations independent of the mesh size. *Landry and Barbot* (2016, 2019) have derived the equations to solve elliptic equations using the Geometric Multigrid in 2D and 3D. While the Geometric Multigrid has superior convergence properties, the Algebraic Multigrid is better suited for more complicated meshes and is scalable to a wide variety of problems as the solver works with the numerical coefficients of the linear system as opposed to the mesh structure. The detailed algorithm is described in *Tatebe* (1993). In addition, we use the built-in multithreading feature of Julia, which enables us to achieve a CPU speed-up of ~ 50 times compared to the original code described in *Kaneko et al.* (2011).

2.3.4 Theoretical Nucleation Estimates and Choice of L_c

In a two-dimensional continuum model, the theoretical estimate of earthquake nucleation for a mode III crack based on energy balance is given by *Rubin and Ampuero* (2005):

$$h^* = \frac{2}{\pi} \frac{\mu L_c b}{\bar{\sigma}(b-a)^2} \tag{2.3}$$

where a, b, and L_c are the rate and state friction parameters, μ is the shear modulus of the near source region and $\bar{\sigma}$ is the effective normal stress. We note that the above estimate of nucleation size is not a unique estimate but is appropriate for our choice of friction parameters (*Rubin and Ampuero*, 2005; *Kaneko and Lapusta*, 2008). Using $L_c = 8\,\mathrm{mm}$ leads to a nucleation size of $3.9\,\mathrm{km}$ in a homogeneous medium. As the nucleation size is proportional to the rigidity of the near-source medium (*Rubin and Ampuero*, 2005; *Kaneko et al.*, 2011), it is reduced by a factor of ~ 3 in a damaged medium with a shear wave velocity reduction of 40% (*Huang*, 2018). The theoretical estimate of the nucleation size in a layered medium (h^*_{lay}) for a mode III rupture is derived by *Kaneko et al.* (2011) using linear stability analysis:

$$h^*_{lay} \tanh\left[2H\frac{\gamma}{h^*_{lay}} + \operatorname{arctanh}\left(\frac{\mu_D}{\mu}\right)\right] = h^*_{hom} \tag{2.4}$$

where μ and μ_D are the rigidity of the host rock and the layer respectively, $\gamma\ (= \pi/4)$ is an empirical parameter dependent on the geometry, h^*_{hom} is the theoretical nucleation size in the homogeneous medium with reduced shear modulus, and H is the thickness of the layered medium. The parameter choice of width and shear wave velocity contrast and their corresponding nucleation sizes are shown in Fig. 2.3. A smaller nucleation size would allow smaller earthquakes to nucleate successfully, therefore incorporating a wider range of magnitudes. We use 5 Gauss-Lobatto-Legendre nodes inside each spectral element, such that the average node spacing is $20\,\mathrm{m}$. For a well resolved simulation, the cohesive zone size (*Day et al.*, 2005; *Kaneko et al.*, 2008) should contain at least 3 node points. Based on the frictional parameters and rigidity of fault damage zone, the quasi-static cohesive zone size in our models is $\sim120\,\mathrm{m}$ and encompasses sufficient nodes. We demonstrate the convergence of our model with respect to different node spacing in section 2.6.

2.4   Results

2.4.1   Complexity in Fault Slip Due to Damage Zone

We discuss the slip-complexity due to reduction in nucleation size in a homogeneous medium and subsequently due to a fault damage zone as a layered medium. The theoretical nucleation size of a mode III rupture is directly proportional to the rigidity of the medium. Since smaller nucleation sizes also tend to give rise to complexities in earthquake cycles (*Lapusta and Rice*, 2003b), it is imperative to isolate the effects of reduced nucleation size from the effects of dynamic wave reflections and stress heterogeneities due to fault damage zones. In this section, we analyze three simulations, all having comparable nucleation sizes: (a) A homogeneous-medium simulation with a reduced characteristic slip distance (Fig. 2.4a), (b) A homogeneous-medium simulation with a reduced shear modulus, i.e., the entire medium is damaged (Fig. 2.4b), (c) A simulation with a fault damage zone modeled as a narrow low-velocity layer (Fig. 2.4 c,d,e). The simulation parameters for each of these models are discussed in Table 2.2. We see that Fig. 2.4a and Fig. 2.4b host earthquakes with uniform sizes and hypocenter locations. We also observe an increase in recurrence intervals and accumulated slip in Fig. 2.4b compared to Fig. 2.4a, which can be attributed to a reduced shear modulus in the medium. Despite these differences, we do not observe complexities such as variations in hypocenter locations or earthquake sizes. In contrast, Fig. 2.4c-e shows significant variability in both earthquake size and hypocenter location, which is attributed to dynamic wave reflections. The damaged medium also has a much larger coseismic slip when compared to an undamaged medium. Fig. 2.4f shows

the comparison of slip rate and shear stress evolution at $7\,\mathrm{km}$ for the three representative models (Fig. 2.4a-c), demonstrating the effect of dynamic wave reflections on stress heterogeneities. We see a clear reflection phase from the free surface in all the models, but the slip-rate and the shear stress is much more heterogeneous in our fault damage zone model. The dynamic wave reflections generate peaks in the shear stress profile that persist through multiple earthquake sequences. It is clear from this comparison that inertial dynamics play an important role in the earthquake sequences, especially in layered medium such as our fault damage zone models.

Our results show that the presence of the fault damage zone promotes complexity in the earthquake slip distribution and variability in their magnitudes, especially for large rigidity contrast between the fault damage zone and the host rock. Given the friction parameters and initial stress conditions in our simulations (Table 2.2), the homogeneous medium hosts periodic earthquakes with exactly the same hypocenter locations and magnitudes, whereas the fault surrounded by a fault damage zone shows a more complex slip distribution with variable earthquake sizes and hypocenter locations through multiple earthquake cycles (Fig. 2.4 c-e). We use comparable nucleation sizes for the homogeneous medium and damaged models to highlight the effects of dynamic waves. We also observe ruptures with multiple slip pulses and more complex slip distribution in the flower structure scenario (Fig. 2.4e, Fig. 2.5b).

Previous dynamic rupture simulations show that fault zone wave reflections can induce pulse-like ruptures (*Harris and Day*, 1997; *Huang and Ampuero*, 2011; *Huang et al.*, 2014b). We observe the imprint of these wave reflections in the spatiotemporal slip rate evolution of fault damage zone simulations (Fig. 2.5). These Slip pulses become a dominant feature during earthquake rupture as the waves are reflected from the damage zone boundaries in our earthquake cycle simulations. Similar pulse-like ruptures are also observed in homogeneous-medium earthquake cycle simulations for specific sets of heterogeneous friction parameters and fault asperity dimensions (*Michel et al.*, 2017). Our results suggest that stress heterogeneities generated by slip pulses due to seismic wave reflections are primarily responsible for the complexities in accumulated slip and variation in hypocenter distributions.

We compute the moment magnitudes of simulated earthquakes to investigate the relation between the magnitudes and cumulative number of earthquakes. The start and end of a rupture is defined based on a threshold slip velocity of $0.001\,\mathrm{m\,s^{-1}}$. The seismic moment is calculated as the product of the elastic shear modulus (μ), the coseismic slip (D) integrated along the depth, and the rupture area. The rupture length (L) is defined as the part of the fault where slip is greater than 1% of the maximum coseismic slip during a certain

earthquake. Since our simulation is two-dimensional, we assume the rupture width (W) is the same as the rupture length. The seismic moment (M_o) is defined as:

$$M_o = \mu(LW)D = \int dL \int \mu(dL)D(L) \tag{2.5}$$

The moment magnitude is computed using the relation of Kanamori (1975) : $Mw = 2/3\log_{10} M_o - 10.7$, where M_o is the seismic moment measured in $\mathrm{dyne\,cm}$.

In our simulations, the model with homogeneous medium hosts one large earthquake every ~ 100 years. The recurrence intervals and magnitude of the earthquakes are also fairly uniform throughout the seismic cycle. In the presence of the fault damage zone, we observe more complex slip history with varying earthquake magnitudes and hypocenter locations. To further understand the simulated earthquake catalog, we investigate the number of earthquakes for each magnitude range (i.e., magnitude-frequency distribution). We combine the magnitudes for all the fault zone simulations in order to emulate a natural setting where there are multiple faults with varying fault damage zone properties and show their cumulative magnitude frequency distribution in Fig. 2.6a. We observe a decrease in the number of earthquakes as the magnitude increases from 3 to 4.5, after which the number of earthquakes stagnates for intermediate magnitudes of 4.5 to 6. Finally we see a sharp decrease in the number of earthquakes for the largest earthquakes. This combined magnitude-frequency distribution is different from the Gutenberg-Richter distribution.

To understand the gap in the intermediate magnitude earthquakes, we examine the envelope of the coseismic slip distributions representing the rupture area for all the simulated earthquakes (Fig. 2.6b). The rupture areas of smaller earthquakes are confined within the depth range of $3\,\mathrm{km}$ to $11\,\mathrm{km}$ (Fig. 2.6b). The rupture area and final slip for these subsurface events are ~ 10 times smaller than those of the surface-rupturing events. Therefore there is two orders of gap in the moment magnitudes between the small and large events. Since the effective normal stress and hence the fault strength is low at depths shallower than $3\,\mathrm{km}$, it is harder to stop dynamic ruptures once they reach this shallow depth. When the rupture breaks through the free surface, the magnitude of the earthquakes tend to be much larger, which may explain the lack of intermediate magnitude earthquakes. Another potential reason is that there is no along-strike rupture termination in our 2D models. Generating a Guternberg-Richter type earthquake catalogue may require a reduction in earthquake nucleation size (*Cattania*, 2019), additional frictional or material heterogeneities, or along-strike termination of spontaneous ruptures.

2.4.2 Variability in Earthquake Hypocenters

Earthquakes on crustal strike-slip faults tend to occur within the top $15\,\mathrm{km}$ to $20\,\mathrm{km}$ of the crust, known as the seismogenic zone. However, these earthquakes are not uniform along depth, and are more correlated with the shallow crustal structure (*Marone and Scholz*, 1988). *Mai et al.* (2005) have performed Kolmogorov-Smirnov tests on a database of finite-source inversions and showed that the uniformity of hypocenters along depth can be statistically rejected, especially for strike-slip faults. Other studies (*Marone and Scholz*, 1988; *Hauksson and Meier*, 2019) have shown that the depth distribution of earthquake hypocenters may be more bimodal, with strong clustering of earthquakes at shallow ($\sim 5\,\mathrm{km}$) and deeper ($\sim 15\,\mathrm{km}$) depths. A bimodal distribution for rupture sizes has also been observed in thrust fault settings (*Dal Zilio*, 2020). Shallow seismicity is usually interpreted as short-term strain transients or changes in the frictional and rheological properties of rocks along depth. The abrupt decrease in deeper seismicity ($\leq 15\,\mathrm{km}$) is attributed to the thermo-mechanical behavior of rocks at these depths. We provide an alternate explanation for the bimodal distribution of seismicity along strike-slip faults based on the geometrical extent of fault damage zones, wherein the structural boundary of the fault damage zone produces additional stress concentration that promotes earthquake nucleation near the boundary. Our results also suggest that frictional and rheological effects may be a dominant mechanism for hypocenter variability when the damaged structure is shallower than $8\,\mathrm{km}$.

The depth distributions of earthquake hypocenters for various fault zone depths, widths and velocity contrasts are shown in Fig. 2.7. In contrast to the homogeneous medium, the hypocenter locations vary considerably for the fault zone simulations, and the depth extent of the fault damage zone has a pronounced effect on the hypocenter location. As demonstrated by Fig. 2.7a, the maximum variability in hypocenter locations is observed when the fault damage zone extends to the earthquake nucleation sites. As the fault zone becomes deeper, we see a systematic downward shift in the average hypocenter location, which saturates for a very deep fault zone extending throughout the seismogenic zone. We attribute this variability to the sharp material discontinuity between the fault damage zone and the host rock where shear stress changes tend to be concentrated (*Bonafede et al.*, 2002; *Rybicki and Yamashita*, 2002), resulting a number of earthquakes nucleating near this interface. For the same depth below the shallower fault zone, the deeper fault zone leads to a smaller nucleation size due to the reduction in elastic shear modulus, thus allowing earthquakes to nucleate at a deeper location as the fault is loaded from below. However, when the damage zone is very shallow, in the order of $\sim 6\,\mathrm{km}$ depth (Fig. 2.7a-i), most of the earthquakes nucleate below the damage zone. This suggests that the interplay between the earthquake nucleation site and damage zone boundary is an important factor influenc-

ing earthquake hypocenter locations. Despite additional stress concentration at the fault damage zone boundary, fault loading conditions and frictional boundary have a dominant effect on earthquake hypocenters for very shallow fault zone. But as the fault damage zone penetrates to the nucleation site, the fault zone effects become more critical in determining the depth distribution of seismicity. In other words, the seismicity distribution is influenced by both the material and frictional boundaries.

In fault damage zones extending throughout seismogenic depths, the increase of damage zone width also leads to an increase in the average hypocenter depths (Fig. 2.7b). This is consistent with the idea that the nucleation size is reduced as the width increases, which should lead to a downward shift in earthquake hypocenters when the fault loaded from below. The hypocenter locations also tend to be deeper for a higher shear wave velocity contrast, again due to a smaller nucleation size (Fig. 2.7c).

Our simulations highlight the variable depth distribution of earthquake hypocenters on strike-slip faults. In certain cases, a shallow fault damage zone exhibits more bimodal distribution of hypocenters (Fig. 2.7a-iii), whereas deeper fault damage zones tend to exhibit more unimodal distribution (Fig. 2.7b-ii). We also see a bimodal distribution when the shear wave velocity contrast is very low (Fig. 2.7c-iv), which can be attributed to frictional stress concentrations. We show the hypocenter distributions from two representative simulations of a shallow and a deep fault damage zone against various observations (Fig. 2.8a), wherein the shallower damage zone shows a more bimodal distribution as compared to a deeper damage zone (Fig. 2.8b). It is pertinent to note that most of the observations of seismicity depth distribution is limited to small earthquakes, because we do not have enough record of large earthquakes along single faults. Nevertheless, we are qualitatively able to compare the simulated earthquake hypocenter locations with the observed hypocenter locations.

2.4.3 Evolution of Peak Slip Rate and Fault Shear Stresses

We show the peak slip rate evolution for our simulations in Fig. 2.9. A homogeneous-medium simulation shows large recurring earthquakes, whereas smaller events emerge in a damaged medium, caused by the interplay between the fault damage zone boundary and the nucleation along the fault. In addition, we observe multiple 'slow events' in the presence of the fault damage zone that do not grow to fully dynamic earthquakes. The complexities in the number of these 'slow events' are elevated for a shallow fault damage zone extending to the nucleation site (Fig. 2.9c). The flower structure shows a more complex peak slip rate function (Fig. 2.9d) despite having fewer slow events because the inner damage

zone extends deep within the seismogenic zone. These slow events in our models occur at $\sim 10\,\text{km}$ depth (Fig. 2.4 d,e), close to the nucleation site and also close to the damage boundary in the case of shallower fault damage zone (Fig. 2.4d). They can be interpreted as accelerations in the slip rate that cannot grow to fully dynamic earthquakes because the stresses are not large enough to reach the dynamic regime, i.e., a failed nucleation (*Noda and Hori*, 2014; *Barbot*, 2019a). We observe a combination of slow events and dynamic ruptures in the velocity weakening regime. Our results imply that the geometry of the damaged medium can cause additional source complexities that are similar to seismic observations. We infer that a mature fault zone is more likely to exhibit slow events compared to immature fault zones in strike-slip tectonic settings.

In order to understand the mechanism underlying the variability of earthquake hypocenter locations and the scale of stress heterogeneities, we show the temporal evolution of fault shear stresses for different types of fault zones. Fig. 2.10 shows the shear stress evolution for the largest earthquake in homogeneous medium, a deeper fault damage zone, a shallow fault damage zone, and the 2D flower structure, respectively. Ruptures in the fault zone undergo a transition from cracks to pulses predominantly after the waves are reflected from the fault damage zone boundaries (Fig. 2.5a), while the homogeneous-medium simulations maintain crack-like ruptures. We observe shear stress heterogeneities emerging during the nucleation phase in the damage zone simulations (Fig. 2.10b), whereas they are absent in homogeneous medium (Fig. 2.10a). The interference of multiple stress peaks very close to the nucleation site are responsible for the variability in earthquake hypocenter locations and sizes in the fault zone simulations. The emergence of smaller earthquakes (Mw ~ 3.0) and the slow events are prominent when a fault damage zone extends to the nucleation site of the earthquakes. Although earthquake rupture velocities are slower in the fault damage zone, the stress peak amplitudes are larger than the homogeneous medium. Overall, the two key effects of the fault damage zoned in fully dynamic earthquake sequences are: (a) multiple stress peaks near the nucleation site, (b) small-scale stress heterogeneities due to dynamic wave reflections.

2.5   Discussion and Conclusions

We present fully dynamic earthquake cycle models that incorporate near-fault material heterogeneities represented by a fault damage zone. We show that the fault zone waves can lead to earthquakes with variable magnitudes and hypocenter locations. The depth distribution of earthquake hypocenters is strongly affected by the fault damage zone depth, with shallower fault zones favoring shallower hypocenters. We also see a bimodal depth

distribution of earthquake hypocenters in shallow damage zones and a more unimodal distribution in deeper damage zones. The variable nucleation locations originate from the interaction between stress heterogeneity induced by dynamic fault zone waves and the rate and state fault. In the shallow fault zone, the stress peaks are concentrated near the bottom of the fault damage zone and directly correlated with the earthquake nucleation locations, whereas the complex nucleation phase is absent in the homogeneous media.

Most existing studies that have discussed complexities in earthquake sequences with a damaged zone use a radiation damping approximation in a quasi-dynamic framework to accommodate the effects of inertia. A major shortcoming in the quasi-dynamic framework is the absence of radiated waves. We have demonstrated that the reflected wave from a fault damage zone can have strong effects on shear stress distribution, and these effects can lead to complexities in the earthquake behavior such as the earthquake size and the hypocenter location. *Thomas et al.* (2014) have shown a detailed comparison of quasi-dynamic vs fully-dynamic earthquake cycle simulations and they demonstrate significant quantitative and some qualitative differences between the two. In particular, the radiation damping approximation tends to show crack-like behavior whereas pulse-like behavior is easily obtained in fully dynamic simulations. The addition of enhanced dynamic weakening leads to significant changes in the earthquake behavior simulated using fully dynamic simulations. The effects of full inertial dynamics have not been explored on the entire parameter space consisting of different ratios of the velocity-weakening size to the nucleation size due to the huge computation cost associated with simulating these fully dynamic earthquake sequences. Even in homogeneous-medium simulations without a fault damage zone, it is not clear if models accounting for full inertial dynamics would lead to the same conclusion as *Barbot* (2019a) and *Cattania* (2019). Nevertheless, previous studies such as *Thomas et al.* (2014) and our current work suggest that major changes are expected, and the quasi-dynamic approximation should be used with caution. In particular, we have demonstrated that for the same nucleation size, the dynamic wave reflections lead to pulses-like behavior and therefore additional complexity in the earthquake sequences.

Previous static and quasi-dynamic simulations have shown that perturbations in shear and normal stress can give rise to complex seismicity (*Ben-Zion*, 2001; *Perfettini et al.*, 2003). Furthermore, observations and numerical experiments suggest that the tectonic stresses on real faults are spatially heterogeneous (*Townend and Zoback*, 2000; *Rivera and Kanamori*, 2002), implying that the stress amplitudes are not smooth but oscillatory over space. The emergence of persistent slip pulses after initial few seconds of rupture propagation contribute to stress heterogeneity in our simulations. Another key observation is the emergence of smaller, slower events in the damaged medium that do not grow to dynamic

earthquakes. These slow events are more prominent in the shallow fault zones where the depth of the fault damage zone intersects the nucleation zone but does not extend deeper to the seismogenic zone. This suggests that the material heterogeneities strongly influence the nucleation phase in addition to generating dynamic reflected waves.

We find that the shape and properties of damage zone can affect the stress distribution and significantly contribute to complex seismicity even without smaller-scale frictional heterogeneities along fault. Earthquake magnitudes show significant variability when compared to a homogeneous medium, but the log-linearity of the magnitude-frequency distribution is difficult to infer due to the limited number of earthquakes generated in the simulations. Observations in regional and global earthquake catalogues generally show a log-linear decay of magnitude with increasing number of earthquakes, in agreement with the Gutenberg-Richter distribution. However, large earthquakes along individual faults or fault sections deviate from this behavior, showing a relatively elevated number of 'characteristic earthquakes' (*Schwartz and Coppersmith*, 1984; *Wesnousky*, 1994; *Parsons et al.*, 2018) that follow a gaussian distribution in addition to smaller earthquakes adhering to the Gutenberg-Richter distribution. This characteristic distribution is used as a basis for rupture forecast models, (e.g., *Field et al.*, 2017). We have combined the earthquakes from multiple simulations to emulate a regional catalogue where we may have multiple faults with different fault zone characteristics, but we ignore the interactions between these faults. In order to reproduce a Gutenberg-Richter distribution, more complexities in the model are required. One way to reproduce the log-linearity of the Gutenberg-Richter distribution would be to reduce the nucleation size in relation to the width of the velocity-weakening region. The question still remains whether frictional heterogeneities only, or additional material heterogeneities in combination with frictional heterogeneities and stress heterogeneities emulate the Gutenberg-Richter behavior in nature. The current model is an idealized approximation of the material effects of fault damage zones with small fractures. More realistic approximations would include the incorporation of viscoelastic and plasticity effects (*Allison and Dunham*, 2018; *Erickson et al.*, 2017), variable pore pressure effects with depth, and time-dependent frictional parameters and initial stresses. Despite these approximations, our models provide a physical description of the effects of material heterogeneities on the long-term behavior of strike-slip faults.

Our future work will be directed towards understanding the effect of fault damage zone evolution through multiple seismic cycles. Paleoseismic studies of large strike-slip earthquakes, limited to the past 1000-1200 years, suggest that the recurrence of large events is non-uniform, possibly even chaotic, with large gap in seismic activity followed by multiple seismic episodes (*Grant and Sieh*, 1992; *Seitz et al.*, 1997; *Fumal et al.*, 2002; *Toké et al.*,

2006). A time-dependent stressing history, possibly driven by the evolution of the fault damage zone through multiple seismic episodes and aseismic creep, may better explain the observed non-uniform recurrence intervals along mature faults. Previous experiments and observations (*Peng and Ben-Zion*, 2006a; *Stanchits et al.*, 2006) have shown that the damage can be enhanced during seismic episodes and be healed during interseismic periods. The amount and localization of damage depends on the earthquake sizes, the interseismic duration for which the fault is allowed to heal, and recurrence intervals of large earthquakes (*Vidale and Li*, 2003a; *Yang*, 2015). Incorporating the evolution of fault damage zone would provide more realistic outlook on long-term structural evolution and source characteristics of mature strike-slip faults.

2.6 Numerical Convergence in the Simulations

We perform numerical convergence tests for the simulations with a narrow fault damage zone extending throughout the model domain. The half-width of the fault damage zone is 150 m, and the shear wave velocity reduction is 40%. We use an average node-spacing of $10\,\mathrm{m}$, $20\,\mathrm{m}$ and $40\,\mathrm{m}$. The comparison between the peak slip rate and the differential slip for a large earthquake is shown in Fig. 2.11. The comparison of peak slip rate for simulations with different node spacings demonstrates that the onset of earthquakes are the same for the different node spacings. Furthermore, Fig. 2.11b shows that the differential slip for different node spacings are the same, implying that the earthquake size is independent of mesh size. The shape of the differential slip shown in the inset zoom figure (Fig. 2.11b) suggests all the features are not preserved for an average node spacing of $40\,\mathrm{m}$, but they are preserved for all the other node spacings. We also show the slip rate as a function of time for the first and the fifth rupture to illustrate the comparable timing of the dynamic rupture in Fig. 2.12(a-b). This figure demonstrates that while the timing of dynamic rupture is comparable for all the node spacings, the node spacing of $40\,\mathrm{m}$ shows numerical oscillations whereas the $20\,\mathrm{m}$ and $10\,\mathrm{m}$ node spacings are adequately resolved. Fig. 2.12(c-d) shows the stress drops for the first and the fifth event along depth, and it is well resolved for all the node spacings. Based on this convergence study, we have chosen an average node spacing of $20\,\mathrm{m}$ for our study.

2.7   Figures - Chapter 2

(a) Fault Damage Zones in California

Legend:
- Hayward Maacama
- San Andreas
- San Jacinto
- Calico
- Landers
- Big Bear
- Hector Mine
- South Napa

San Francisco
Parkfield
Los Angeles

(b) Fault Zone Schematic

Damage Zone
Host Rock
Outer partially damaged zone
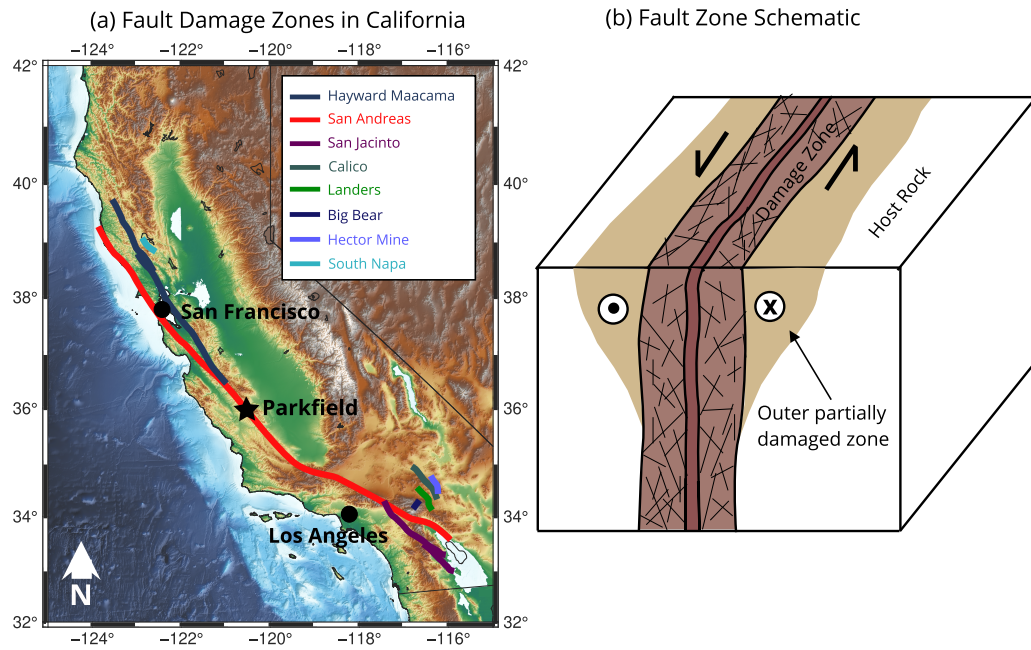
Figure 2.1: (a) Map of California faults with documented fault damage zones. (b) A schematic of mature fault zone structure that includes a fault core shown as the central dark-brown zone surrounded by an inner narrow zone of damage extending through the seismogenic zone, and an outer partially-damaged zone resembling a flower structure. Our models represent a two-dimensional vertical cross section across the fault.
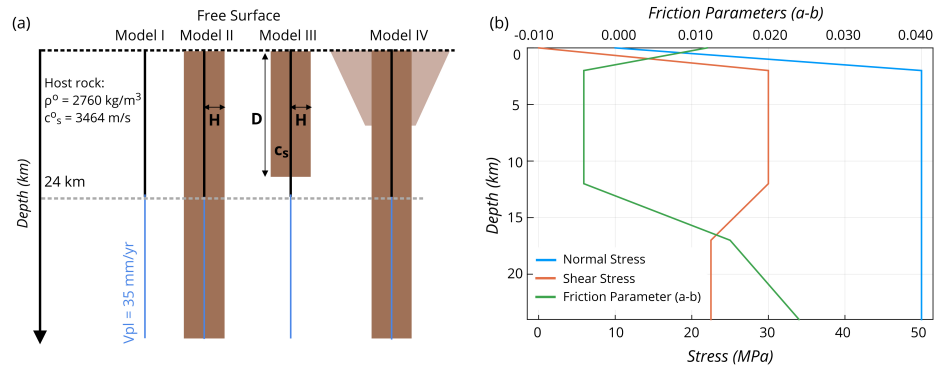
Figure 2.2: (a) Model description of four different scenarios. We consider a vertical strike-slip fault $24\,\mathrm{km}$ deep loaded from below by a plate motion rate of $35\,\mathrm{mm\,yr^{-1}}$. Model I: Homogeneous medium used as a reference model. Model II: A narrow fault damage zone extending throughout the seismogenic zone. Model III: A narrow fault damage zone truncating at a shallower depth, and Model IV: Two-dimensional approximation of flower structure damage. (b) Friction parameters $(a-b)$ and initial stresses along the fault dip. The seismogenic zone, i.e., the velocity weakening region, is the overstressed patch between 2 and $15\,\mathrm{km}$ depth.
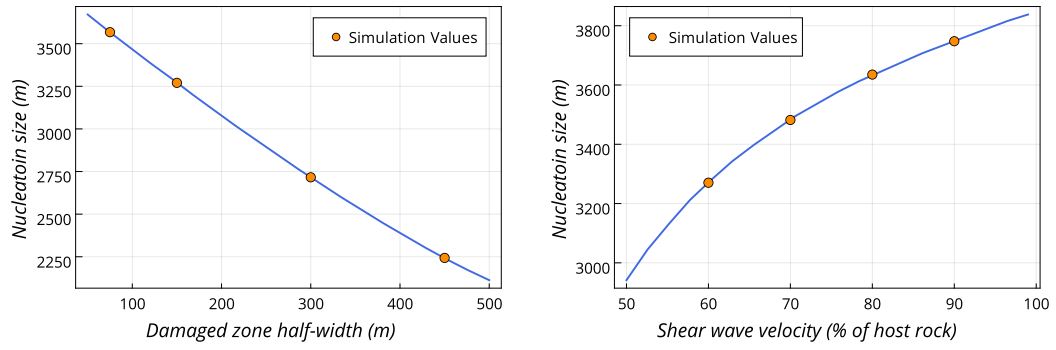
Figure 2.3: Variation of theoretical nucleation sizes in a layered medium. The left figure shows the variation due to fault damage zone widths, and the right figure shows the variation due to shear wave velocity. The orange dots show the theoretical nucleation sizes for the parameters chosen in our simulations.
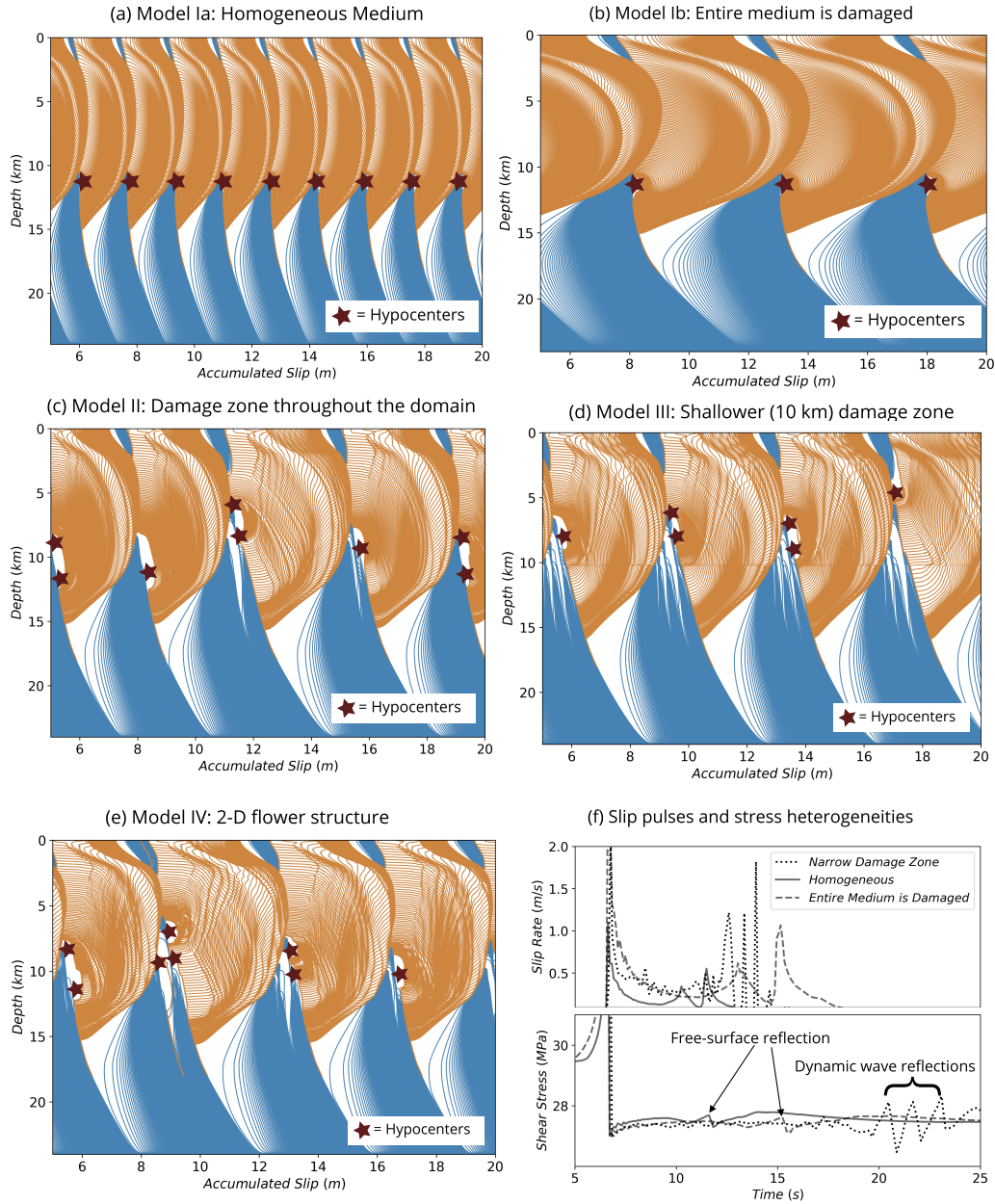
Figure 2.4: Cumulative slip contours with hypocenters shown as red stars. Multiple hypocenters close to each other represent smaller (Mw ~3) and larger (Mw ~7) earthquakes. The orange lines are plotted every $0.1\,\mathrm{s}$ during an earthquake and the blue lines are plotted every $2\,\mathrm{yr}$ during the interseismic period. The different models include (a) Homogeneous medium with smaller $L_c = 4\,\mathrm{mm}$, (b) Homogeneous medium with reduced shear modulus $\mu = 10\,\mathrm{GPa}$ such that the entire medium is damaged, (c) A narrow fault damage zone extending throughout the fault, (d) A narrow fault zone truncated at shallow depth, (e) 2D flower structure. (f) Comparison of slip-rate and shear stress for a single rupture of three models shown in Fig. 4a,b,c.

24
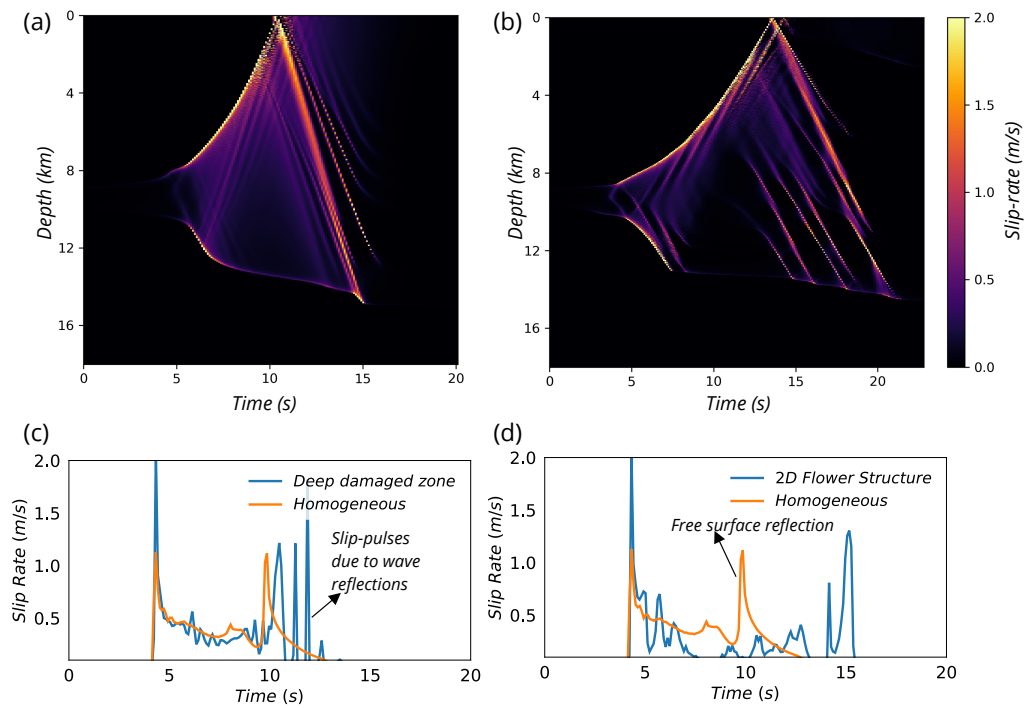
Figure 2.5: Spatiotemporal slip rate evolution demonstrating dynamic wave reflections for (a) fault damage zone extending throughout the domain, and (b) trapezoid shaped nested fault damage zone. (c) and (d) show the slip rate at a depth of $7\,\mathrm{km}$ for (a) and (b) respectively as compared to a homogeneous medium. The ruptures begin as crack but transition to pulses due to the wave reflections.
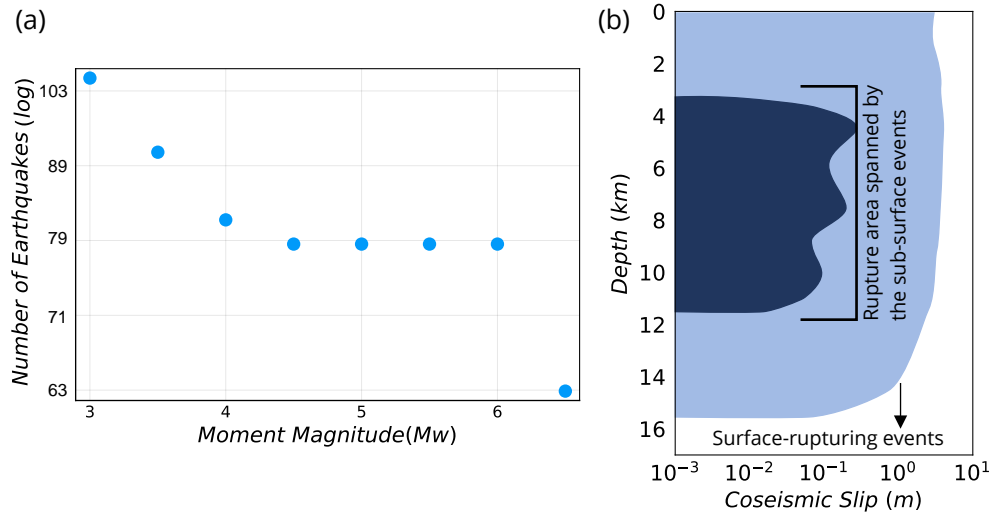
Figure 2.6: (a) Cumulative magnitude-frequency distribution for the combined simulations with multiple fault damage zone widths, depths, and rigidity contrasts. (b) The envelope of coseismic slip for the larger and smaller earthquakes against are plotted against the fault depth. We show the cumulative rupture length (and therefore rupture area) for all the larger and smaller earthquakes combined as the shaded region.
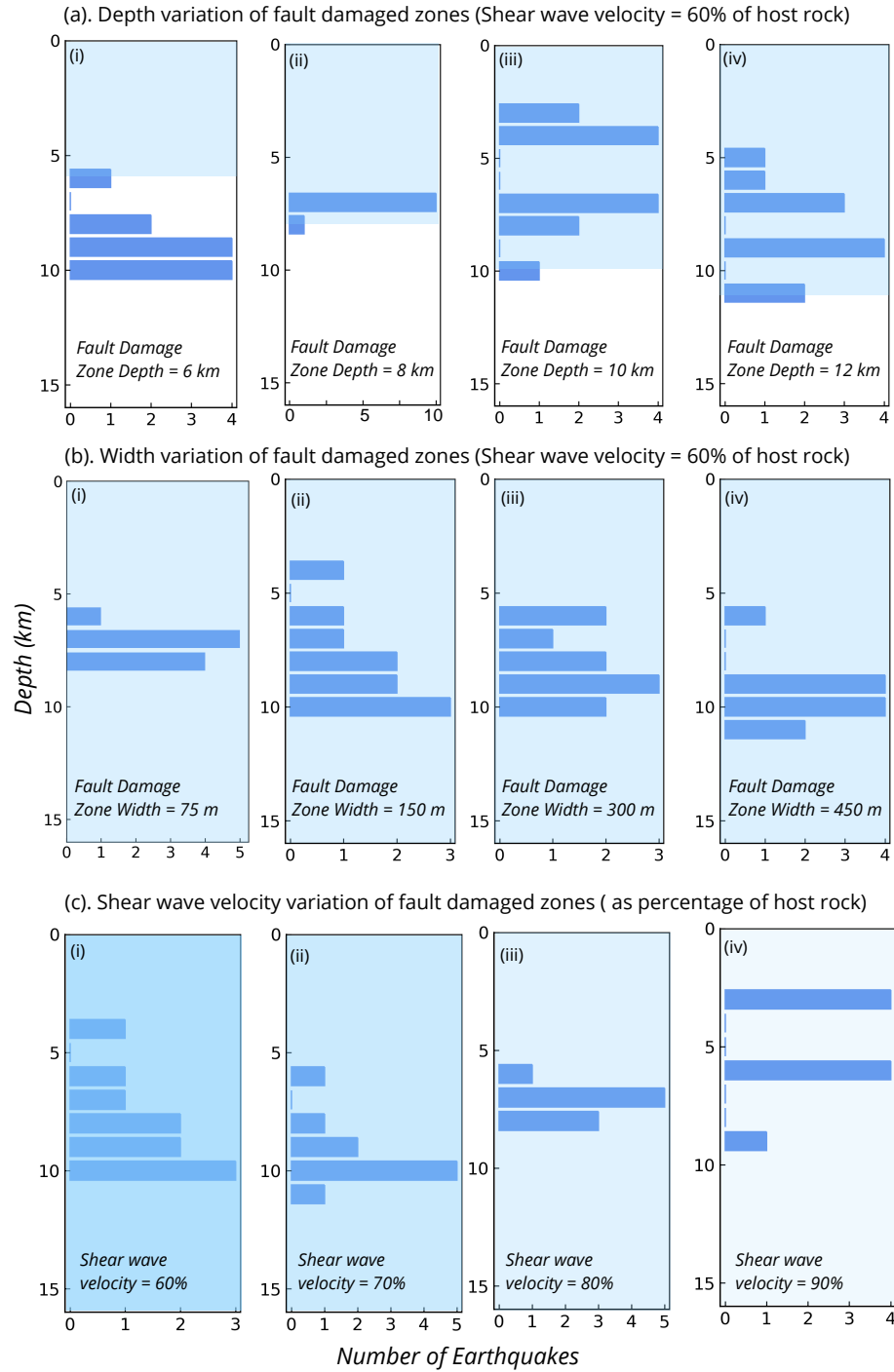
Figure 2.7: Earthquake hypocenter distribution for simulations with varying (a) fault damage zone depths, (b) widths, and (c) shear wave velocity contrasts. The shaded region shows the depth extent of damage zone and the intensity of shading shows the shear wave velocity contrast. All the models are shown to a depth of 16 km, which is the transition from velocity-weakening to velocity-strengthening regime.
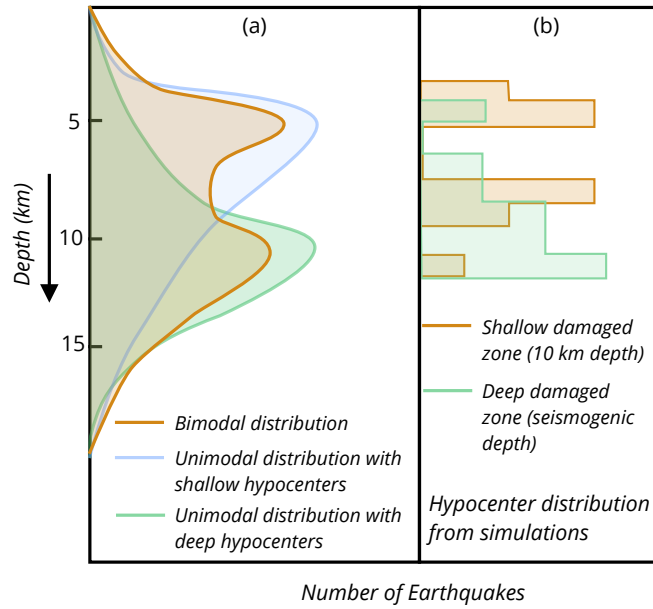
Figure 2.8: a). Observed seismicity distribution along strike-slip faults. We show bimodal distribution, unimodal distribution with shallow hypocenters, and unimodal distribution with deep hypocenters. (b) Simulated hypocenter distribution for a shallow and a deep damage zone. The models correspond to Fig. 7a-iii and 7b-ii.
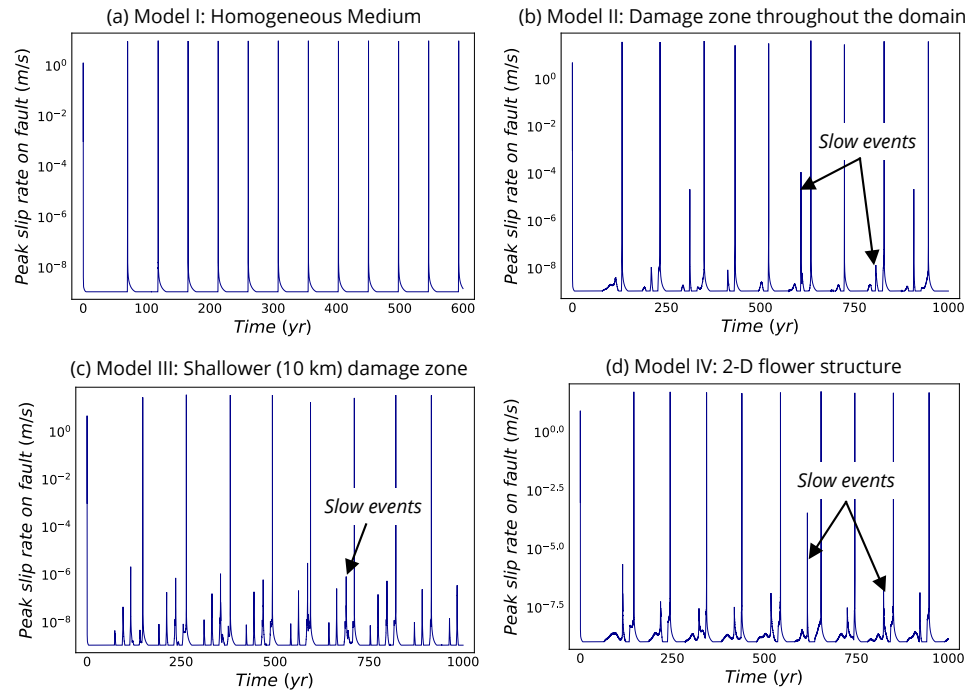
Figure 2.9: Peak slip rate function for (a) homogeneous medium, (b) deep fault damage zone, (c) shallow fault damage zone, (d) two-dimensional flower structure.
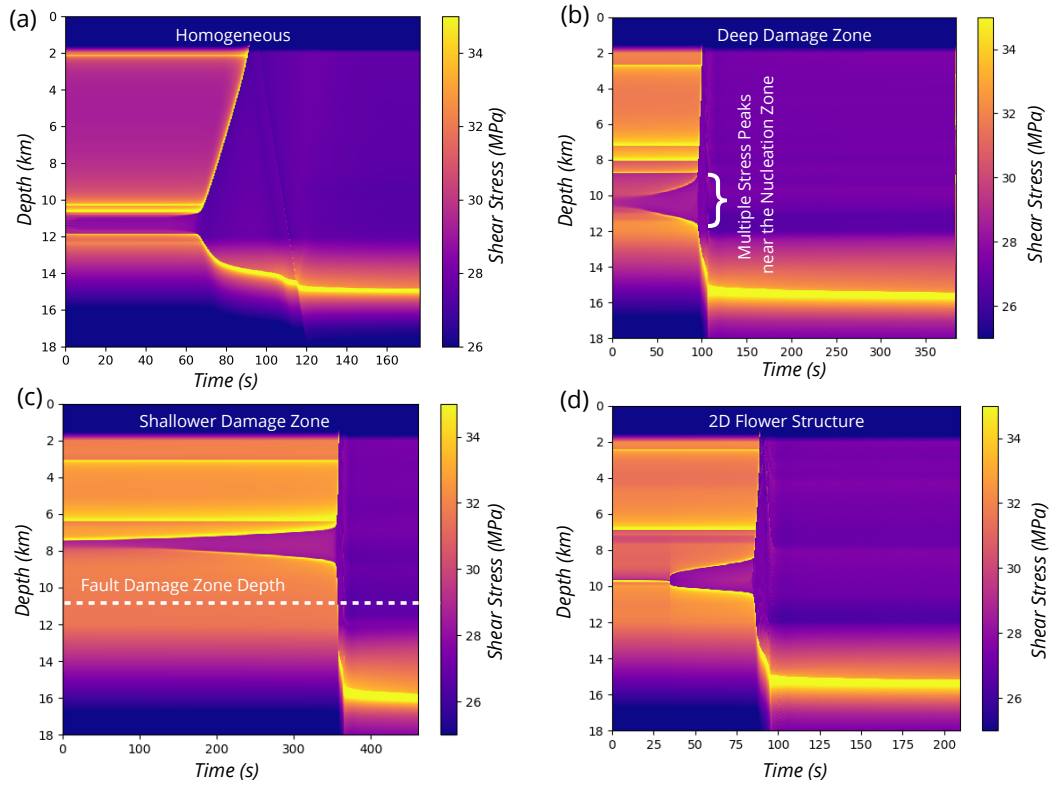
Figure 2.10: Shear stress evolution of a single earthquake including the nucleation phase shown along the fault for (a) homogeneous medium, (b) deep fault zone, (c) shallower fault zone, (d) two-dimensional flower structure.
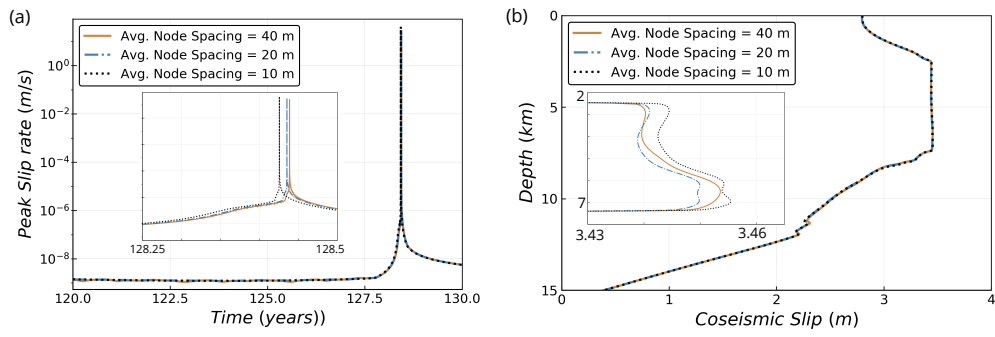
Figure 2.11: (a) Peak slip rate shown for multiple node spacings, (b) Differential slip of one earthquake shown for multiple node spacings.
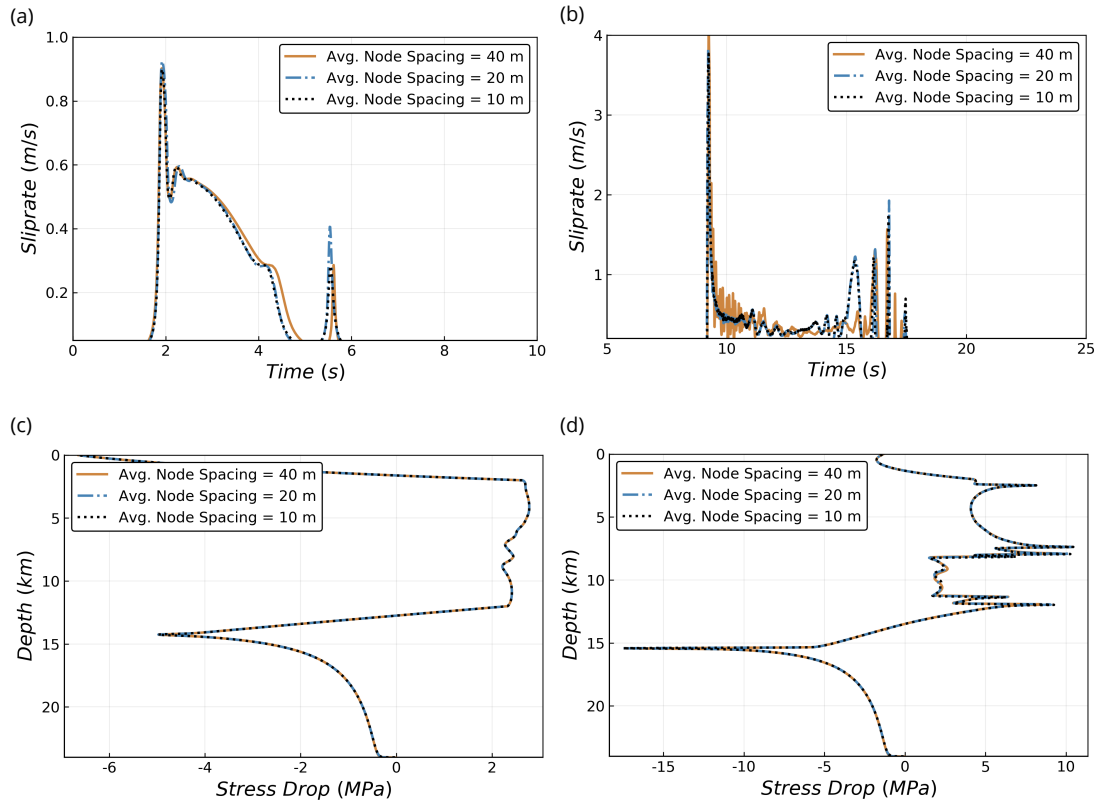
Figure 2.12: (a-b) Resolution tests showing the slip rate function for (a) first, and (b) fifth event at $7\,\mathrm{km}$ depth. (c-d) The stress drop along depth of the fault for (c) first, and (d) fifth event shown for multiple node spacings.

Table 2.1: Geometry of fault damage zone along Parkfield segment of San Andreas Fault as constrained by different studies.

References	Geometry	Width Inference	Depth Inference
Resistivity and MT *Unsworth et al.* (1997)	Wide at the top, narrow at depth	500 m: inner damage, 5 km: outer damage	4 km, with a deeper damage zone less resolved
Trapped seismic waves *Lewis and Ben-Zion* (2010)	Tabular low-velocity zone	150 m to 300 m	5 km to 7 km
Seismic wave velocities *Thurber et al.* (2003a)	Wide at the top and at seismogenic depth, narrow in between	500 m to 600 m	8 km
Geology: SAFOD *Lockner et al.* (2011)	Tabular	200 m	2 km

Table 2.2: Parameters used in numerical simulations of earthquake cycles. The parameters shown at the beginning are the same for all the simulations and other parameters are shown for each model that we use. The normal and shear stresses represent the values for the velocity-weakening region.

Parameter	Symbol	Value
Static friction coefficient	μ_0	0.6
Reference velocity	V_0	$1 \times 10^{-6}\,\mathrm{m\,s^{-1}}$
Plate loading rate	V_{pl}	$35\,\mathrm{mm\,yr^{-1}}$
Evolution effect	b	0.019
Effective normal stress	$\bar{\sigma}$	$50\,\mathrm{MPa}$
Initial shear stress	τ_0	$30\,\mathrm{MPa}$
Steady-state velocity dependence in the seismogenic region	$(b-a)$	-0.004
Width of seismogenic zone	W	$10\,\mathrm{km}$
Average node spacing	dx	$20\,\mathrm{m}$
Seismic slip-rate threshold	V_{th}	$1\,\mathrm{mm\,s^{-1}}$
Model Ia: Undamaged medium		
Characteristic weakening distance	L_c	$4\,\mathrm{mm}$
Shear modulus	μ	$32\,\mathrm{GPa}$
Model Ib: Entire medium is damaged		
Characteristic weakening distance	L_c	$8\,\mathrm{mm}$
Shear modulus	μ	$16\,\mathrm{GPa}$
Model II & III: Layered medium		
Characteristic weakening distance	L_c	$8\,\mathrm{mm}$
Shear modulus of host rock	μ	$32\,\mathrm{GPa}$
Shear modulus of damaged rock	μ_D	$10\,\mathrm{GPa}$
Model IV: 2-D flower structure		
Characteristic weakening distance	L_c	$8\,\mathrm{mm}$
Shear modulus of host rock	μ	$32\,\mathrm{GPa}$
Shear modulus of inner damage zone	μ_{Di}	$18\,\mathrm{GPa}$
Shear modulus of outer damage zone	μ_{Do}	$10\,\mathrm{GPa}$

CHAPTER 3

Influence of Fault Zone Maturity on Fully Dynamic Earthquake Cycles [*]

Abstract

We study the mechanical response of two-dimensional vertical strike-slip fault to coseismic damage evolution and interseismic healing of fault damage zones by simulating fully dynamic earthquake cycles. Our models show that fault zone structure evolution during the seismic cycle can have pronounced effects on mechanical behavior of locked and creeping fault segments. Immature fault damage zone models exhibit small and moderate subsurface earthquakes with irregular recurrence intervals and abundance of slow-slip events during the interseismic period. In contrast, mature fault damage zone models host pulse-like earthquake ruptures that can propagate to the surface and extend throughout the seismogenic zone, resulting in large stress drop, characteristic rupture extents, and regular recurrence intervals. Our results suggest that interseismic healing and coseismic damage accumulation in fault zones can explain the observed differences of earthquake behaviors between mature and immature fault zones and indicate a link between regional seismic hazard and fault structural maturity.

3.1 Introduction

Active faults are usually surrounded by narrow regions of localized deformation extending several hundred meters to a few kilometers in width across the fault. This deformation zone consisting of a dense fracture network is macroscopically viewed as an elastic layer with low seismic wave velocities and referred to as a fault damage zone (*Ben-Zion and Sammis*,

2003). The strength of the fault damage zone evolves throughout the seismic cycle, but the details of the evolution mechanism and the nature of this evolution remain elusive.

Fault zone maturity can be defined and quantified by the total slip accumulated over time in field geologic and geodetic studies (*Dolan and Haravitch*, 2014), with larger slip corresponding to higher maturity. Fig. 3.1 shows a conceptual model of how a strike-slip fault system may evolve through multiple earthquake cycles. Immature fault zones (Fig. 3.1a) are characterized by a distributed network of damage, and as the fault zone matures (Fig. 3.1c), the damage becomes localized. The faulting itself becomes more localized, transitioning from multiple and discontinuous slip surfaces to a more throughgoing fault. Other parameters such as the total fault length, the slip rate, and the initiation age have also been used to determine fault zone maturity (*Perrin et al.*, 2016). However, the surface slip expression for immature faults usually underestimate slip at depth by about $10\,\%$ to $60\,\%$ (*Dolan and Haravitch*, 2014). *Perrin et al.* (2016) have shown that structural maturity of a strike-slip fault zone is well correlated with the seismic wave velocity of near-fault materials, which decreases as the fault zone becomes progressively more mature. Such velocity reductions are well documented along mature fault zones such as the San Andreas fault zone (*Li et al.*, 2006; *Lewis and Ben-Zion*, 2010), San Jacinto fault zone (*Lewis et al.*, 2005), Nojima fault zone (*Mizuno et al.*, 2008), and Wenchuan fault zone (*Pei et al.*, 2019). Examples of immature fault zones that exhibit less evidence of localized damage include the northern part of the San Andreas fault zone (*Waldhauser and Ellsworth*, 2002), the Bam fault in Iran (*Fielding et al.*, 2009), the Jiuzhaigou earthquake near Kunlun fault zone in China (*Li et al.*, 2020), and Peloponnese fault zone in Greece (*Feng et al.*, 2010). Previous studies have shown that a more compliant or mature fault damage zone enables ruptures to propagate as slip pulses (*Harris and Day*, 1997; *Huang and Ampuero*, 2011; *Huang et al.*, 2014a; *Thakur et al.*, 2020; *Idini and Ampuero*, 2020). Geodetic observations (e.g., *Goldberg et al.*, 2020; *Feng et al.*, 2010) have shown earthquake slip distributions are complex in an immature fault zone, and they become more uniform as the fault zone matures. Understanding the long-term earthquake behavior during the structural evolution of the fault damage zone is key to unraveling the locations, recurrence intervals, stressing history, and the probability of subsequent earthquakes in an active fault zone.

Observations of seismic wave velocity changes within the fault damage zone ($< 1\,\mathrm{km}$ from the fault; (e.g., *Vidale and Li*, 2003b; *Li et al.*, 2003, 2006; *Wu et al.*, 2009; *Peng and Ben-Zion*, 2006b; *Zhao and Peng*, 2009; *Roux and Ben-Zion*, 2014)) documented a sharp decrease in pressure- and shear-wave velocities following earthquakes as well as a subsequent logarithmic increase in wave velocity with time. Other observations further away from the fault zone (e.g., *Taira et al.*, 2009; *Chen et al.*, 2015; *Pei et al.*, 2019) revealed

coseismic reduction and interseismic increase of seismic wave velocities in the surrounding region. Laboratory experiments have shown similar change in seismic wave velocities (*Johnson and Jia*, 2005; *Kaproth and Marone*, 2014; *Snieder et al.*, 2016) wherein they observe compaction during holds (i.e., interseismic period) and dilation during fault slip (i.e., seismic events). Mechanisms for damage accumulation in active fault zones are likely a combination of processes including dilation, compaction, cracking, shear driven pulverization, and fabric generation (*Gratier et al.*, 2003). The observed coseismic velocity drop is potentially related to brecciation, cataclasis, and damage accumulation, implying a magnitude dependence of this velocity drop (*Li et al.*, 2003; *Rubinstein and Beroza*, 2005; *Brenguier et al.*, 2008).

During the interseismic period, time-dependent fault zone healing may occur due to a combination of rheological restrengthening, inelastic strain, mineral precipitation, and fluid pressure recovery (*Vidale and Li*, 2003b). There is some debate on whether this healing time is significant in contributing to fault zone stress redistribution and therefore influencing long-term seismicity (*Vidale and Li*, 2003b; *Mizuno et al.*, 2008). It is hard to accurately quantify fault zone healing time because it requires long-term continuous monitoring of seismic wave velocities. Active seismic studies along the Landers fault zone (*Vidale and Li*, 2003b) and Longmenshan fault zone (*Pei et al.*, 2019) suggest that it may take years or decades to heal completely, whereas other studies (*Peng and Ben-Zion*, 2006b; *Mizuno et al.*, 2008; *Wu et al.*, 2009) suggest that the healing time may not be longer than the typical timescales of postseismic afterslip, i.e., a couple of months. Another study by *Roux and Ben-Zion* (2014) along the North Anatolian Fault suggests a recovery rate over a timescale of few days. It is worthwhile noting that some of these studies may have a lower spatial resolution than others which might affect the inference of fault zone recovery rate.

We use numerical simulations to understand the effects of fault zone damage accumulation after multiple cycles of earthquakes and healing during the interseismic period on a two-dimensional vertical strike-slip fault. We model the fault zone structure evolution as changes in the shear wave velocity of an elastic layer surrounding a strike-slip fault. This elastic fault damage zone has a lower shear wave velocity, and therefore, a lower rigidity compared to the surrounding host rock. We assume a constant density in our numerical simulations as the changes in shear-wave velocity has a more significant effect on the rigidity of the material. Throughout the remainder of this article, we will use the term "rigidity ratio", which is the percentage ratio of the fault zone shear modulus to the host rock shear modulus, to parameterize the fault zone evolution through time. Fig. 3.1b shows a representative rigidity ratio evolution through time. We constrain the coseismic damage accumulation and the rate of interseismic healing using shear-wave velocity observations

from Wenchuan (*Pei et al.*, 2019), Landers (*Vidale and Li*, 2003b), Nojima (*Mizuno et al.*, 2008), and North Anatolian Fault zones (*Peng and Ben-Zion*, 2006b). We describe the numerical procedure and the fault zone healing mechanism in section 3.2. The results of our models are described in section 3.3. We show that an immature fault zone tends to produce more slow-slip events and irregular earthquake sequences with predominantly subsurface events. In contrast, a more mature fault damage zone tends to produce a more regular sequence of earthquakes with a combination of surface-reaching and subsurface events. In section 3.4, we discuss the implications of our results for earthquake cycle behaviors of strike-slip fault zones.

3.2 Model Description

We use two-dimensional earthquake cycle models of strike-slip faults with mode III rupture where the displacement is out of the plane of interest and stresses and friction vary with depth. For simplicity, we use a narrow fault-parallel layer as a proxy for the damage zone and its geometry remains constant throughout the simulated sequence. This is equivalent taking a vertical cross-section across Fig. 3.1c, and the fault zone maturity in the damage evolution model corresponds to the change in rigidity ratio without changing the geometry of the fault zone (Fig. 3.1b). The frictional properties and initial conditions are chosen to keep the frictional complexities at a minimum. Here we focus the discussion on fault zone properties.

Since there are very few long-term observations (10,000-100,000 years) documenting the changes in permanent damage through multiple earthquake cycles, we limit ourselves to modeling short earthquake sequences for several hundred years each, with each sequence intended to represent different stages of fault zone maturity, including an immature stage and a mature stage, both of which accumulate no permanent damage. We also consider a transition stage which incorporates permanent damage, i.e., a reduction in rigidity after each earthquake. The distinction between immature and mature fault zones in our models depends on the rigidity ratio of the damage zone to the host rock. Typically, larger velocity reductions (35 % to 50 %) and lower rigidities (25 % to 45 % of host rock) are measured around mature fault zones, whereas smaller velocity reductions (8 % to 10 %) and higher rigidities (80 % to 90 % of host rock) are measured around immature fault zones (*Perrin et al.*, 2016). Based on these seismic wave velocity measurements, we choose a rigidity ratio changing between 80 % and 85 % of host rock for the immature fault zone and a rigidity ratio changing between 40 % and 45 % of the host rock for the mature fault zone. While mature fault zones can have lower rigidities as well, the chosen values lie well within

what is observed for mature and immature fault zones.

Another important parameter is the coseismic velocity drop. While its value is not well constrained by observations and can vary significantly ($0.1\,\%$ to $5\,\%$) between different fault zones such as Parkfield (*Li et al.*, 2006), Wenchuan (*Pei et al.*, 2019), and Landers (*Li et al.*, 2003), it is dependent on the size of the earthquake with smaller earthquakes showing smaller coseismic drop. Since our simulations are two-dimensional and do not have any along-strike constraints on the earthquake size, we use a magnitude-independent coseismic damage accumulation of $5\,\%$ rigidity change in order to facilitate a better comparison between different simulation cycles.

Our current models are a purely elastic approximation of how a fault damage zone may evolve over time through multiple earthquake sequences. This ignores the energy dissipated through the damage process (e.g., *Okubo et al.*, 2019), including that required for secondary crack formation (*Lyakhovsky et al.*, 2005). Additionally, the coseismic velocity drop in our models approximates the damage evolution and crack propagation over smaller timescales during each event to a step change that occurs after the event is over. Other plausible mechanisms such fault roughness evolution (*Heimisson*, 2020), or alternate modeling approaches such as elastic impact (*Tsai and Hirth*, 2020) might influence the dynamics of earthquake sequences. While incorporating these complexities may affect the overall fault slip behavior, they are computationally very expensive to implement and beyond the scope of the current study.

Our damage evolution model is described by a change in the rigidity ratio with respect to the host rock. We parameterize this ratio of shear modulus of the damage zone to the shear modulus of the surrounding host rock using three variables: A: the coseismic damage accumulation, which shows the amount of damage increase after an earthquake, T: the healing time, which shows the interseismic duration it takes the fault zone to heal to its maximum level, and P: the permanent damage, which shows the amount of damage that the fault zone never recovers. The rigidity ratio evolves through time based on the following relation:

$$\frac{\mu_D}{\mu} = \begin{cases} A_0, & \text{after each earthquake} \\ A(1 - \exp(-(\frac{1}{T})(t - t_{\text{start}}))) + A_0, & \text{during interseismic period} \end{cases} \tag{3.1}$$

where t and t_{start} are the current timestep and the start time of the previous earthquake in years, $\frac{1}{T}$ is the inverse of healing time (in years), A_0 is the prescribed damage after the earthquake. For the simulations with zero permanent damage (Fig. 3.2 and Fig. 3.3), A_0 is zero. For the simulation with permanent damage (Fig. 3.4), the permanent damage P is set

up by decreasing A_0 after each earthquake to $A_0 - nP$, where n is the earthquake number.

We use a spectral element method to simulate fully dynamic ruptures and aseismic deformation on a two-dimensional fault with mode-III rupture (*Kaneko et al.*, 2011; *Thakur et al.*, 2020). Adaptive time-stepping is used to switch from aseismic to seismic events based on a threshold slip velocity of $0.5\,\mathrm{mm\,s^{-1}}$ (*Erickson et al.*, 2020). The fault is 24 km deep, with the seismogenic zone extending from 3 km to 16 km. The rest of the fault creeps aseismically. Our two-dimensional rectangular domain is twice the fault length in the dip direction and 30 km in the off-fault direction. The bottom of the fault is loaded with a plate loading rate of $35\,\mathrm{mm\,yr^{-1}}$. Free surface is imposed on the top boundary of the domain, whereas the other three boundaries have absorbing boundary conditions. The frictional resistance of the fault to sliding is described by laboratory derived rate- and state-dependent friction laws, which were developed empirically (*Dieterich*, 1979; *Ruina*, 1983; *Blanpied et al.*, 1991) and is widely used in numerical models to simulate earthquake sequences (*Rice*, 1993; *Lapusta et al.*, 2000). We use rate- and state- dependent friction with aging law for the state-evolution to simulate earthquake sequences on the fault (*Dieterich*, 1979; *Ruina*, 1983; *Scholz*, 1998). We use the regularized form of the rate-and-state model (*Lapusta et al.*, 2000; *Rice and Ben-Zion*, 1996), which relates the shear strength (T) to the slip rate ($\dot{\delta}$) as follows:

$$T = a\bar{\sigma}\,\mathrm{arcsinh}\left[\frac{\dot{\delta}}{2\dot{\delta}_o}e^{\frac{f_o+b\ln(\dot{\delta}\theta/L_c)}{a}}\right] \tag{3.2}$$

where $\bar{\sigma}$ is the effective normal stress (i.e., the difference between lithostatic stress and the pore fluid pressure), f_o is a reference friction coefficient corresponding to a reference slip rate $\dot{\delta}_o$, L_c is the characteristic distance over which the contact asperity slips, and a and b are empirical constants dependent on the mechanical and thermal properties of the contact surface. The state variable θ, interpreted as the average lifetime of the contact asperity, evolves as follows:

$$\frac{d\theta}{dt} = 1 - \frac{\dot{\delta}\theta}{L_c} \tag{3.3}$$

Barbot (2019a) has shown that the state variable θ is the age of contact strengthening. Depending on the values of L_c, $(a-b)$, and the ratio $\frac{a}{b}$, we can determine the frictional stability of the fault wherein we can have an unstable slip for a steady state velocity weakening frictional regime ($a-b < 0$), or a stable sliding for a steady state velocity strengthening frictional regime ($a-b > 0$). Fault dynamics is controlled by R_u, the ratio of the velocity-weakening patch size to the nucleation size, and the ratio $\frac{b-a}{a}$ that controls the relative importance of strengthening and weakening effects and the ratio of static to dynamic stress

drops. For higher values of R_u, we can obtain more chaotic rupture styles such as partial and full ruptures, aftershock sequence, and a wide range of events (*Barbot*, 2019a; *Cattania*, 2019). In our simulations, we use relatively simple values for the theoretical nucleation size of ~ 2 km, and the width of velocity weakening region of ~ 10 km, implying that the value of R_u is ~ 5, which predicts single-period full ruptures in a homogeneous medium *Barbot* (2019a).

The fault damage zone extends throughout the domain and is symmetric across the fault. We use temporal changes in the rigidity ratio of the fault damage zone for modeling the damage accumulation and healing through time. We use a constant half-width of 1 km for the fault zone geometry. This facilitates easier comparison between mature and immature fault zones and is coherent with the observations (*Ben-Zion and Sammis*, 2003; *Perrin et al.*, 2016). The host rock has a shear wave velocity of 3464 km/s and a density of $2670\,\mathrm{kgm}^{-3}$ implying that the shear modulus is 32 GPa. We start with the same initial shear wave velocity in the fault damage zone but with a density of $2500\,\mathrm{kgm}^{-3}$ which remains constant throughout the simulation (*Kaneko et al.*, 2008; *Kaneko et al.*, 2011). Since density does not contribute as much to the rigidity as the shear wave velocity, any changes in the rigidity of the fault damage zone are directly related to the changes in shear wave velocity, which is an observable from seismic monitoring experiments. The initial rigidity ratio ($\frac{\mu_D}{\mu}$) is approximately 0.94, which primarily stems from the density difference between the host rock and the fault damage zone. The parameters tested for this study are discussed in Tables 3.1 and 3.2. The parameters shown in the results are shown in bold in Table 3.2.

The time-evolution of the shear modulus, described in equation A1, is operative only during the quasi-static part of the deformation, i.e., when the inertia is negligible and the fault is creeping aseismically. Since the time-steps are large in this part of the simulation, the deformation is essentially slow-enough such that the stress-strain relationship is linear throughout the numerical simulation. During the dynamic earthquakes, the shear modulus remains constant till the inertial effects are dissipated, after which it drops by a prescribed amount. This ensures that we can study the effects of coseismic damage accumulation and interseismic healing using parameters inspired by seismic observations, but still pertain to an elastic deformation regime.

Fig. 3.4 shows the fault slip evolution in a simulation that includes permanent damage after each earthquake.

3.3 Results

We have tested a range of parameters in our simulations that account for fault zone maturity, coseismic damage accumulation, and healing time. Here the fault zone maturity can be described by the initial rigidity ratio (Fig. 3.1b). These parameters are described in Tables 3.1 and 3.2. For brevity, we choose to show representative cases for a healing time of 8 years and a coseismic velocity drop of 5% in the following subsections. Changing these parameters (e.g., healing time between 1 and 20 years) have some effects on the location and timing of individual earthquakes but does not affect the overall interpretation of our results.

3.3.1 Effects of Fault Damage Zone Maturity

The initial rigidity ratio of fault damage zones with respect to the surrounding host rock can have significant effects on seismicity evolution. A higher initial rigidity ratio implies a less mature fault zone and vice versa. While keeping the permanent damage at zero, we compare an immature fault zone evolution characterized by rigidity ratio changing between 80% and 85%, against a mature fault zone evolution characterized by rigidity ratio changing between 40% and 45% (Figs. 3.2a and b). For the sake of simplicity, the fault zone accumulates damage by the same amount irrespective of the earthquake size.

For the models with a constant healing time, a mature fault zone tends to show more regular earthquake sequences with full (surface-reaching) ruptures, whereas a less mature fault zone shows irregular earthquake sequences with partial (subsurface) ruptures and more slow-slip events (Figs. 3.2c and d). The cumulative slip demonstrates events with variable sizes and depths throughout the seismogenic zone, but we do not see ruptures spanning the entire seismogenic region in the immature fault zone. Instead, we only see ruptures extending across a fraction of the seismogenic zone, and these partial ruptures persist throughout multiple seismic cycles. This phenomenon of partial ruptures occurs only in immature fault zone model with healing, which tend to have crack-like ruptures and overall lower slip velocities. In contrast, mature fault zone model exhibit higher slip-velocities and pulse-like ruptures, which tend to produce surface-reaching ruptures. Such pulse-like ruptures can be identified by looking at the cumulative slip of earthquake cycles in mature fault zones (Fig. 3.2d), where the final slip distribution is nearly flat, a characteristic of pulse-like ruptures (*Heaton*, 1990).

We measure shear stress before and after a representative earthquake from each of these simulations to understand the depth distribution of stress drop and the mechanisms accounting for different earthquake behaviors in mature and immature fault zones. Figs. 3.2e and

f show the depth distribution of shear stress for an earthquake in the immature and mature fault zone models, respectively. We see that the mature fault zone model exhibits a large, uniform stress drop along the fault dip (Fig. 3.2f) such that stress peaks after the earthquake are concentrated only towards the edges of the velocity-weakening segment due to ruptures propagating throughout the seismogenic zone. On the other hand, the immature fault zone model (Fig. 3.2e) results in a partial stress drop as the rupture is arrested before reaching the edges of the asperity. In this context, a partial stress drop refers to the stresses being released only in a small portion of the velocity-weakening segment along the fault. The partial stress drop in immature fault zones leads to residual stress peaks concentrated within the velocity-weakening region, which may cause subsequent ruptures or slow-slip events near those stress peaks. As discussed in more detail in section 3.2, the slow-slip events can delay the next earthquake rupture and result in irregular recurrence intervals between earthquakes.

We also include permanent damage after each earthquake in our model to demonstrate the transition from an immature fault zone to a mature fault zone (i.e., P is nonzero in Fig. 3.1b). While faults in nature need several tens of thousands of years to transition from immature to mature stages, it is not computationally feasible to perform such simulations with full inertial effects. The choice of the amount of coseismic velocity reduction and interseismic healing in our simulations allows the transition from immature to mature fault zones within 300-400 years. Fig. 3.4 shows the accumulated slip contours for the earthquake cycle in this scenario. We begin with an initial rigidity ratio of 90% and drop it down by 5% after each earthquake (Fig. 3.4). We allow the fault to recover 80% of the coseismic drop in rigidity during the interseismic period therefore accommodating a permanent damage of 1% rigidity reduction after each earthquake, though smaller recovery percentages may be achieved if the next earthquake occurs before the fault has healed completely (Fig. 3.4b). We see a progressive increase in the rupture length from partial to full ruptures as the fault zone becomes more mature (Fig. 3.4a). We distinguish between an immature and a mature fault damage zone based on when we start observing surface-reaching events that rupture the entire seismogenic zone. Surface-reaching ruptures become prevalent when the rigidity ratio falls below 60% of the host rock. Furthermore, earthquakes become more regular and frequent as the fault zone matures. This simulation informs us that the transition from immature to mature fault zone is gradual, and we can see a mixture of surface-reaching and subsurface events during this transition stage.

3.3.2 Effects of Healing: Slow-Slip Events and Irregularity in Recurrence Intervals

Interseismic healing has significant effects on the dynamics of earthquakes and aseismic fault slip, including creep accumulation within the nominally velocity-weakening region, inhibition of surface-reaching events, restriction of earthquake sizes, and generation of slow-slip events also within the velocity-weakening region. Here we discuss the effects of healing in an immature fault zone in more detail and demonstrate how slow-slip events affect seismicity by comparing a simulation with fault zone rigidity ratio ranging between $60\,\%$ and $65\,\%$ against a fault zone with the same initial rigidity ratio but without healing (i.e., a constant rigidity ratio of $60\,\%$). This range of rigidity ratio still lies in the immature fault zone parameter space discussed in the previous section but leads to fewer slow-slip events compared to the $80\,\%$ to $85\,\%$ range. It allows us to analyze the healing effect and slow-slip events more clearly.

In our numerical simulations, slow-slip events are manifested as accelerated slip that fail to reach the seismic threshold velocity but release finite stress on the slip patch along a portion of the fault. The slip rate of slow slip events in our simulations can vary from $1 \times 10^{-8}\,\mathrm{m\,s^{-1}}$ to $1 \times 10^{-4}\,\mathrm{m\,s^{-1}}$ (Fig. 3.3). Besides slow-slip events, the events below the seismic threshold in our simulations also encompass aseismic creep and afterslip (Fig. 3.3b). Aseismic creep is characterized by slip rate that is close to the tectonic plate rate ($\leq 1 \times 10^{-9}\,\mathrm{m\,s^{-1}}$). Afterslip is another category of transient slow-slip that releases stresses from recent earthquakes during the postseismic stage (*Avouac*, 2015; *Bürgmann*, 2018). The slip rate of afterslip is typically below the seismic slip rate of $1\,\mathrm{mm\,s^{-1}}$ and can go down to $1 \times 10^{-5}\,\mathrm{m\,s^{-1}}$. Afterslip can be distinguished from the slow-slip events by when and where they occur, i.e., away from peak-slip regions of earthquakes.

Figs. 3.3a and b show the slip-rate evolution for a fault zone without and with healing during the seismic cycle. The simulation without healing (Fig. 3.3a) shows large surface-reaching ruptures that are periodic in time. This sequence of earthquakes encompasses dynamic events and aseismic creep but does not exhibit any slow-slip events between them. Fig 3.3b shows a wider range of events including multiple slow-slip events in addition to earthquakes and creep. Such slow-slip events can be identified from the peak slip-rate function in these simulations (Figs. 3.2a and b, and Fig. 3.3d) and generally occur during the interseismic stage within the seismogenic zone in our simulations (Figs. 3.3b and d). These slow-slip events are distributed throughout the interseismic period, with no temporal preference before or after an earthquake, though they have a spatial preference in relation to the residual stresses from previous events. Earthquake ruptures and slow-slip events

in our simulations with fault zone healing occur at the edges of previous ruptured region within the velocity-weakening zone (Fig. 3.3b), due to residual stress peaks from those events. The slow-slip events also contribute to the release of stresses during the interseismic period, and in addition, generate stress-peaks within the seismogenic zone, away from its base. This is in contrast to the simulation without healing (Fig. 3.3a), where the stress peaks are predominantly near the base of the seismogenic zone. Other numerical studies (*Barbot*, 2019a; *Idini and Ampuero*, 2020) also showed that slow-slip events can be generated in the velocity-weakening part of the fault using quasi-dynamic continuum models. However, the relative size of seismogenic asperity to nucleation, R_u (*Barbot*, 2019a), for such simulations is much lower than what we use here. Such numerical simulations can exhibit periodic slow-slip events at lower R_u values (< 1) and chaotic slow-slip events at higher R_u values (> 13). Our simulations use an $R_u \sim 5$, which should result in periodic bilateral ruptures, as seen in Fig. 3.3a. Note that the incorporation of healing does not change the R_u values significantly as they lie in the same parameter regime through time. However, interseismic healing helps release the stresses inelastically though time during the quasi-static deformation, which rearranges the stress-peaks and stress shadows along the fault dip, resulting in restriction of earthquake sizes and generation of slow-slip events.

Since the interseismic healing promotes slow-slip events, stresses are released nonuniformly along the fault during this period. This causes partial ruptures to terminate without reaching the free surface. Moreover, these slow-slip events delay the onset of subsequent earthquakes. We see in Figs. 3.3d and f that earthquakes become farther apart in time when there are slow-slip events between them, as compared to consecutive earthquakes occurring without such slow-slip events. This delay, combined with the occurrence of slow-slip events within the velocity-weakening region, gives rise to the irregular recurrence of earthquakes in immature fault zones with healing. We can also infer that the slow-slip events with higher amount of slip release more stresses during the interseismic period, which delays the subsequent earthquake by a larger amount (Fig. 3.3f).

Another notable feature of the simulation with healing is the penetration of aseismic creep into the velocity-weakening part of the fault (Fig. 3.3b). The simulation without healing (Figs. 3.3a and c) shows complete ruptures with regular recurrence intervals, and aseismic creep is constrained to the velocity-strengthening parts of the fault. However, the incorporation of healing during the interseismic period allows the creep to accumulate and build up progressively within the velocity-weakening region (Figs. 3.3b and d). We demonstrate the cumulative rupture and creep extent from all the events in our simulation with healing in relation to the velocity weakening and velocity strengthening regions along the fault on the right side of Fig. 3.3b. We see that the cumulative creep extends through

almost the entire fault, whereas the earthquake rupture extent is predominantly confined to the velocity weakening region. Creeping within the seismogenic zone also causes nonuniform stress release during the interseismic period, similar to the effects of slow-slip events discussed above, albeit to a lesser extent.

This effect of creep buildup within the velocity-weakening region and the abundance of slow-slip events is also observed in our simulation with permanent damage (Fig. 3.4). We observe more slow-slip events during the immature stage of the fault zone which is responsible for irregular recurrence intervals for earthquakes. These slow-slip events become less frequent during the mature stages of the earthquake cycle, and thus there is a more regular sequence of earthquakes. This transition is in accordance with the results from the previous section highlighting the differences between a mature and immature fault damage zone without permanent damage. We show the slip rate range of slow-slip events and fast earthquakes in our simulations, in comparison to those observed on natural faults and in laboratory experiments in Fig. 3.3e. We see that our numerical simulation of a fault zone with healing can produce a wide range of events, both in the fast slipping and slow slipping regime, comparable to those observed along natural faults.

3.4   Discussion and Conclusions

Seismologic and geodetic observations in immature fault zones exhibit complex ruptures and distributed coseismic damage. The damage zones in these faults are wider with poorly defined boundaries, resulting in earthquake sequences exhibiting irregular recurrence and size distributions akin to a Gutenberg-Richter magnitude scaling. Examples of such fault zones include the Ridgecrest sequence where geodetic studies have shown complex, multi-fault, and slow rupture with a heterogeneous static stress change (*Goldberg et al.*, 2020). The study by *DuRoss et al.* (2016) along the immature Wasatch fault zone in Utah suggests partial-segment and multi-segment ruptures with irregular recurrence intervals. Seismic studies after the 2008 earthquake in Peloponnese, Greece have shown negligible surface deformation, i.e., a coseismic slip deficit towards the surface (*Feng et al.*, 2010; *Fielding et al.*, 2009). *Dolan and Haravitch* (2014) compiled multiple fault zone studies to show that the ratio of the surface slip-measurements to the slip at depth is correlated with fault zone maturity, and immature fault zones tend to have lower ratios. These studies imply that immature fault zones lack surface slip during the coseismic phase and exhibit irregular recurrence intervals, which is also corroborated by our models. In contrast, very mature sections of fault zones have been shown to exhibit higher regularity in earthquake recurrence (e.g., Alpine fault in *Berryman et al.*, 2012; *Howarth et al.*, 2021).

Our results unveil how the seismic and aseismic segments in a fault zone interact during the earthquake cycle within an elastic framework. We have shown that the seismogenic zone (velocity-weakening) in our models can have both seismic and aseismic slip episodes, with the latter encompassing slow-slip and creep events. The slow-slip events in our models are distributed within the velocity-weakening segment of the fault and occur throughout the interseismic period. Additionally, we see the aseismic creep penetrating into the velocity-weakening region in our immature fault zone models with healing. Both phenomena contribute to the nonuniform release of stresses during the seismic cycle, with slow-slip events having a dominant effect on the earthquake recurrence. Slow-slip events are very challenging to observe in geologically immature strike-slip faults using seismic or geodetic methods. Certain observations along strike-slip fault zones (e.g., the Northern SAF in *Murray et al.*, 2014) and subduction zones (e.g., Japan subduction zone in *Johnson et al.*, 2016) have shown seismic and aseismic slip episodes occurring in the nominally velocity-weakening region. As subduction zones tend to be old and mature, some local geologic structures like heterogeneous seafloor structure or complex material properties associated with partially coupled subduction zone might be needed to rejuvenate them (*Wang and Bilek*, 2014). Surface creep has been observed on several fault systems including the Maacama and Bartlett Springs (*McFarland et al.*, 2009; *Tong et al.*, 2013), and creep rates in the shallow parts can be locally very high in the order of $1 \times 10^{-6} \, \mathrm{m \, s^{-1}}$ to $1 \times 10^{-9} \, \mathrm{m \, s^{-1}}$ (*Murray et al.*, 2014). This creep is suggested to extend to depths overlapping with some or all of the seismogenic zone in the Northern San Andreas fault system (*Murray et al.*, 2014). *Bruhat and Segall* (2017) have explored models where they discuss that the updip propagation of deep interseismic creep can explain the slip rate profile along the Northern Cascadia subduction zone. These creep episodes may allude to slow-slip events happening in these regions of immature fault zones as well as subduction zones. Such conditions would be expected to extend the time between major earthquakes, and potentially also limit the earthquake size.

To summarize, we performed fully dynamic earthquake cycle simulations in a two-dimensional strike-slip fault surrounded by an elastic damage zone with time-dependent shear modulus evolution that emulates coseismic damage and interseismic healing during seismic and aseismic periods respectively. The models with interseismic healing in immature fault zones can promote aseismic slip episodes including slow-slip events and creep to propagate into the seismogenic zone. Our numerical simulations show that such events in immature fault zones can limit the size of earthquakes and prolong the time between large earthquakes. In these simulations, slow-slip events are abundant and the stress peaks from previous earthquakes and slow-slip events are critical in determining the location of and

timing of subsequent events, thereby creating irregularity in recurrence intervals and partial ruptures. These partial ruptures lead to predominantly sub-surface events in immature fault zones. In contrast, the higher compliance of mature fault zones leads to earthquakes with complete stress drops and rupture extending throughout the seismogenic zone. We demonstrate that such fundamental variations in fault slip behavior can arise due to how the fault zone structure evolves in time, despite using simple elastic damage zone rheology and frictional fault properties. Our results emphasize the importance of monitoring seismic wave velocities and interseismic healing along active faults to help better characterize their first-order mechanical behavior.

3.5 Figures - Chapter 3
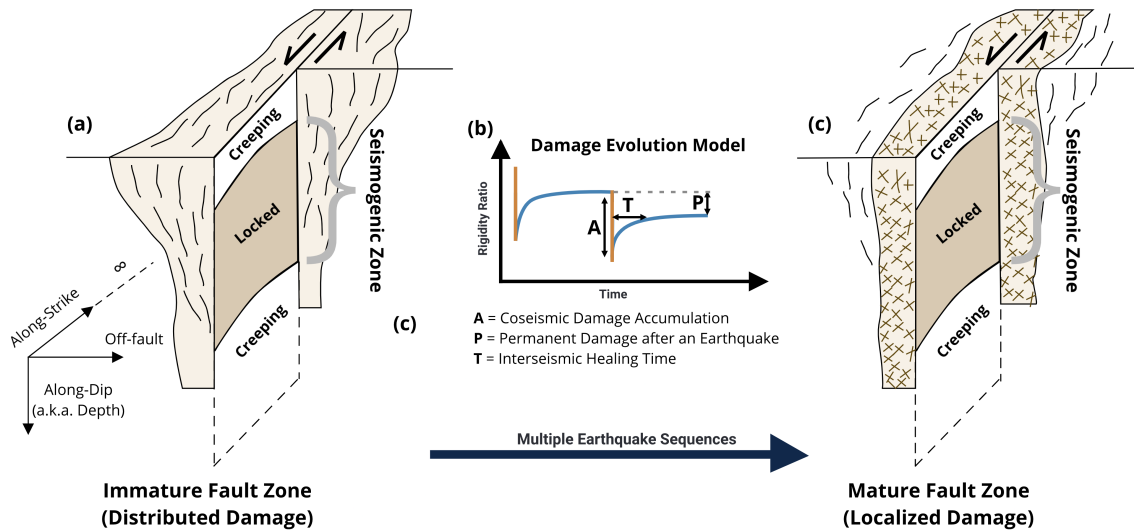
Figure 3.1: A conceptualized evolution of a fault damage zone through multiple earthquake sequences for strike-slip fault systems. (a) Schematic of an immature fault zone with distributed damage increases towards the surface. (b) Parameters considered for an elastic damage evolution model, showing the prescribed change in the rigidity ratio (ratio of shear modulus in damage zone to that in the host rock) through time. (c) Schematic of a mature fault zone with localized damage and a dense fracture network.
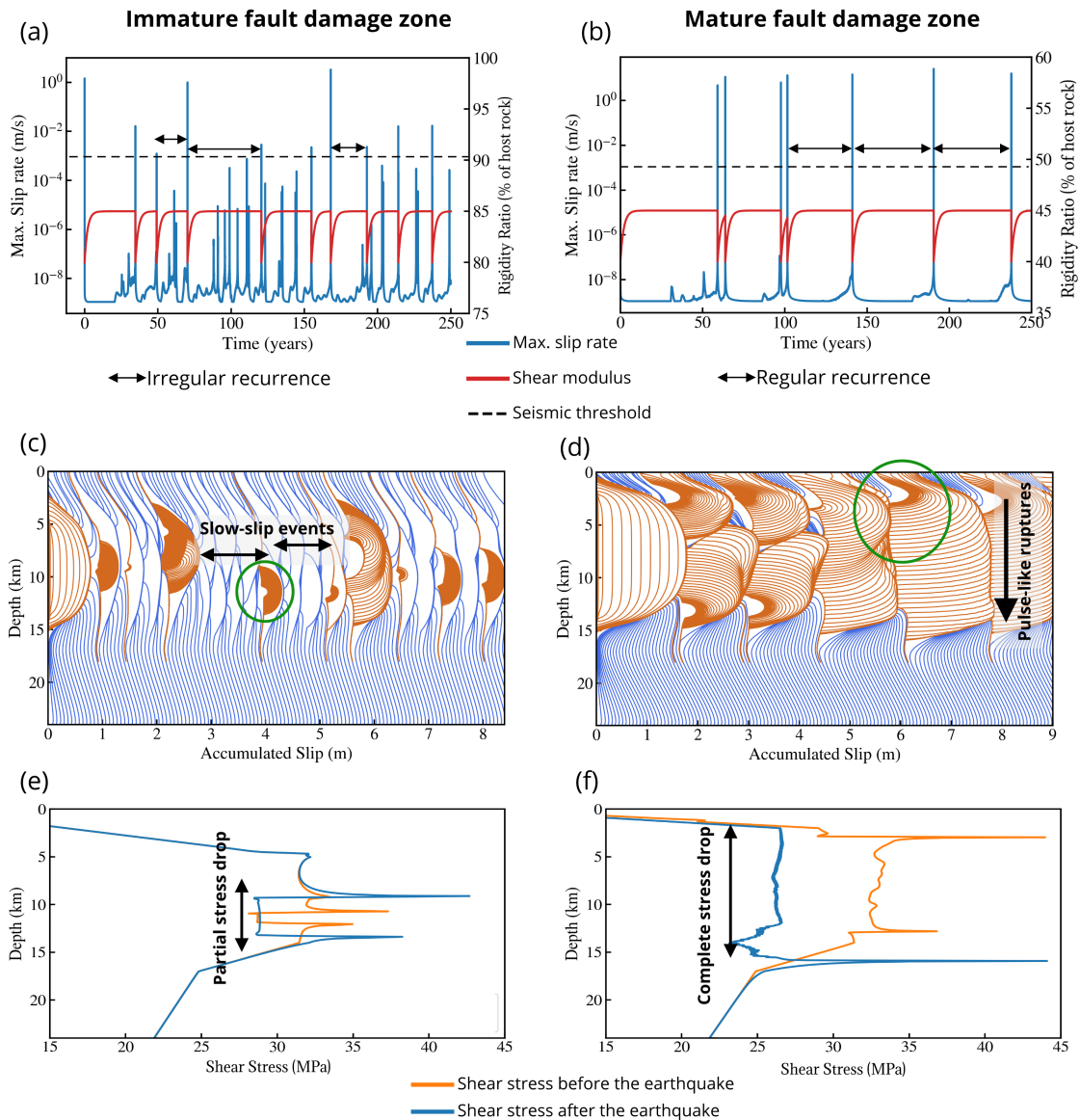
Figure 3.2: Immature vs mature fault damage zone. (a-b) The evolution of slip-rate function (blue) and the rigidity ratio (red) through time. (c-d) Cumulative slip through earthquake sequences shown along depth in mature and immature fault zones. The orange lines are plotted every 0.1 seconds during earthquakes, and the blue lines are plotted every year during interseismic periods. (e-f) The on-fault shear stress before and after a representative earthquake for each case (circled in green in (c) and (d)) demonstrates a partial stress-drop for immature fault zones and a complete stress drop for mature fault zones.

50
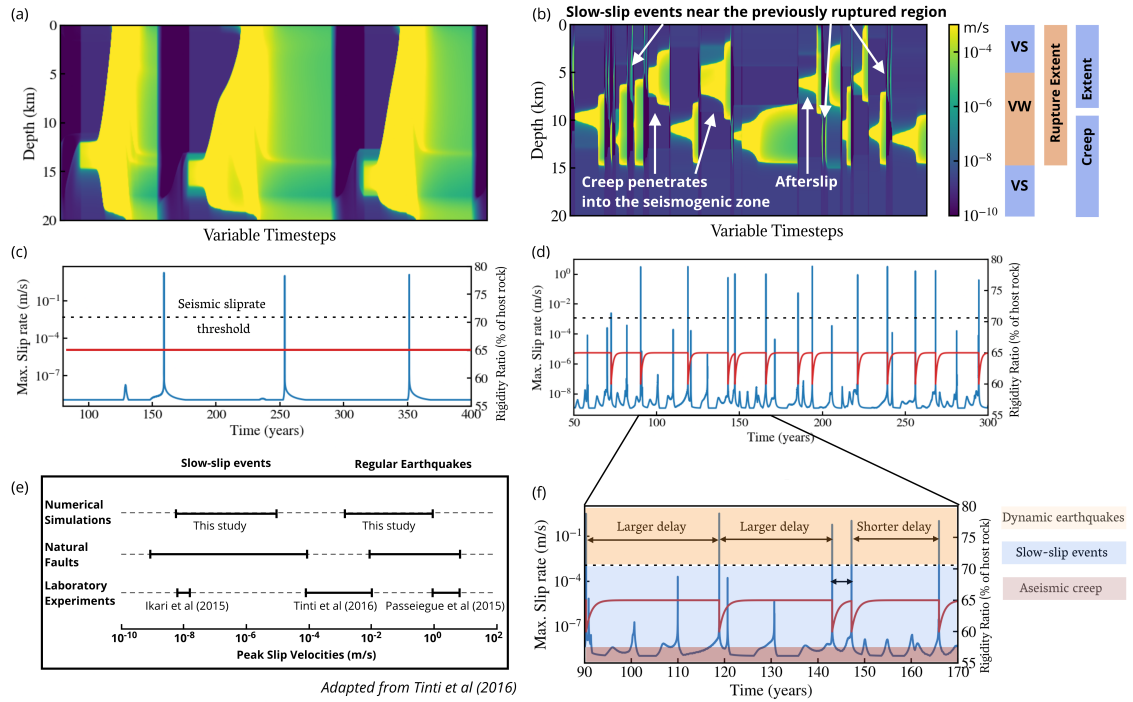
Figure 3.3: (a) The spatiotemporal slip-rate evolution in immature fault zone without healing (see color scale in (b)). (b) The spatiotemporal slip-rate evolution in immature fault zone with healing. The right side shows the depth extent of the frictional parameters delineating the velocity-weakening and the velocity-strengthening region. (c-d) The rigidity ratio and the peak slip-rate function for a segment of the simulation. (e) A compilation of the peak slip-velocity range for slow-slip events from laboratory experiments, natural faults, and our numerical simulations. (f) Zoom in of part (d), showing larger delay in earthquake onset for higher slow slip-rates.
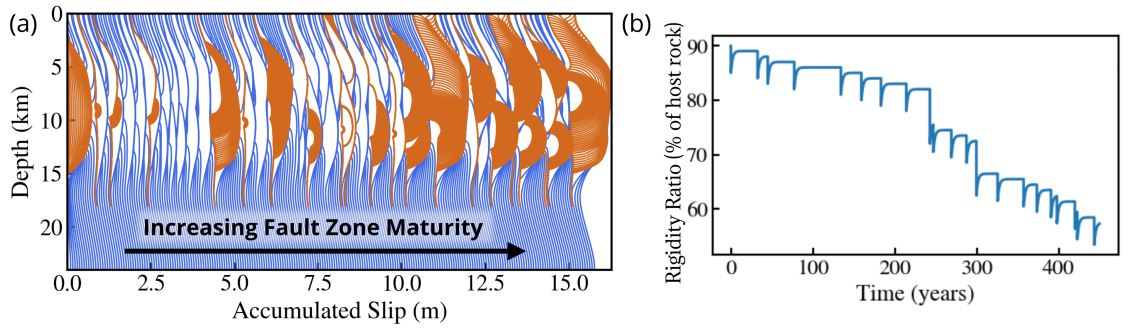
Figure 3.4: Incorporation of permanent damage after each earthquake demonstrates the transition from immature to mature fault zone. (a) The accumulated slip history. (b) Rigidity ratio through time. Here, the transition from immature to mature fault zone occurs within a few hundred years, whereas in nature, the evolution can take millions of years.

Table 3.1: Parameters used in numerical simulations of earthquake cycles. The normal and shear stresses represent the values for the velocity-weakening region.

Parameter	Symbol	Value
Static friction coefficient	μ_0	0.6
Reference velocity	V_0	$1 \times 10^{-6}\,\mathrm{m\,s^{-1}}$
Plate loading rate	V_{pl}	$35\,\mathrm{mm\,yr^{-1}}$
Evolution effect	b	0.019
Effective normal stress	$\bar{\sigma}$	$50\,\mathrm{MPa}$
Initial shear stress	τ_0	$30\,\mathrm{MPa}$
Steady-state velocity dependence in the seismogenic region	$(b-a)$	-0.004
Width of seismogenic zone	W	$10\,\mathrm{km}$
Half-width of damage zone	W	$0.5\,\mathrm{km}$
Average node spacing	dx	$20\,\mathrm{m}$
Seismic slip-rate threshold	V_{th}	$1\,\mathrm{mm\,s^{-1}}$
Characteristic weakening distance	L_c	$8\,\mathrm{mm}$
Shear modulus of host rock	μ	$32\,\mathrm{GPa}$
Shear modulus of damaged rock	μ_D	Variable (see Eq. A1)

Table 3.2: Damage evolution and healing parameters. The parameters in bold represent the simulations presented in the paper. The left column shows the range of rigidity ratio over which the shear modulus drops during earthquake and heals during interseismic period.

Rigidity ratio $\left(\frac{\mu_D}{\mu}\right)$	Healing time (yr)
$40 - 45\%$	**8**, 10, 12, 15
$80 - 85\%$	**8**, 10, 12, 15
$60 - 65\%$	4, **8**, 10, 20
$60 - 70\%$	8
$60 - 80\%$	8

CHAPTER 4

The Effects of Precursory Velocity Changes on Earthquake Nucleation and Stress Evolution in Dynamic Earthquake Cycle Simulations *

Abstract

Seismic velocity changes in earthquake cycles have been observed over a wide range of timescales and may be a good indicator of the onset of future earthquakes. Understanding the effects of precursory velocity changes right before seismic and slow-slip events could potentially elucidate the onset and timing of fault failure. We use numerical models to simulate fully dynamic earthquake cycles in 2D strike-slip fault systems with antiplane geometry, surrounded by a narrow fault-parallel damage zone. By imposing S-wave velocity changes inside fault damage zones, we investigate the effects of these precursors on multiple stages of the seismic cycle, including nucleation, coseismic, postseismic, and interseismic stages. Our modeling results show a wide spectrum of fault slip behaviors including fast earthquakes, slow-slip events, and variable creep. One primary effect of the imposed velocity precursor is the acceleration of an otherwise slow-slip event into a fully dynamic earthquake. Furthermore, the onset time of these precursors has significant effects on the earthquake nucleation phase, and earlier onset of precursors causes the earthquakes to nucleate sooner with a much smaller nucleation size that is not predicted by theoretical equations. Our results highlight the importance of short- and long-term monitoring of fault zone structures for better assessment of regional seismic hazard.

4.1 Introduction

Earthquakes are a complex phenomenon occurring over a wide range of spatial and temporal scales. They are believed to result from a sudden release of accumulated energy manifested either as failure in intact rocks or sudden stick-slip motion on preexisting faults. Predicting the onset and timing of fault failure leading to earthquakes is one of the ultimate goals of seismology. However, our current understanding of earthquake preparation processes, including the nucleation phase that leads to the start of earthquake rupture acceleration, is still limited. One direction towards understanding this process is searching for precursory signals preceding large earthquakes, but the effect of precursory signals on the subsequent earthquake and long-term seismic cycles is yet to be explored.

The commonly observed preseismic signals include the reduction in b-values prior to large earthquakes and slow-slip events leading up to large earthquakes, e.g., the 2011 Mw 9.0 Tohoku-Oki earthquake (*Kato et al.*, 2012; *Nanjo et al.*, 2012; *Ito et al.*, 2015), and the 2014 Mw 8.1 Iquique, Chile earthquake (*Kato and Nakagawa*, 2014). Additionally, changes in seismic wave velocity have been observed along natural faults prior to earthquakes (*Whitcomb et al.*, 1973; *Niu et al.*, 2008). *Whitcomb et al.* (1973) found that both the P- and S-wave velocities significantly decreased about 3.5 years before the 1971 San Fernando earthquake followed by a slower recovery period. They also inferred that this velocity change could be proportional to the size of the effective fault dimension. *Niu et al.* (2008) inferred precursory velocity changes approximately 10 and 2 hours prior to two earthquakes using the travel time data from active source experiments in the SAFOD drill site. Similar precursory signals are seen in surface expression of fault slip, like premonitory slow-slip events before landslides (*Poli*, 2017) or seismic velocity decrease prior to volcanic eruption (*Olivier et al.*, 2019). *Scuderi et al.* (2016) have studied such robust precursory signals in laboratory fault experiments and found systematic reduction in seismic wave velocities during both slow and fast earthquakes, which are believed to start via the same nucleation process (*Kato et al.*, 2012; *Bouchon et al.*, 2013; *Hulbert et al.*, 2019). The mechanisms for these precursory seismic velocity changes are primarily attributed to the accelerating fault deformation, fluid effects, and opening and closure of microcracks due to stress changes (*Scuderi et al.*, 2016; *Poli*, 2017; *Stanchits et al.*, 2003; *Rivet et al.*, 2016). The above discussion begs the questions: is precursory velocity change a robust indicator of the size, onset, or duration of an earthquake? How does the onset duration of such velocity precursors affect the earthquake nucleation and rupture process?

Faults are also geometrically complex, and the surrounding network of fractures with nested hierarchy of localized deformation is referred to as a fault damage zone (*Lewis and*

Ben-Zion, 2010; *Yang et al.*, 2011; *Niu et al.*, 2008). Numerical models of earthquakes in fault damage zones approximated as elastic low-velocity layers suggested that they can influence dynamic rupture styles (*Huang and Ampuero*, 2011; *Huang et al.*, 2014b) as well as long-term seismic cycle behaviors (*Abdelmeguid et al.*, 2019; *Thakur et al.*, 2020; *Nie and Barbot*, 2021). Additionally, these fault damage zones may change in strength throughout the earthquake cycle due to coseismic damage accumulation and interseismic healing (*Thakur and Huang*, 2021, and references therein), which give rise to variability in earthquake size, location, and interevent times in immature and mature fault zones. The long-term behavior of fault slip is also governed by other factors including the variation of initial stress at different scales (*Andrews and Ma*, 2016), and the earthquake nucleation size and duration (*Lapusta and Rice*, 2003a; *Cattania*, 2019). Dynamic rupture models with heterogeneous power-law stress distribution have partially explained the observed scaling of stress drop, moment, and radiated motion (*Ripperger et al.*, 2007; *Andrews and Barall*, 2011; *Dalguer and Mai*, 2011). Models simulating the whole earthquake cycle (*Tal and Hager*, 2018; *Tal et al.*, 2018; *Ozawa et al.*, 2019) also utilize the spatial roughness of faults to induce stress heterogeneities. Therefore, it is evident that both stress and material heterogeneities play important roles in the generation mechanisms of earthquakes in natural fault zones.

Here we investigate the effects of precursors on multiple stages of the seismic cycle, including nucleation, coseismic, postseismic, and interseismic stages, by imposing S-wave velocity changes in fault damage zones. Since a natural fault rarely has uniform background stresses, we also show the effects of such precursory velocity changes in earthquake cycles on a fault with a self-similar distribution of initial normal stress with depth, which may manifest due to apriori stress heterogeneities, local geologic structures, or stress transfer from surrounding faults. Our results show that the onset of precursory S-wave velocity drop causes an earlier nucleation of earthquakes, therefore causing a reduction in recurrence intervals over the seismic cycle. Moreover, precursory velocity changes also promote the acceleration of slow-slip events to dynamic earthquakes, and promote the growth of some intermediate magnitude earthquakes, which do not break through the entire fault asperity, into full ruptures spanning the entire fault width. We also discuss how the heterogeneities in fault shear stress are manifested after multiple earthquakes due to fault damage zones, precursors, and initial self-similar normal stress. Our results highlight the importance of short- and long-term monitoring of fault zone structures for better assessment of regional seismic hazard.

4.2 Methods

We use physics-based numerical models to simulate fully dynamic earthquake cycles in a two-dimensional, vertical strike-slip fault with antiplane geometry. We model all the stages of earthquake cycles including nucleation, dynamic rupture, and post-seismic and interseismic stages using a 2D spectral element method (*Kaneko et al.*, 2011, and references therein). For simplicity, we use a narrow fault-parallel layer as a proxy for the damage zone and its geometry remains constant throughout the simulated sequence (Figs. 4.1a and b). The material is purely elastic with the fault-parallel damage zone having a lower shear modulus compared to the surrounding host rock. On an antiplane fault, the initial conditions of stresses and friction are depth-dependent, and the models do not have any along-strike variable properties. Full inertial effects with explicit time-stepping are considered during dynamic ruptures, and a quasi-static algorithm with implicit adaptive time-stepping is used during the interseismic period (*Lapusta et al.*, 2000). Earthquakes are recorded in our simulation when the on-fault slip velocity exceeds $1\,\mathrm{mm\,s^{-1}}$.

4.2.1 Model Setup

Our model domain extends to $48\,\mathrm{km}$ in depth and $30\,\mathrm{km}$ in width (Fig. 4.1b). Since this setup is symmetric across the fault, we only consider one half of the domain to save computational cost. The top boundary represents the earth's free-surface and is therefore imposed to be stress-free. The fault zone boundary is divided into two parts: the top $24\,\mathrm{km}$ of the boundary is the active fault governed by rate- and state-dependent friction laws, and the bottom $24\,\mathrm{km}$ loads the fault with a constant velocity of $35\,\mathrm{mm\,yr^{-1}}$. The other boundaries are absorbing boundaries that allow seismic waves to pass through. The seismogenic zone, a segment of the fault that accumulates stress during the interseismic period to eventually host earthquakes, extends from $2\,\mathrm{km}$ to $17\,\mathrm{km}$ along the fault as in typical strike-slip fault systems. The rest of the fault creeps aseismically. Mature fault damage zones in our simulations are approximated as elastic layers parallel to the fault with lower shear moduli than the surrounding host rock. The damage zone is $1\,\mathrm{km}$ wide and extends throughout the domain of the simulation. The host rock has a density of $2670\,\mathrm{kg/m^3}$ and an S-wave velocity of $3464\,\mathrm{m\,s^{-1}}$. The damage zone has a density of $2670\,\mathrm{kg/m^3}$ and an S-wave velocity of $2425\,\mathrm{m\,s^{-1}}$, implying a $30\,\%$ velocity reduction, similar to what is observed in nature for mature strike-slip fault zones (*Huang et al.*, 2014b; *Perrin et al.*, 2016; *Thakur et al.*, 2020).

4.2.2 Friction Laws

The laboratory-derived rate- and state-dependent friction laws determine how fast the fault is slipping in relation to the shear strength (*Dieterich*, 1979; *Ruina*, 1983; *Blanpied et al.*, 1991). We use a regularized version of the classic rate- and state- dependent friction, wherein the regularization is interpreted as a thermally activated creep model that relates the shear strength (T) to the slip rate ($\dot{\delta}$) as follows:

$$T = a\bar{\sigma}\operatorname{arcsinh}\left[\frac{\dot{\delta}}{2\dot{\delta}_o}e^{\frac{f_o + b\ln(\dot{\delta}\theta/L)}{a}}\right] \qquad (4.1)$$

where $\bar{\sigma}$ is the effective normal stress (the difference between lithostatic stress and the pore fluid pressure), f_0 is a reference friction coefficient corresponding to a reference slip-rate $\dot{\delta}_o$, and a and b are empirical constants that depend on the mechanical and thermal properties of the interface in contact. The parameter θ is a state variable interpreted as the average lifetime of the surface in contact and L_c is the characteristic length scale over which the contact surface slips. The evolution of the state variable is governed by the aging law (*Ruina*, 1983):

$$\frac{d\theta}{dt} = 1 - \frac{\dot{\delta}\theta}{L} \qquad (4.2)$$

The frictional stability on the fault is determined by the parameter ($a - b$). Fig. 4.1c shows the depth profile for the friction parameter (a-b). The seismogenic zone ($2\,\mathrm{km}$ to $17\,\mathrm{km}$) is prescribed to be velocity weakening at steady state, which means it has potential to develop unstable slip. The rest of the fault is prescribed to be velocity strengthening at steady state, implying a stable sliding behavior. This profile is similar to what is expected at equivalent depths from laboratory and numerical experiments (*Blanpied et al.*, 1991; *Lapusta et al.*, 2000). Earthquake dynamics are determined by the parameters a/b and L_c. A lower value of L_c relative to the size of the velocity-weakening asperity results in more chaotic rupture styles (*Cattania*, 2019; *Barbot*, 2019a), whereas a/b controls the relative importance of strengthening and weakening effects and the ratio of static to dynamic stress drops (*Barbot*, 2019a).

The nucleation length and the cohesive zone size can have important effects on the spatiotemporal patterns of fault slip behavior and need to be well resolved (*Rubin and Ampuero*, 2005; *Erickson et al.*, 2020). We set $L_c = 2\,\mathrm{mm}$ in our first set of results (Sections 4.3.1-4.3.3) which implies an approximate nucleation size of 500 m within the damage zone. We use an average spatial resolution of 33 m, which ensures that we have more than 15 elements within the nucleating region and that the simulations are well resolved (*Thakur*

et al., 2020). Additionally, we show another set of results in Section 4.3.4 with $L_c = 8\,\mathrm{mm}$ in order to understand the effects of precursory velocity changes in earthquake cycles with full, periodic ruptures.

4.2.3   Precursory Velocity Change Setup

We model the velocity precursor as changes in the S-wave velocity of the fault damage zone surrounding a strike-slip fault. While the laboratory experiments have documented a change in the P-wave velocity (*Scuderi et al.*, 2016), natural faults often show equivalent changes in P- and S-wave velocities in the absence of fluid effects (*Thurber et al.*, 2003b). Our models are two-dimensional and under antiplane strain approximation. Therefore the models only have SH waves and we assume that similar changes in material properties during the nucleation phase would lead to SH wave velocity reduction as well. Since fully dynamic earthquake cycle models do not provide any constraint on the earthquake location and timing except the initial stress and friction values, we use the maximum slip velocity on the fault as a threshold for prescribing the precursory velocity drop (Fig. 4.2). Once the on-fault slip-rate exceeds the threshold, the S-wave velocity drops instantaneously by $0.5\,\%$. This velocity change is about a half of the observed P-wave velocity drop in fast stick-slip experiments (*Scuderi et al.*, 2016). It is imperative to note that this drop happens only within the fault damage zone, where the S-wave velocity is already $30\,\%$ lower than the surrounding host rock. Once the earthquake has completely ruptured and the on-fault acceleration reaches 0, the fault zone S-wave velocity is set up to increase back to its original value logarithmically with time. This healing happens over 21 days in our models, which is chosen to be short enough so that it does not affect subsequent earthquakes in the sequence (Fig. 4.2a). The evolution of the shear modulus in the fault damage zone with respect to the host rock (μ_D/μ) is given as follows:

$$
\frac{\mu_D}{\mu} = \begin{cases} A_0, & \text{if } V_{max} \geq V_{threshold} \\ (1 - \exp(-r(t - t_{\text{start}}))), & \text{if } \frac{\mu_D}{\mu} < A_0 \end{cases}
\tag{4.3}
$$

where A_0 is the specified amplitude of the precursory velocity drop, r is the healing rate, and $t - t_{\text{start}}$ is the timestep relative to the previous earthquake. Healing starts after the current earthquake is over, while t_{start} refers to the start time of that earthquake.

The evolution of on-fault peak slip-rate with time shows the precursor onset duration (Fig. 4.2b), and we can see that there is a sharp log-linear acceleration of fault slip-rate due to the incorporation of this precursory velocity drop. We note that the actual duration of precursor prior to an earthquake does not have a strict relation with the slip-rate thresh-

old we use, and we need to calculate the actual duration after running the simulations. In theory, a lower slip-rate threshold leads to a longer precursor duration. The measured precursor durations suggest that they follow a nonlinear decreasing relationship with increasing precursor slip-rate threshold for $L_c = 2\,\mathrm{mm}$ and $L_c = 8\,\mathrm{mm}$ (Fig. 4.2c), but more data points are needed to establish a quantitative relationship.

We also observe a significant reduction in earthquake nucleation size in the presence of precursory velocity reductions. The theoretical equation for nucleation size in a layered medium (*Kaneko et al.*, 2011) predicts that it should depend only on the shear modulus of the near-fault material given that other parameters are constant. This theoretical relationship overestimates the nucleation size observed in our models with precursors. We measure the nucleation size using the patch of the fault having higher slip-rate than the threshold velocity of $1\,\mathrm{mm\,s^{-1}}$ at the start of the earthquakes. Fig. 4.2d shows that the nucleation size can be reduced by more than a half with increasing precursor duration for a constant 0.5% precursory velocity drop. This is seen across both $L_c = 2\,\mathrm{mm}$ and $L_c = 8\,\mathrm{mm}$ simulations. Additionally, since the slip-rate threshold used for setting up the precursor onset duration cannot be lower than the background creep rate of $1 \times 10^{-9}\,\mathrm{m\,s^{-1}}$, the decrease in nucleation size will plateau as the precursor onset duration increases. Our results suggest that the nucleation size is also a function of precursory onset time, with a longer precursor duration leading to a smaller nucleation size.

4.3 Results

4.3.1 Reference Model: Fully Dynamic Earthquake Cycles with a Fault Damage Zone

Our reference model consists of a fault-parallel damage zone extending throughout the depth of the domain, and a characteristic slip distance of $L_c = 2\,\mathrm{mm}$. This reference model does not have any precursory velocity drop. However, the presence of damage zone, along with the small nucleation size, gives rise to complexities in the earthquake sequence such as variability in earthquake magnitudes and hypocenter locations as well as the presence of slow-slip events. These complexities result from a combination of stress heterogeneities generated by fault zone reflected waves during dynamic rupture (*Thakur et al.*, 2020) as well as multi-sized earthquake ruptures due to the relatively small nucleation size compared to the fault asperity size (*Cattania*, 2019; *Barbot*, 2019a). The cumulative slip contours show that dynamic wave reflections affect seismic slip in large and small earthquakes (Fig. 4.3a). The spatiotemporal slip-rate of a representative earthquake (marked in yellow

star) shown in Fig. 4.3b highlights multiple dynamic wave reflections, where parts of the fault have sub-seismic slip-rate ($< 1\,\mathrm{mm\,s^{-1}}$) while other parts have seismic slip-rate. The rupture also propagates as slip pulses at any given depth. Additionally, our reference model has abundant slow-slip events between large earthquakes, as shown by the peak slip-rate along the fault in Fig. 4.3c. In Fig. 4.3d, the shear stress before the earthquake highlights the overstressed nucleating region near $14\,\mathrm{km}$ depth, while the shear stress after the earthquake is very heterogeneous in space, primarily because of dynamic wave reflections.

4.3.2   Effects of Precursory Velocity Changes on Earthquake Cycles

We present four models with different precursory durations for $L_c = 2\,\mathrm{mm}$. Comparing the cumulative slip for the simulations with precursors (Fig. 4.4a-d) to the reference simulation (Fig. 4.3a, cumulative slip between $5\,\mathrm{m}$ to $8\,\mathrm{m}$), we can see that the precursory simulations host a greater number of surface-reaching earthquakes for an equivalent amount of accumulated slip. Note that for $L_c = 2\,\mathrm{mm}$ the nucleation size decreases with increasing precursor duration and reaches 0.5 times the theoretical estimate for the 30-day precursor (Fig. 4.2d). Therefore, an earlier onset of precursory velocity drop results in an earlier onset of earthquakes as demonstrated by the peak slip-rate in these simulations (Fig. 4.4e). The reference model and the 1-hour precursor model only have one earthquake between 25-70 years. As the precursor duration becomes longer, the earthquake recurrence time also decreases and we have additional slow events for the 2-day and 20-day precursors and an additional earthquake for the 30-day precursor.

We further examine the magnitude-frequency distribution and the depth distribution of earthquake hypocenters (Fig. 4.5). The earthquake magnitude is calculated by integrating fault slip over the rupture length given the fault zone shear modulus, and the rupture width is assumed to be the same as the rupture length in our 2D approximation. The cumulative magnitude-frequency distribution shows a sharp decrease in the number of earthquakes beyond magnitude 6 as well as a log-linear trend for smaller earthquakes for all the simulations. However, the reference simulation has several intermediate magnitude earthquakes (Mw 4-6), whose number decreases log-linearly with increasing magnitude but has a different slope than the smaller earthquakes. These intermediate magnitude earthquakes disappear in our simulations with precursors, which predominantly exhibit larger surface-reaching events and very small earthquakes. As the precursory velocity drop occurs, the slip-rate accelerates at a faster rate compared to the reference simulation, which causes the nucleation phase to accelerate and promotes earthquake rupture to break through the free surface. Additionally, the simulation with 30-day precursor has more intermediate

magnitude earthquakes compared to the other precursor durations, but still fewer than the reference simulation (Fig. 4.5a).

Similarly, we see that the hypocenter locations of earthquakes in 20-day and 30-day precursor simulations look more similar to those in the reference simulation, whereas the 1-hour and 2-day precursors give rise to a different distribution of earthquake hypocenters along depth (Fig. 4.5b). Moreover, the 2-day precursor simulation shows that most of the earthquakes nucleate at a very shallow depth. Since the shallow earthquakes in this simulation are also large events that occur more infrequently than smaller events, the total number of earthquakes in this case is lower than in the other cases when larger earthquakes nucleate at the base of the seismogenic zone (Fig. 4.5a).

To understand the nucleation phase of these events with precursory velocity drop, we compare the spatiotemporal slip-rate history in our 20-day precursor simulation with our reference simulation. A comparison between Fig. 4.6a and Fig. 4.6b shows that there are fewer slow-slip events in the presence of velocity precursors. In other words, there is a lower number of earthquakes but a higher number of slow-slip events when there are no precursors. By zooming in to the nucleation phase, we find the incorporation of precursory velocity drop results in a much shorter nucleation phase (Fig. 4.6c-d). Without precursors (Fig. 4.6c), the fault accelerates for 21 hours with peak fault slip-rate oscillating within the slow-slip regime ($< 1 \times 10^{-4} \, \mathrm{m \, s^{-1}}$) before growing into an earthquake. In contrast, precursory velocity drop (Fig. 4.6d) shortens the duration of the nucleation phase to 3 hours before the seismic event, and the peak slip-rate oscillations are also fewer and restricted to less than 1 hour before the event, implying that it is easier for larger earthquakes to nucleate. Again we observe that certain events that would have been slow-slip events in our reference simulation (Fig. 4.6a) grow into dynamic earthquakes in the presence of precursory velocity drop (Fig. 4.6b).

4.3.3   Heterogeneous Stress with and without Precursors

Natural faults manifest complexity in a variety of ways including fault roughness, stress transfer from nearby faults, and background stress heterogeneity (*Smith and Heaton*, 2011). Fault segments with relatively high shear stresses serve as asperities that facilitate rupture nucleation and propagation, whereas those with relatively low shear stresses provide barriers that tend to stop rupture. Modulated by fault friction, geometry, and fault zone material properties, fault stress state also evolves with cycles of earthquakes and long-term interseismic slip. To investigate whether the effects of precursory velocity changes are persistent along faults with prior stress heterogeneities, we simulate earthquake cycles with a

self-similar normal stress distribution along depth, hereafter referred to as heterogeneous normal stress, in addition to velocity precursor and a fault damage zone. We use one-dimensional stochastic, fractal like model to simulate heterogeneous stress, as described in *Smith and Heaton* (2011).

The incorporation of self-similar normal stress influences the earthquake nucleation size (*Rubin and Ampuero*, 2005; *Kaneko et al.*, 2011), thereby making the nucleation variable with depth. We see that the simulation with heterogeneous normal stress shows a rough slip profile for the aseismic part as well, in contrast to the reference model that only shows a rough coseismic slip profile (Fig. 4.7a). The heterogeneous normal stress model also delays earthquake nucleation as compared to the reference model (Fig. 4.7c). However, with the incorporation of precursory velocity drop 20 days prior to earthquake, the earthquakes nucleate much earlier even when the initial normal stress is heterogeneous, similar to what is seen in Fig. 4.4. Figs. 4.7b and d show the magnitude-frequency distribution and the depth distribution of earthquake hypocenters for our simulations with heterogeneous normal stress. While we see a greater number of earthquakes nucleating near the base of the seismogenic zone than our reference model (Fig. 4.4), the overall distribution looks similar between models with and without precursory velocity changes. This implies that though the precursory velocity changes can strongly affect the onset of earthquake nucleation, it has a weaker effect on the earthquake size and depth distribution than the fault damage zone structure as well as heterogeneous normal stress and frictional parameters.

We further compare the shear stresses before and after one representative earthquake for simulations with and without precursory velocity drop and initial heterogeneous normal stress (Fig. 4.8). Our reference simulation with the fault damage zone exhibits heterogeneous shear stress after the earthquake within the seismogenic zone ($2\,\mathrm{km}$ to $17\,\mathrm{km}$ in Fig. 4.8a), while the shear stress before the earthquake does not have heterogeneities except for some stress peaks near the nucleation region and the frictional transition boundary. This is because the stress heterogeneities are caused by dynamic wave reflections and only in the region of rupture propagation. Moreover, the location and number of such stress peaks in the reference simulation are affected by the stress heterogeneities of previous earthquake, but they are not heterogeneous at every point along the fault. With the incorporation of precursory velocity drop (Fig. 4.8b), we see that the shear stress before the earthquake is more heterogeneous within the seismogenic zone. With additional initial heterogeneous normal stress, the creeping regions of the fault exhibit more heterogeneities in the shear stress as well which are amplified in the presence of velocity precursors (Figs. 4.8c and d).

4.3.4 Precursory Velocity Change with a Larger Nucleation Size ($L_c = 8\,\mathrm{mm}$)

In this section, we carry out more simulations using $L_c = 8\,\mathrm{mm}$ while keeping other parameters the same as the above sections. The larger L_c results in a proportionately larger nucleation size and therefore periodic, full ruptures are exclusively observed in these simulations. Fig. 4.9a shows the cumulative slip for four simulations with different precursor durations. Note that the simulation with a precursory velocity drop 1 second before the earthquake shows a very slow rupture propagation during the start of rupture, demonstrated by very dense cumulative slip contours during the seismic event. We see a clear reduction in nucleation size as the precursor duration increases (Fig. 4.9a) and thus earlier earthquake rupture onsets (Figs. 4.9b and c). The incorporation of precursory velocity changes also results in a log-linear acceleration of slip-rate as discussed previously (Fig. 4.9c). The nucleation size for $L_c = 8\,\mathrm{mm}$ can drop by more than half of the theoretical nucleation size (Fig. 4.2d), which suggests that the nucleation size reduction is relatively larger for larger L_c for an equivalent precursory velocity onset. As the material and frictional properties are the same across these simulations with $L_c = 8\,\mathrm{mm}$, the reduction in nucleation size is caused solely due to the onset of precursory velocity drop. However, the reduction in nucleation size does not cause additional earthquake complexities such as small earthquakes and variable hypocenter locations. Across all these simulations, the resulting earthquake magnitude remains unchanged for these large, periodic events. Since our models are two-dimensional, the earthquake magnitude predominantly depends on the rupture length along the dip direction. Our results show that precursory velocity drop does not contribute to any change in rupture length for large periodic events, though earthquake magnitudes along natural faults may also be affected by the rupture width along the strike direction.

4.4 Discussion and Conclusions

Earthquake recurrence predictability has been a long standing question in seismology. Two time-dependent seismicity models for the recurrence of earthquakes, including the time-predictable and slip-predictable models, have been proposed by *Shimazaki and Nakata* (1980). In these models, the earthquake recurrence, or the time interval between two large earthquakes is proportional to the slip amount of the preceding earthquake (time-predictable) or the slip amount of the next large earthquake (slip-predictable). These models are based on the Reid's elastic rebound theory, i.e., the earthquakes are a sudden elastic rebound of the gradually accumulated stresses in the earth's crust. A schematic of cumula-

tive displacement with time is shown for these two models in Fig. 4.10a.

To compare our results with the classic time-predictable and slip-predictable models, we show the cumulative slip against time for our representative models, including the reference model, a model with 20-day precursor, a model with self-similar normal stress (heterogeneous stress), and a model with both precursors and heterogeneous stress in Fig. 4.10b-e. Since the recurrence models are based on coseismic slip of large earthquakes (*Shimazaki and Nakata*, 1980; *Rubinstein et al.*, 2012) while our numerical models capture all the events, we consider our models to exhibit a time-predictable behavior if the cumulative coseismic slip is larger than the accumulated creep, and to be slip-predictable if the cumulative coseismic slip is smaller than the accumulated creep. We see that our models show a complex sequence of earthquakes with a mixture of time-predictable and slip-predictable behaviors. Furthermore, there are some significant differences between the surface slip and the average slip in terms of earthquake predictability and recurrence, primarily for the reference simulation (Fig. 4.10b). As discussed earlier, this model has more sub-surface intermediate magnitude earthquakes, and therefore the surface slip may not be representative of the slip at depth for these earthquakes. The surface slip of our reference model begins with a time-predictable behavior but later transitions to a slip-predictable behavior. However, the average slip along depth shows a mixed behavior between 300 and 500 years before transitioning to a slip-predictable behavior. The model with precursors (Fig. 4.10c) shows a similar behavior for the surface and average slip, where the first 220 years of earthquakes exhibit a time-predictable behavior and they transition to a mixed behavior later in the sequence, with a short slip-predictable stage between 400 and 500 years. Our simulations with heterogeneous normal stress, with and without precursors (Fig. 4.10d, e), show predominantly a time-predictable behavior with a mixed behavior later in the earthquake cycle. Note that there may be some effects of the initial spin-up in our simulations that are not considered when looking at these recurrence models.

The magnitude-frequency distribution of earthquakes usually follow a power-law relationship, best described by the Gutenberg-Richter (G-R) distribution. Most observations of global and regional seismicity agree with the G-R distribution (*Page and Felzer*, 2015; *Rundle*, 1989). However, certain observations of magnitude-frequency distributions along more planar faults (e.g., the San Andreas Fault) have shown a "characteristic earthquake" distribution, wherein the largest earthquake of a characteristic size recurs with an approximately regular interval. The period between two such characteristic earthquakes is generally quiescent except for low-level seismic activity (*Schwartz and Coppersmith*, 1984; *Wesnousky*, 1994). While our reference simulation shows a more log-linear decrease of earthquake size, the simulations with precursory velocity changes are more akin to a characteristic dis-

tribution with a dearth of intermediate magnitude earthquakes (Fig. 4.5a, 4.7d). Despite the similarities, the slope of the distribution is different from what is observed in nature, primarily due to our choice of friction parameters and the two-dimensional model approximations.

In this study, we have focused on imposing precursors and self-similar stresses under an elastic approximation to study their effects on earthquake cycles. However, we have not considered the physical mechanisms that may be responsible for such material properties and stress changes through the earthquake cycle, e.g., incorporating plasticity (*Erickson and Dunham*, 2014) or continuum damage rheology (*Lyakhovsky et al.*, 1997; *Thomas and Bhat*, 2018) within the fault damage zone. Incorporation of inelastic behavior in the fault zone promotes the accumulation of permanent deformation throughout the fault zone evolution. Such deformation may lead to a complex feedback between the evolving fault zone medium and seismic events, generating unique off-fault rupture patterns (*Thomas and Bhat*, 2018) and self-consistent healing and damage accumulation (*Lyakhovsky et al.*, 1997). *Mia et al.* (2022) have shown that the off-fault plastic accumulation may lead to partial ruptures and clustering of seismic events in time. In our simulations, these mechanisms will likely affect the slow-slip generation during the aseismic phase and modulate the shear stress evolution throughout the seismic cycle. Additionally, due to the huge computational costs, we have not explored the detailed parameter space for the choice of damage zone geometry as well as precursory velocity onset and amplitude, which are likely to reveal additional fault zone physics in relation to the velocity precursors. Despite these approximations in our study, our simulations with prescribed precursory velocity drop before the earthquake highlights the importance of monitoring such velocity changes in natural faults, which can potentially aid in seismic hazard assessment.

We present two-dimensional, fully dynamic earthquake cycle simulations with an elastic fault damage zone and analyze the effects of precursory velocity changes with variable onset durations. We further investigate the effects of additional apriori stress heterogeneities with and without such precursory velocity changes. Our models demonstrate that the earthquake nucleation size reduces by more than half due to a precursory velocity change of 0.5%, depending on how early this change occurs prior to the earthquake. Furthermore, compared to a reference scenario without precursory velocity drop, the earthquakes nucleate earlier in the seismic cycle, with earlier precursor onset resulting in earlier earthquake onset. Despite this significant reduction in the earthquake nucleation phase, we find that the magnitude of earthquakes are comparable across different models for our simulations with $L_c = 8\,\mathrm{mm}$, whereas they can be highly variable for simulations with $L_c = 2\,\mathrm{mm}$, suggesting that the complexities in earthquake sequences might depend on

the characteristic slip distance L_c and not solely on the nucleation size. Our models also highlight the relative effects of heterogeneous stress evolution in the presence of fault damage zones and precursory velocity reductions. Fault stress heterogeneities generated by rupture in fault damage zones can affect the rupture nucleation and propagation of future earthquakes. However, the incorporation of preexisting self-similar stresses promotes the heterogeneous distribution of stresses during both rupture propagation and the aseismic creep. For homogeneous initial stress conditions, precursory velocity changes affect the earthquake statistics like the magnitude-frequency distribution and the hypocenter location, while for a heterogeneous initial stress condition, the earthquake statistics are not affected significantly. Our dynamic earthquake cycle models explore a range of complexities due to precursory velocity drop and heterogeneous normal stresses, suggesting that more detailed and frequent observations in nature can help us better estimate the size and timing of future earthquakes.

4.5 Figures - Chapter 4
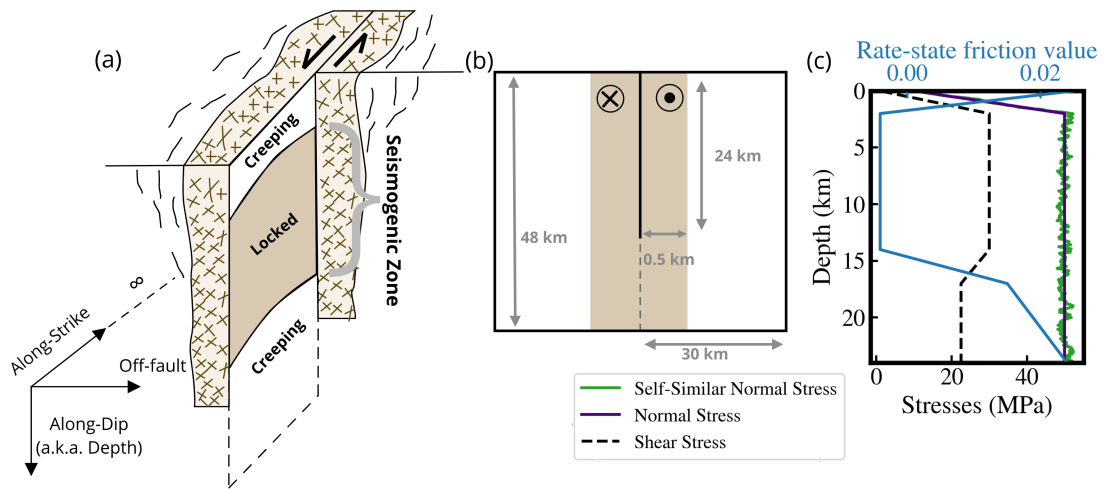
Figure 4.1: Model description and setup. (a) A schematic fault damage zone along a strike-slip fault. (b) The model geometry for our numerical simulation. It represents a vertical cross-section across the fault zone schematic in Fig. 1a, with a fixed fault damage zone width. The model is infinite along strike. (c) The initial stresses and friction parameters along the fault depth.
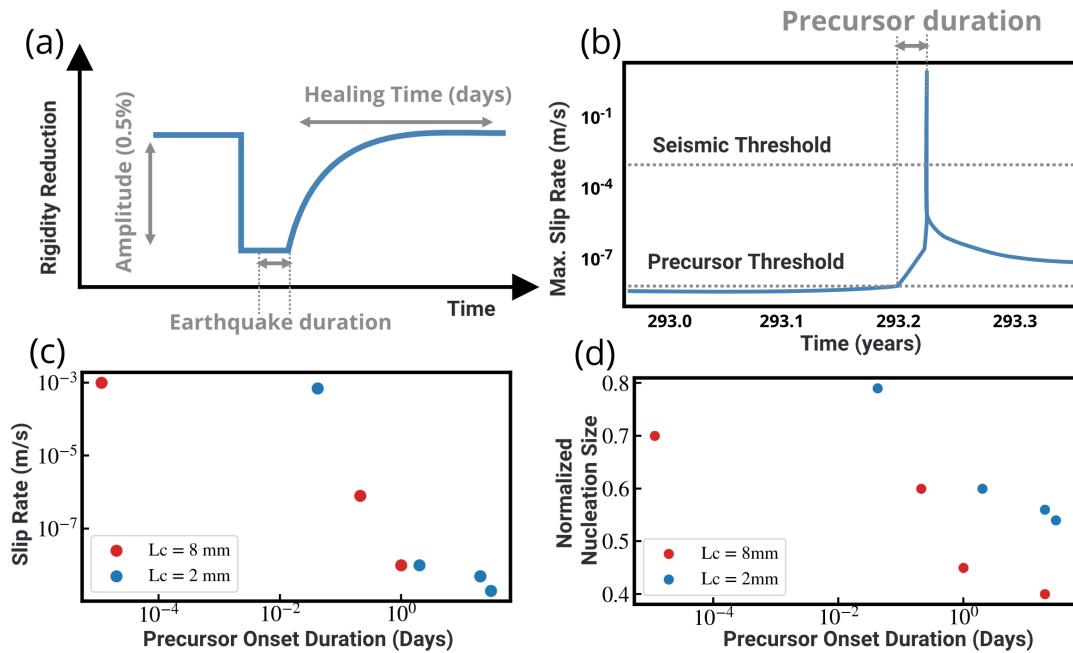
Figure 4.2: Precursor setup and simulation parameters. (a) The rigidity evolution with time showing the setup of precursory velocity change. (b) A representative earthquake from our simulations highlighting the onset of precursory velocity reduction given a seismic slip-rate threshold. (c) Slip-rate thresholds used in our simulations to set up precursor durations. (d) Observed nucleation size which is normalized against the theoretical estimates is shown for the different precursor onset duration.
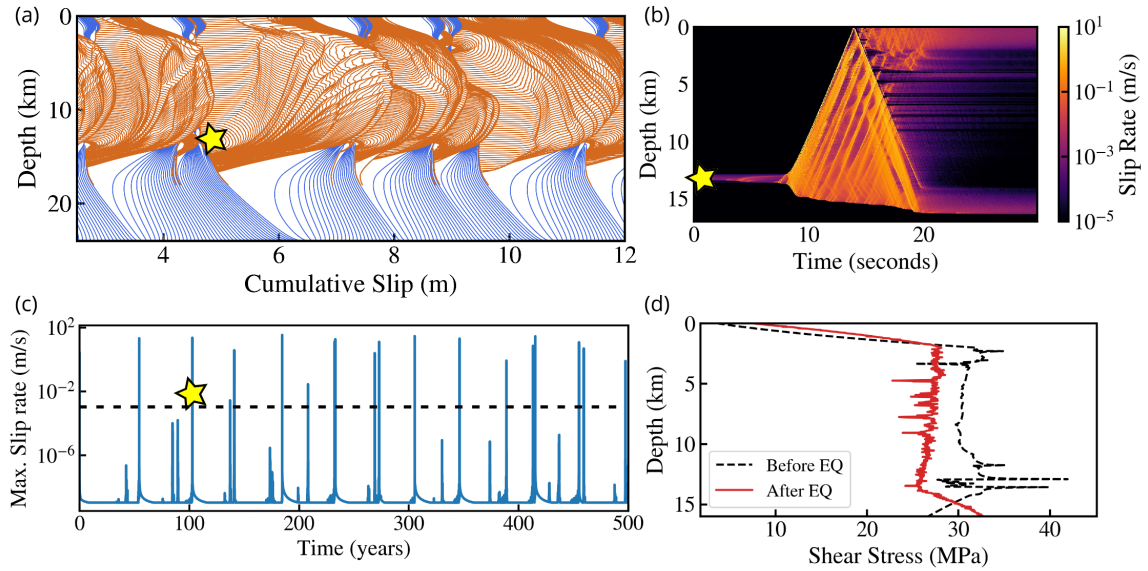
Figure 4.3: Reference model with fault damage zone. (a) Cumulative slip through earthquake sequences shown along depth. The orange lines are plotted every 0.1 s during earthquakes, and the blue lines are plotted every two years during interseismic periods. (b) Spatiotemporal slip-rate for one representative large earthquake along depth and time. (c) The peak slip-rate on fault is shown in time, demonstrating a range of fast and slow events. The dashed line shows the seismic threshold. (d) The shear stress along depth before and after a representative earthquake. The yellow star shows the location of the representative earthquake highlighted in (b) and (d).
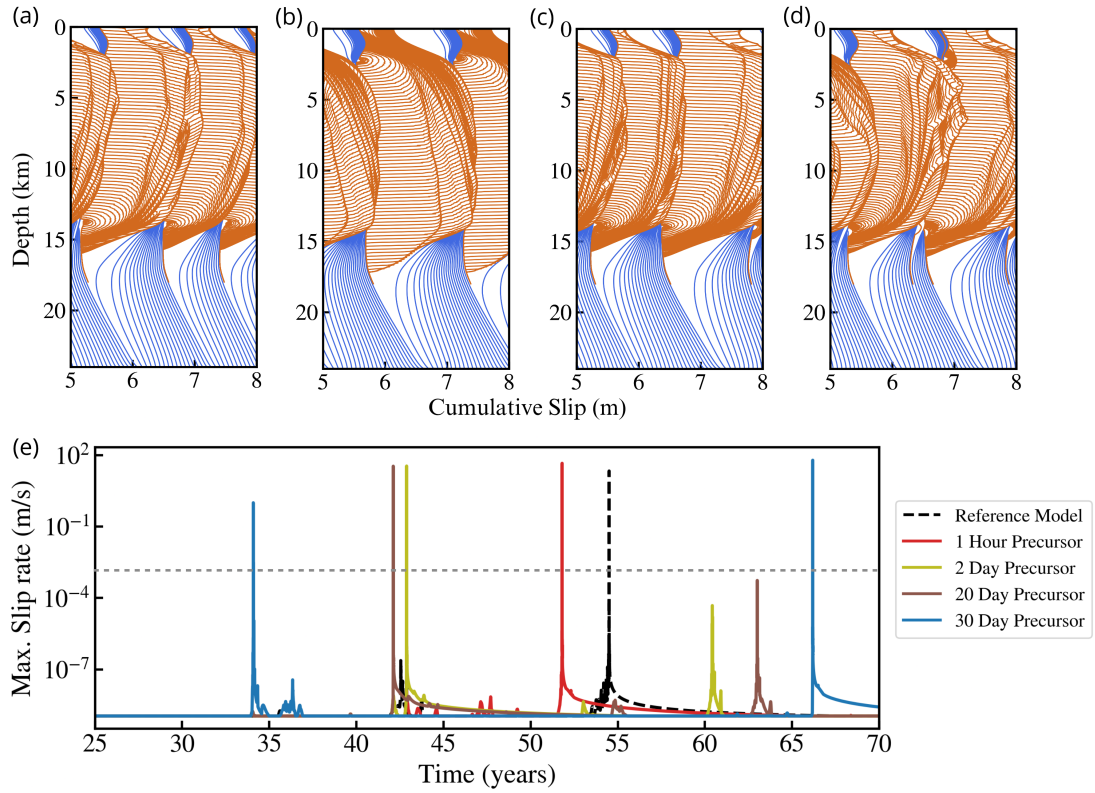
Figure 4.4: A comparison of earthquake cycle models with different precursory velocity onset. (a-d) Cumulative slip for a section of the earthquake sequence for precursor onsets of (a) 1 hour, (b) 2 days, (3) 20 days, and (4) 30 days before earthquakes. The orange lines are plotted every 0.1 seconds and the blue lines are plotted every 1 year. (e) Peak slip-rate on the fault shown in time for different precursor onsets and the reference simulation. The dashed grey line shows the seismic threshold.
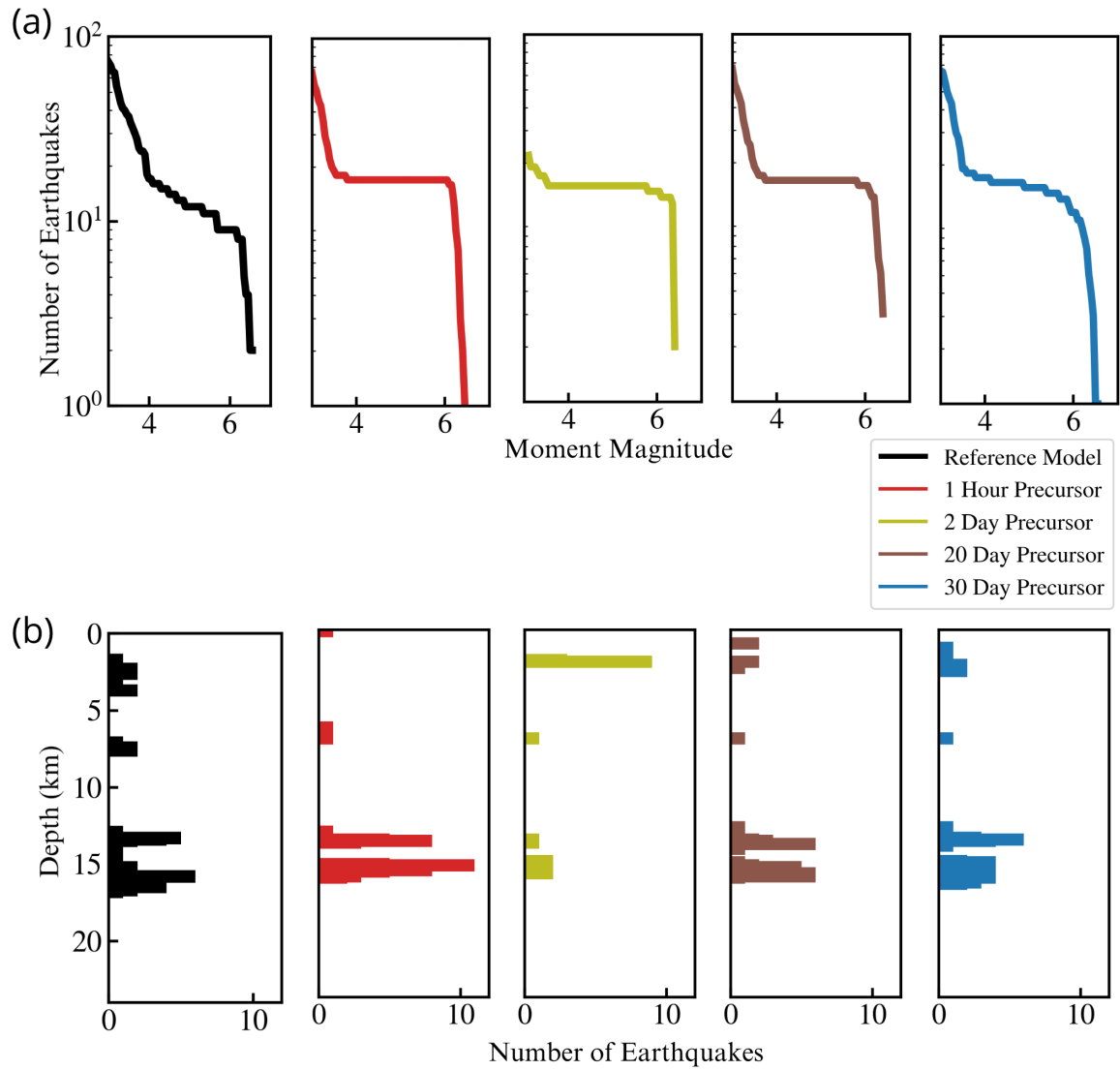
Figure 4.5: (a) Magnitude-frequency distribution for our reference simulation and different precursor onset durations. (b) Depth distribution of earthquake hypocenters for the same simulations.
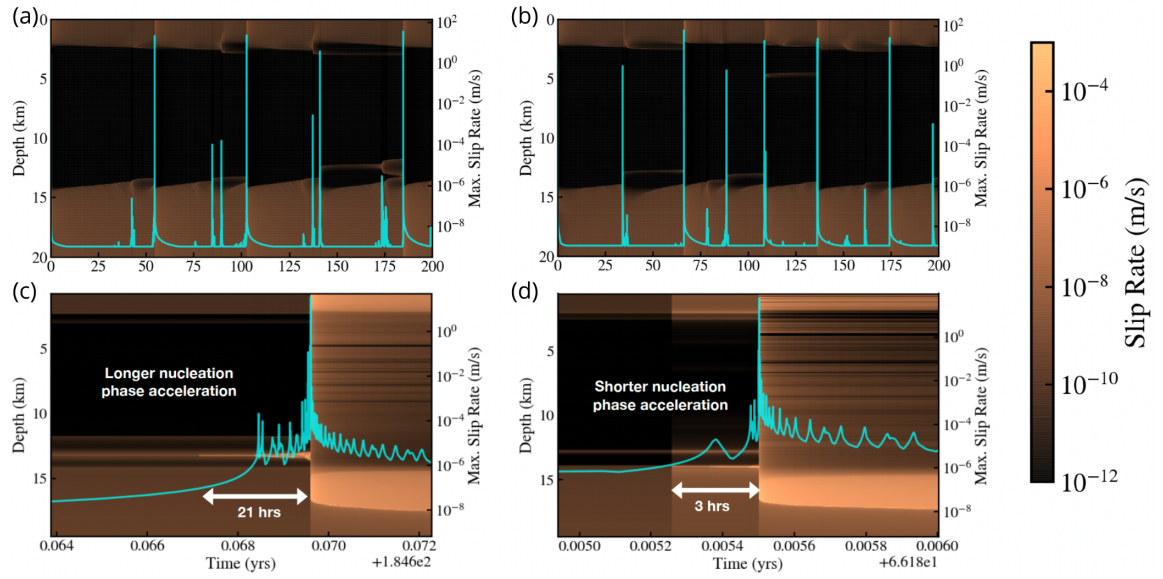
Figure 4.6: a-c) Spatiotemporal slip-rate history of the reference simulation. (b-d) Spatiotemporal slip-rate history of the 20-day precursor. The bottom figures show the zoom-in of one representative earthquake from each simulation.
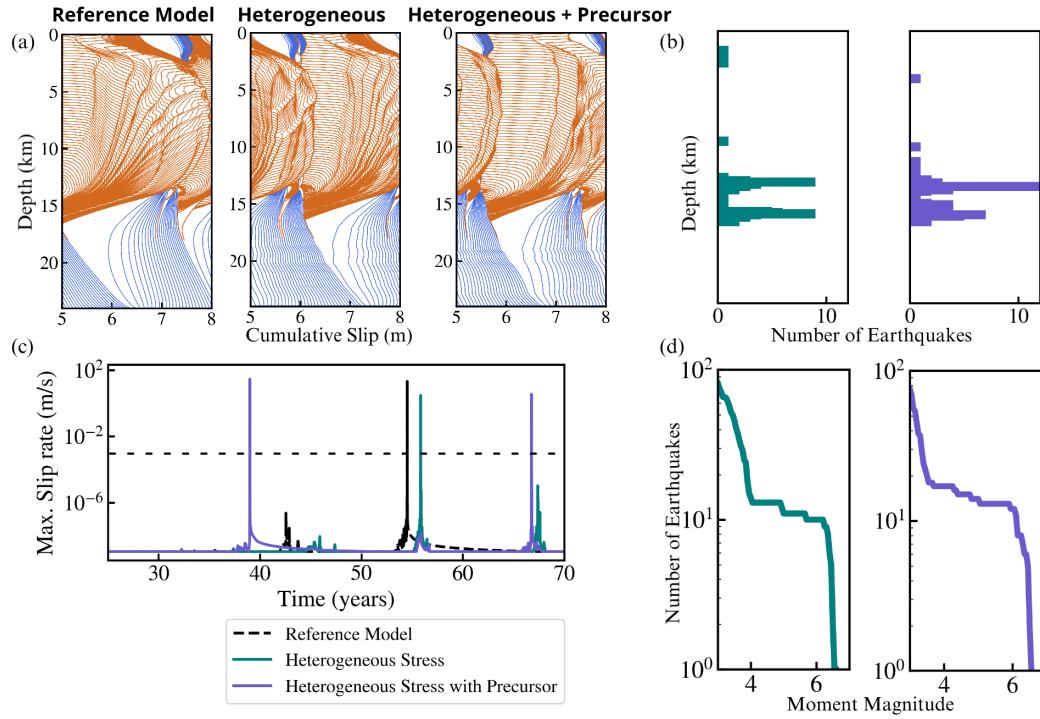
Figure 4.7: Earthquake cycle simulations with self-similar (heterogeneous) initial normal stress. (a) A comparison of cumulative slip contours for three simulations: the reference model, the heterogeneous stress without precursors, and the heterogeneous stress with precursors. The orange lines are plotted every 0.1 seconds and the blue lines are plotted every 1 year. (b) Depth distribution of earthquake hypocenters. (c) A comparison of peak slip-rate on the fault. The dashed line shows the seismic threshold. (d) Depth distribution of earthquake hypocenters. The magnitude-frequency and depth distribution of reference model are discussed in Fig. 4.

75
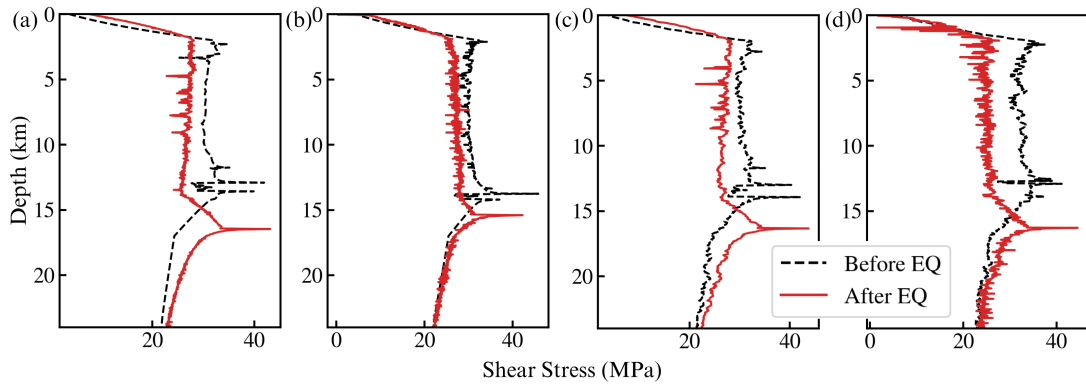
Figure 4.8: Shear stress before and after one large earthquake. (a) Reference Simulation. (b) 20-Day Precursor. (c) Heterogeneous initial normal stress without precursor. (d) Heterogeneous initial normal stress with 20-day precursor.
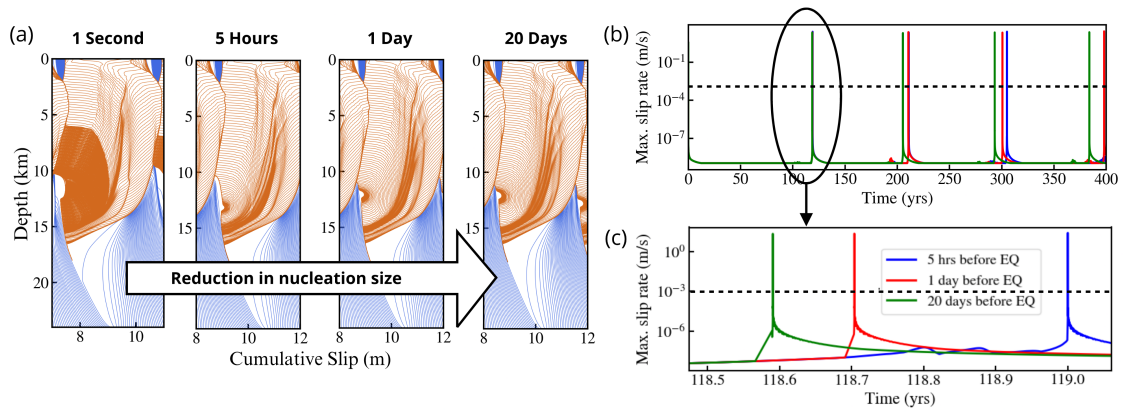
Figure 4.9: (a) Cumulative slip profiles for simulations with different precursor onset durations. The orange lines are plotted every 0.1 seconds and the blue lines are plotted every 1 year. (b) A comparison of peak slip-rate on the fault for three precursor durations. (c) Zoom-in of Fig. 9b showing the earlier nucleation of earthquakes with earlier precursor onset times. The dashed lines show the seismic threshold.
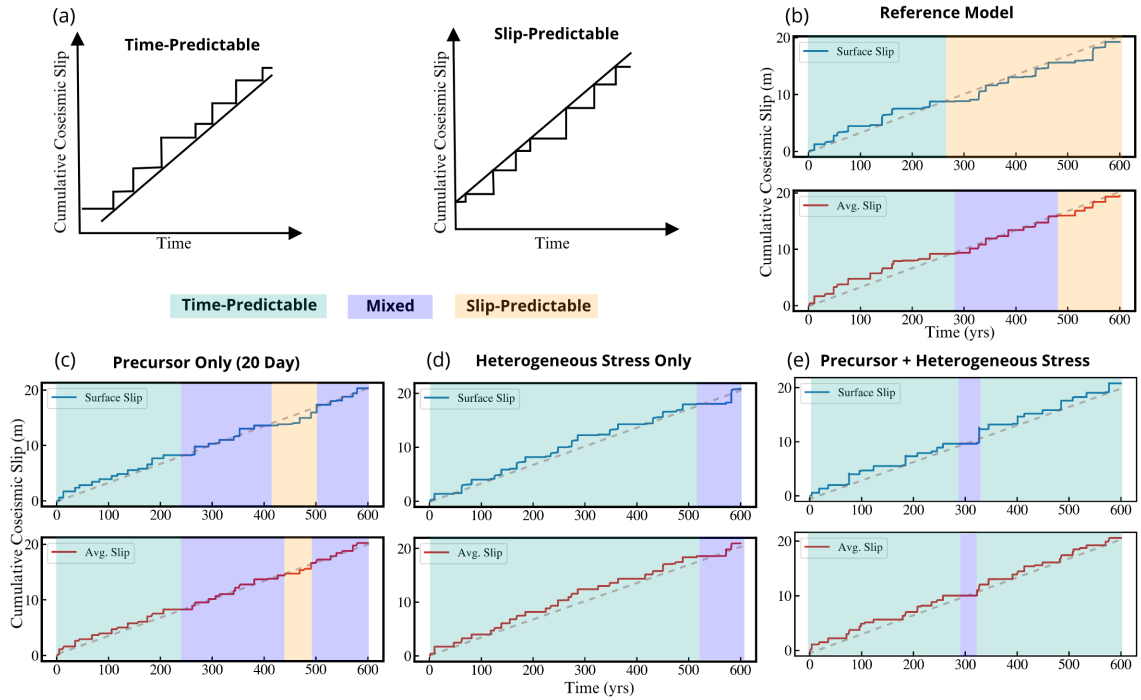
Figure 4.10: (a) Earthquake recurrence models, modified after Shimazaki and Nakata (1980). (b-e) Modeled cumulative surface and average slip during the coseismic phase along depth showing a mixture of time-predictable and slip-predictable behavior. The dashed grey lines represent the creep along the fault boundary that would have accumulated due to the plate motion.

CHAPTER 5

Conclusions

Earthquake cycle simulations help to the study of both earthquakes and interseismic deformation and to reconcile seismologic, geodetic, and geologic datasets over various time scales. Seismological and geological observations from mature faults like San Andreas, San Jacinto, and Northern Anatolian faults show that the seismicity on mature faults is constrained by the material properties and the spatial extent of the damaged fault zones. This thesis focuses on modeling fault damage zones, well-known structures of localized deformation around faults, and study their effects on seismicity evolution and aseismic transients in strike-slip fault systems.

We presented fully dynamic simulations of earthquake cycles in mature strike-slip fault zones in chapter 2. We showed that the geometry and material properties of the fault damage zone can significantly influence the spatial and temporal seismicity distribution. In particular, the fault zone waves can lead to earthquakes with variable magnitudes and hypocenter locations that are absent in an otherwise homogeneous material. The depth distribution of earthquake hypocenters is strongly affected by the fault damage zone depth, with shallower fault zones favoring shallower hypocenters. Shallow fault damage zones produce a bimodal depth distribution of earthquakes that depends on both the frictional and material boundaries along depth. The variable nucleation locations originate from the interaction between stress heterogeneity induced by dynamic fault zone waves and the rate and state fault. These results build new links between material properties of fault damage zones, which can be directly measured using geologic, seismic and geodetic methods, and the characteristics of earthquake sources.

Fault damage zone structure also evolves over time, resulting in damage accumulation and healing. Paleoseismic studies of large strike-slip earthquakes, limited to the past 1,000 to 1,200 yrs, suggest that the recurrence of large events is non-uniform, possibly even chaotic, with large gap in seismic activity followed by multiple seismic episodes (*Grant and Sieh*, 1992; *Fumal et al.*, 2002; *Toké et al.*, 2006). In chapter 3, we presented fully dynamic simulations in which damage accumulation and healing are modeled as changes

in seismic wave velocities within the fault damage zones. The reduction of seismic wave velocity and rate of interseismic healing are constrained by observations in Wenchuan, Landers and Nojima. Our results unveil how the seismic and aseismic segments in a fault damage zone interact during the earthquake cycle within an elastic framework. Both phenomena contribute to the nonuniform release of stresses during the seismic cycle, with slow-slip events having a dominant effect on the earthquake recurrence. Our simulations also show that permanent damage limits the maximum sizes of earthquakes. The slow slip events in our models are distributed within the velocity-weakening segment of the fault and occur throughout the interseismic period. Fault zone healing promotes the penetration of aseismic creep into the velocity-weakening region and reduces the fault asperity sizes that host earthquakes. The results indicate that the damage and healing of fault damage zones can have a pronounced effect on the temporal evolution of locked and creeping regions.

In chapter 4, we modeled precursory velocity changes in seismic cycles, often observed in laboratory experiments (*Scuderi et al.*, 2016), on strike-slip faults with homogeneous and heterogeneous initial stresses. We demonstrated that an earlier onset time of precursory velocity drop causes an earlier nucleation of earthquakes and a reduction in recurrence intervals over the seismic cycle. Precursory velocity changes allow some intermediate magnitude earthquakes, that do not break through the entire fault asperity, and some slow-slip events to grow into full ruptures spanning the entire fault width. We also analyzed the evolution of on-fault shear stress with time in the presence of different types of stress heterogeneities, stemming from fault damage zones, precursory velocity changes, and apriori self-similar normal stress. Each of these sources of stress heterogeneities contribute to the evolution of heterogeneous shear stress along different regions of the fault zone, and a combination of them amplifies the shear stress heterogeneity.

Future research direction would include developing a unified computational framework to model earthquake cycles in both two and three dimensions, and reconcile them with observational data, e.g., creating synthetic seismograms along the azimuth of fault zones. Additionally, various multiphysical aspects of fault systems have been simplified in our models to an elastic approximation. Incorporation of inelastic behavior in the fault zone promotes the accumulation some permanent deformation throughout the fault zone evolution. Such deformation may lead to a complex feedback between the evolving fault zone medium and seismic events, generating unique off-fault rupture patterns (*Thomas and Bhat*, 2018) and self-consistent healing and damage accumulation. In our simulations, these mechanisms will likely affect the generation of slow-slip events during the aseismic phase and modulate the shear stress evolution throughout the seismic cycle. Despite these approximations, the earthquake cycle models presented in this thesis can provide a more realistic description

of the physics and statistics of earthquakes in mature strike-slip fault systems, and can be theoretically extended to certain dip-slip systems as well. The past few decades have seen an exponential growth in earthquake physics research, and the coming decades promise us with a lot more computational power and data, therefore now is a good time to delve into understanding earthquakes.

BIBLIOGRAPHY

Abdelmeguid, M., X. Ma, and A. Elbanna (2019), A novel hybrid finite element-spectral boundary integral scheme for modeling earthquake cycles: Application to rate and state faults with low-velocity zones, *Journal of Geophysical Research: Solid Earth*.

Albertini, G., and D. S. Kammer (2017), Off-fault heterogeneities promote supershear transition of dynamic mode ii cracks, *Journal of Geophysical Research: Solid Earth*, *122*(8), 6625–6641.

Allison, K. L., and E. M. Dunham (2018), Earthquake cycle simulations with rate-and-state friction and power-law viscoelasticity, *Tectonophysics*, *733*, 232–256.

Andrews, D. J., and M. Barall (2011), Specifying Initial Stress for Dynamic Heterogeneous Earthquake Source Models, *Bulletin of the Seismological Society of America*, *101*(5), 2408–2417, doi:10.1785/0120110012.

Andrews, D. J., and S. Ma (2016), Validating a Dynamic Earthquake Model to Produce Realistic Ground Motion, *Bulletin of the Seismological Society of America*, *106*(2), 665–672, doi:10.1785/0120150251.

Avouac, J.-P. (2015), From geodetic imaging of seismic and aseismic fault slip to dynamic modeling of the seismic cycle, *Annual Review of Earth and Planetary Sciences*, *43*, 233–271.

Barbot, S. (2019a), Slow-slip, slow earthquakes, period-two cycles, full and partial ruptures, and deterministic chaos in a single asperity fault, *Tectonophysics*, *768*, 228,171.

Barbot, S. (2019b), Modulation of fault strength during the seismic cycle by grain-size evolution around contact junctions, *Tectonophysics*, *765*, 129–145.

Barbot, S., Y. Fialko, and D. Sandwell (2008), Effect of a compliant fault zone on the inferred earthquake slip distribution, *Journal of Geophysical Research: Solid Earth*, *113*(B6).

Barbot, S., Y. Fialko, and D. Sandwell (2009), Three-dimensional models of elastostatic deformation in heterogeneous media, with applications to the eastern california shear zone, *Geophysical Journal International*, *179*(1), 500–520.

Barbot, S., N. Lapusta, and J.-P. Avouac (2012), Under the hood of the earthquake machine: Toward predictive modeling of the seismic cycle, *Science*, *336*(6082), 707–710, doi: 10.1126/science.1218796.

Ben-David, O., G. Cohen, and J. Fineberg (2010), The dynamics of the onset of frictional slip, *Science*, *330*(6001), 211–214.

Ben-Zion, Y. (2001), Dynamic ruptures in recent models of earthquake faults, *Journal of the Mechanics and Physics of Solids*, *49*(9), 2209–2244.

Ben-Zion, Y., and C. G. Sammis (2003), Characterization of fault zones, *Pure and Applied Geophysics*, *160*(3-4), 677–715.

Ben-Zion, Y., Z. Peng, D. Okaya, L. Seeber, J. G. Armbruster, N. Ozer, A. J. Michael, S. Baris, and M. Aktar (2003), A shallow fault-zone structure illuminated by trapped waves in the karadere–duzce branch of the north anatolian fault, western turkey, *Geophysical Journal International*, *152*(3), 699–717.

Berryman, K. R., U. A. Cochran, K. J. Clark, G. P. Biasi, R. M. Langridge, and P. Villamor (2012), Major earthquakes occur regularly on an isolated plate boundary fault, *Science*, *336*(6089), 1690–1693.

Bezanson, J., A. Edelman, S. Karpinski, and V. B. Shah (2017), Julia: A fresh approach to numerical computing, *SIAM review*, *59*(1), 65–98.

Bhat, H. S., R. Dmowska, G. C. King, Y. Klinger, and J. R. Rice (2007), Off-fault damage patterns due to supershear ruptures with application to the 2001 mw 8.1 kokoxili (kunlun) tibet earthquake, *Journal of Geophysical Research: Solid Earth*, *112*(B6).

Blanpied, M., D. Lockner, and J. Byerlee (1991), Fault stability inferred from granite sliding experiments at hydrothermal conditions, *Geophysical Research Letters*, *18*(4), 609–612.

Blanpied, M. L., D. A. Lockner, and J. D. Byerlee (1995), Frictional slip of granite at hydrothermal conditions, *Journal of Geophysical Research: Solid Earth*, *100*(B7), 13,045–13,064.

Bonafede, M., B. Parenti, and E. Rivalta (2002), On strike-slip faulting in layered media, *Geophysical Journal International*, *149*(3), 698–723.

Bouchon, M., V. Durand, D. Marsan, H. Karabulut, and J. Schmittbuhl (2013), The long precursory phase of most large interplate earthquakes, *Nature Geoscience*, *6*(4), 299–302, doi:10.1038/ngeo1770, number: 4 Publisher: Nature Publishing Group.

Brenguier, F., M. Campillo, C. Hadziioannou, N. M. Shapiro, R. M. Nadeau, and E. Larose (2008), Postseismic Relaxation Along the San Andreas Fault at Parkfield from Continuous Seismological Observations, *Science*, *321*(5895), 1478–1481, doi:10.1126/science.1160943, publisher: American Association for the Advancement of Science Section: Report.

Bruhat, L., and P. Segall (2017), Deformation rates in northern Cascadia consistent with slow updip propagation of deep interseismic creep, *Geophysical Journal International*, *211*(1), 427–449, doi:10.1093/gji/ggx317.

Bürgmann, R. (2018), The geophysics, geology and mechanics of slow fault slip, *Earth and Planetary Science Letters*, *495*, 112–134.

Burridge, R., and L. Knopoff (1967), Model and theoretical seismicity, *Bulletin of the seismological society of america*, *57*(3), 341–371.

Caine, J. S., J. P. Evans, and C. B. Forster (1996), Fault zone architecture and permeability structure, *Geology*, *24*(11), 1025–1028.

Carlson, J. M., and J. Langer (1989), Properties of earthquakes generated by fault dynamics, *Physical Review Letters*, *62*(22), 2632.

Cattania, C. (2019), Complex earthquake sequences on simple faults, *Geophysical Research Letters*, *46*(17-18), 10,384–10,393.

Chen, K. H., T. Furumura, and J. Rubinstein (2015), Near-surface versus fault zone damage following the 1999 Chi-Chi earthquake: Observation and simulation of repeating earthquakes, *Journal of Geophysical Research: Solid Earth*, *120*(4), 2426–2445, doi:https://doi.org/10.1002/2014JB011719, _eprint: https://agupubs.onlinelibrary.wiley.com/doi/pdf/10.1002/2014JB011719.

Chester, F., and J. M. Logan (1986), Implications for mechanical properties of brittle faults from observations of the punchbowl fault zone, california, *Pure and applied geophysics*, *124*(1-2), 79–106.

Chester, F. M., J. P. Evans, and R. L. Biegel (1993), Internal structure and weakening mechanisms of the san andreas fault, *Journal of Geophysical Research: Solid Earth*, *98*(B1), 771–786.

Cochard, A., and R. Madariaga (1996), Complexity of seismicity due to highly rate-dependent friction, *Journal of Geophysical Research: Solid Earth*, *101*(B11), 25,321–25,336.

Cochran, E. S., Y.-G. Li, P. M. Shearer, S. Barbot, Y. Fialko, and J. E. Vidale (2009), Seismic and geodetic evidence for extensive, long-lived fault damage zones, *Geology*, *37*, 315–318, doi:10.1130/G25306A.1.

Dal Zilio, L. (2020), Bimodal seismicity in the himalaya controlled by fault friction and geometry, in *Cross-Scale Modeling of Mountain Building and the Seismic Cycle: From Alps to Himalaya*, pp. 67–93, Springer.

Dalguer, L. A., and P. M. Mai (2011), Near-Source Ground Motion Variability from M˜6.5 Dynamic Rupture Simulations, IASPEI and IAEE, accepted: 2017-06-09T18:16:39Z.

Day, S. M., L. A. Dalguer, N. Lapusta, and Y. Liu (2005), Comparison of finite difference and boundary integral solutions to three-dimensional spontaneous rupture, *Journal of Geophysical Research: Solid Earth*, *110*(B12).

Dieterich, J. H. (1979), Modeling of rock friction: 1. experimental results and constitutive equations, *Journal of Geophysical Research: Solid Earth*, *84*(B5), 2161–2168, doi:10. 1029/JB084iB05p02161.

Dolan, J. F., and B. D. Haravitch (2014), How well do surface slip measurements track slip at depth in large strike-slip earthquakes? The importance of fault structural maturity in controlling on-fault slip versus off-fault surface deformation, *Earth and Planetary Science Letters*, *388*, 38–47, doi:10.1016/j.epsl.2013.11.043.

DuRoss, C. B., S. F. Personius, A. J. Crone, S. S. Olig, M. D. Hylland, W. R. Lund, and D. P. Schwartz (2016), Fault segmentation: New concepts from the Wasatch Fault Zone, Utah, USA, *Journal of Geophysical Research: Solid Earth*, *121*(2), 1131–1157, doi:https://doi.org/10.1002/2015JB012519, _eprint: https://agupubs.onlinelibrary.wiley.com/doi/pdf/10.1002/2015JB012519.

Erickson, B. A., and E. M. Dunham (2014), An efficient numerical method for earthquake cycles in heterogeneous media: Alternating subbasin and surface-rupturing events on faults crossing a sedimentary basin, *Journal of Geophysical Research: Solid Earth*, *119*(4), 3290–3316.

Erickson, B. A., E. M. Dunham, and A. Khosravifar (2017), A finite difference method for off-fault plasticity throughout the earthquake cycle, *Journal of the Mechanics and Physics of Solids*, *109*, 50 – 77, doi:https://doi.org/10.1016/j.jmps.2017.08.002.

Erickson, B. A., J. Jiang, M. Barall, N. Lapusta, E. M. Dunham, R. Harris, L. S. Abrahams, K. L. Allison, J.-P. Ampuero, S. Barbot, et al. (2020), The community code verification exercise for simulating sequences of earthquakes and aseismic slip (seas), *Seismological Research Letters*, *91*(2A), 874–890.

Feng, L., A. V. Newman, G. T. Farmer, P. Psimoulis, and S. C. Stiros (2010), Energetic rupture, coseismic and post-seismic response of the 2008 MW 6.4 Achaia-Elia Earthquake in northwestern Peloponnese, Greece: an indicator of an immature transform fault zone, *Geophysical Journal International*, *183*(1), 103–110, doi:10.1111/j.1365-246X. 2010.04747.x.

Fialko, Y., D. Sandwell, D. Agnew, M. Simons, P. Shearer, and B. Minster (2002), Deformation on nearby faults induced by the 1999 hector mine earthquake, *Science*, *297*(5588), 1858–1862.

Field, E. H., R. J. Arrowsmith, G. P. Biasi, P. Bird, T. E. Dawson, K. R. Felzer, D. D. Jackson, K. M. Johnson, T. H. Jordan, C. Madden, et al. (2014), Uniform california earthquake rupture forecast, version 3 (ucerf3)—the time-independent model, *Bulletin of the Seismological Society of America*, *104*(3), 1122–1180.

Field, E. H., T. H. Jordan, M. T. Page, K. R. Milner, B. E. Shaw, T. E. Dawson, G. P. Biasi, T. Parsons, J. L. Hardebeck, A. J. Michael, et al. (2017), A synoptic view of the third uniform california earthquake rupture forecast (ucerf3), *Seismological Research Letters*, *88*(5), 1259–1267.

Fielding, E. J., P. R. Lundgren, R. Bürgmann, and G. J. Funning (2009), Shallow fault-zone dilatancy recovery after the 2003 bam earthquake in iran, *Nature*, *458*(7234), 64–68.

Fumal, T., R. Weldon, G. Biasi, T. Dawson, G. Seitz, W. Frost, and D. Schwartz (2002), Evidence for large earthquakes on the san andreas fault at the wrightwood, california, paleoseismic site: Ad 500 to present, *Bulletin of the Seismological Society of America*, *92*(7), 2726–2760.

Goldberg, D. E., D. Melgar, V. J. Sahakian, A. M. Thomas, X. Xu, B. W. Crowell, and J. Geng (2020), Complex Rupture of an Immature Fault Zone: A Simultaneous Kinematic Model of the 2019 Ridgecrest, CA Earthquakes, *Geophysical Research Letters*, *47*(3), e2019GL086,382, doi:https://doi.org/10.1029/2019GL086382, _eprint: https://agupubs.onlinelibrary.wiley.com/doi/pdf/10.1029/2019GL086382.

Grant, L., and K. Sieh (1992), Irregular recurrence times and increased seismic hazard from earthquakes on the carrizo segment of the san andreas fault, southern california, in *Proc. of the 35th Ann. Meeting of the Assoc. of Engineering Geologists*, pp. 2–9.

Gratier, J.-P., P. Favreau, and F. Renard (2003), Modeling fluid transfer along California faults when integrating pressure solution crack sealing and compaction processes, *Journal of Geophysical Research: Solid Earth*, *108*(B2), doi:https://doi.org/10.1029/2001JB000380, _eprint: https://agupubs.onlinelibrary.wiley.com/doi/pdf/10.1029/2001JB000380.

Harris, R. A., and S. M. Day (1997), Effects of a low-velocity zone on a dynamic rupture, *Bulletin of the Seismological Society of America*, *87*(5), 1267–1280.

Hauksson, E., and M.-A. Meier (2019), Applying depth distribution of seismicity to determine thermo-mechanical properties of the seismogenic crust in southern california: comparing lithotectonic blocks, *Pure and Applied Geophysics*, *176*(3), 1061–1081.

Heaton, T. H. (1990), Evidence for and implications of self-healing pulses of slip in earthquake rupture, *Physics of the Earth and Planetary Interiors*, *64*(1), 1–20, doi: 10.1016/0031-9201(90)90002-F.

Heimisson, E. R. (2020), Crack to pulse transition and magnitude statistics during earthquake cycles on a self-similar rough fault, *Earth and Planetary Science Letters*, *537*, 116,202.

Herrendörfer, R., T. Gerya, and Y. van Dinther (2018), An invariant rate-and state-dependent friction formulation for viscoeastoplastic earthquake cycle simulations, *Journal of Geophysical Research: Solid Earth*, *123*(6), 5018–5051.

Hillers, G., Y. Ben-Zion, and P. M. Mai (2006), Seismicity on a fault controlled by rate- and state-dependent friction with spatial variations of the critical slip distance, *Journal of Geophysical Research (Solid Earth)*, *111*, B01403, doi:10.1029/2005JB003859.

Howarth, J. D., N. C. Barth, S. J. Fitzsimons, K. Richards-Dinger, K. J. Clark, G. P. Biasi, U. A. Cochran, R. M. Langridge, K. R. Berryman, and R. Sutherland (2021), Spatiotem- poral clustering of great earthquakes on a transform fault controlled by geometry, *Nature Geoscience*, *14*(5), 314–320.

Huang, Y. (2018), Earthquake rupture in fault zones with along-strike material heterogene- ity, *Journal of Geophysical Research: Solid Earth*.

Huang, Y., and J.-P. Ampuero (2011), Pulse-like ruptures induced by low-velocity fault zones, *Journal of Geophysical Research: Solid Earth*, *116*(B12).

Huang, Y., J.-P. Ampuero, and D. V. Helmberger (2014a), Earthquake ruptures modulated by waves in damaged fault zones, *Journal of Geophysical Research: Solid Earth*, *119*(4), 3133–3154, doi:https://doi.org/10.1002/2013JB010724, _eprint: https://agupubs.onlinelibrary.wiley.com/doi/pdf/10.1002/2013JB010724.

Huang, Y., J.-P. Ampuero, and D. V. Helmberger (2014b), Earthquake ruptures modulated by waves in damaged fault zones, *Journal of Geophysical Research: Solid Earth*, *119*(4), 3133–3154.

Hulbert, C., B. Rouet-Leduc, P. A. Johnson, C. X. Ren, J. Rivière, D. C. Bolton, and C. Marone (2019), Similarity of fast and slow earthquakes illuminated by machine learn- ing, *Nature Geoscience*, *12*(1), 69–74, doi:10.1038/s41561-018-0272-8, number: 1 Pub- lisher: Nature Publishing Group.

Idini, B., and J.-P. Ampuero (2020), Fault-zone damage promotes pulse-like rupture and rapid-tremor-reversals.

Ito, Y., R. Hino, S. Suzuki, and Y. Kaneda (2015), Episodic tremor and slip near the Japan Trench prior to the 2011 Tohoku-Oki earthquake, *Geophys- ical Research Letters*, *42*(6), 1725–1731, doi:10.1002/2014GL062986, _eprint: https://onlinelibrary.wiley.com/doi/pdf/10.1002/2014GL062986.

Jiang, J., and N. Lapusta (2016), Deeper penetration of large earthquakes on seismically quiescent faults, *Science*, *352*, 1293–1297, doi:10.1126/science.aaf1496.

Johnson, K. M., A. Mavrommatis, and P. Segall (2016), Small interseismic asperities and widespread aseismic creep on the northern Japan subduction interface, *Geophysical Research Letters*, *43*(1), 135–143, doi:https://doi.org/10.1002/2015GL066707, _eprint: https://agupubs.onlinelibrary.wiley.com/doi/pdf/10.1002/2015GL066707.

Johnson, P. A., and X. Jia (2005), Nonlinear dynamics, granular media and dynamic earth- quake triggering, *Nature*, *437*(7060), 871–874, doi:10.1038/nature04015, number: 7060 Publisher: Nature Publishing Group.

Kaneko, Y., and N. Lapusta (2008), Variability of earthquake nucleation in continuum models of rate-and-state faults and implications for aftershock rates, *Journal of Geophysical Research: Solid Earth*, *113*(B12).

Kaneko, Y., N. Lapusta, and J.-P. Ampuero (2008), Spectral element modeling of spontaneous earthquake rupture on rate and state faults: Effect of velocity-strengthening friction at shallow depths, *Journal of Geophysical Research: Solid Earth*, *113*(B9).

Kaneko, Y., J.-P. Ampuero, and N. Lapusta (2011), Spectral-element simulations of long-term fault slip: Effect of low-rigidity layers on earthquake-cycle dynamics, *Journal of Geophysical Research (Solid Earth)*, *116*, B10313, doi:10.1029/2011JB008395.

Kaproth, B. M., and C. Marone (2014), Evolution of elastic wave speed during shear-induced damage and healing within laboratory fault zones, *Journal of Geophysical Research: Solid Earth*, *119*(6), 4821–4840, doi:https://doi.org/10.1002/2014JB011051, _eprint: https://agupubs.onlinelibrary.wiley.com/doi/pdf/10.1002/2014JB011051.

Kato, A., and S. Nakagawa (2014), Multiple slow-slip events during a foreshock sequence of the 2014 Iquique, Chile Mw 8.1 earthquake, *Geophysical Research Letters*, *41*(15), 5420–5427, doi:10.1002/2014GL061138, _eprint: https://onlinelibrary.wiley.com/doi/pdf/10.1002/2014GL061138.

Kato, A., K. Obara, T. Igarashi, H. Tsuruoka, S. Nakagawa, and N. Hirata (2012), Propagation of Slow Slip Leading Up to the 2011 Mw 9.0 Tohoku-Oki Earthquake, *Science*, *335*(6069), 705–708, doi:10.1126/science.1215141, publisher: American Association for the Advancement of Science.

Landry, W., and S. Barbot (2016), Gamra: Simple meshing for complex earthquakes, *Computers & Geosciences*, *90*, 49–63.

Landry, W., and S. Barbot (2019), Fast, accurate solutions for 3d strain volumes in a heterogeneous half space, *Computers & geosciences*, *125*, 109–114.

Lapusta, N., and J. R. Rice (2003a), Nucleation and early seismic propagation of small and large events in a crustal earthquake model, *Journal of Geophysical Research: Solid Earth*, *108*(B4), doi:10.1029/2001JB000793, _eprint: https://onlinelibrary.wiley.com/doi/pdf/10.1029/2001JB000793.

Lapusta, N., and J. R. Rice (2003b), Nucleation and early seismic propagation of small and large events in a crustal earthquake model, *Journal of Geophysical Research: Solid Earth*, *108*(B4).

Lapusta, N., J. R. Rice, Y. Ben-Zion, and G. Zheng (2000), Elastodynamic analysis for slow tectonic loading with spontaneous rupture episodes on faults with rate- and state-dependent friction, *Journal of Geophysical Research: Solid Earth*, *105*(B10), 23,765–23,789, doi:10.1029/2000JB900250.

Lewis, M., Z. Peng, Y. Ben-Zion, and F. Vernon (2005), Shallow seismic trapping structure in the san jacinto fault zone near anza, california, *Geophysical Journal International*, *162*(3), 867–881.

Lewis, M. A., and Y. Ben-Zion (2010), Diversity of fault zone damage and trapping structures in the parkfield section of the san andreas fault from comprehensive analysis of near fault seismograms, *Geophysical Journal International*, *183*(3), 1579–1595.

Li, Y., R. Bürgmann, and B. Zhao (2020), Evidence of Fault Immaturity from Shallow Slip Deficit and Lack of Postseismic Deformation of the 2017 Mw 6.5 Jiuzhaigou Earthquake, *Bulletin of the Seismological Society of America*, *110*(1), 154–165, doi: 10.1785/0120190162.

Li, Y.-G., and P. Leary (1990), Fault zone trapped seismic waves, *Bulletin of the Seismological Society of America*, *80*(5), 1245–1271.

Li, Y.-G., and F. L. Vernon (2001), Characterization of the san jacinto fault zone near anza, california, by fault zone trapped waves, *Journal of Geophysical Research: Solid Earth*, *106*(B12), 30,671–30,688.

Li, Y.-G., J. E. Vidale, S. M. Day, D. D. Oglesby, and E. Cochran (2003), Postseismic Fault Healing on the Rupture Zone of the 1999 M 7.1 Hector Mine, California, Earthquake, *Bulletin of the Seismological Society of America*, *93*(2), 854–869, doi: 10.1785/0120020131, publisher: GeoScienceWorld.

Li, Y.-G., P. Chen, E. S. Cochran, J. E. Vidale, and T. Burdette (2006), Seismic evidence for rock damage and healing on the san andreas fault associated with the 2004 m 6.0 parkfield earthquake, *Bulletin of the Seismological Society of America*, *96*(4B), S349–S363.

Lindsey, E. O., V. J. Sahakian, Y. Fialko, Y. Bock, S. Barbot, and T. K. Rockwell (2014), Interseismic strain localization in the san jacinto fault zone, *Pure and Applied Geophysics*, *171*(11), 2937–2954.

Lockner, D., H. Naka, H. Tanaka, H. Ito, and R. Ikeda (2000), Permeability and strength of core samples from the nojima fault of the 1995 kobe earthquake, in *Proceedings of the international workshop on the Nojima fault core and borehole data analysis*, vol. 129, pp. 147–152, Citeseer.

Lockner, D. A., C. Morrow, D. Moore, and S. Hickman (2011), Low strength of deep san andreas fault gouge from safod core, *Nature*, *472*(7341), 82.

Lyakhovsky, V., Y. Ben-Zion, and A. Agnon (1997), Distributed damage, faulting, and friction, *Journal of Geophysical Research: Solid Earth*, *102*(B12), 27,635–27,649, doi:10.1029/97JB01896, _eprint: https://onlinelibrary.wiley.com/doi/pdf/10.1029/97JB01896.

Lyakhovsky, V., Y. Ben-Zion, and A. Agnon (2005), A viscoelastic damage rheology and rate-and state-dependent friction, *Geophysical Journal International*, *161*(1), 179–190.

Ma, X., and A. Elbanna (2015a), Effect of off-fault low-velocity elastic inclusions on supershear rupture dynamics, *Geophysical Journal International*, *203*(1), 664–677.

Ma, X., and A. Elbanna (2015b), Effect of off-fault low-velocity elastic inclusions on supershear rupture dynamics, *Geophysical Journal International*, *203*(1), 664–677.

Mai, P. M., P. Spudich, and J. Boatwright (2005), Hypocenter locations in finite-source rupture models, *Bulletin of the Seismological Society of America*, *95*(3), 965–980.

Marone, C., and C. Scholz (1988), The depth of seismic faulting and the upper transition from stable to unstable slip regimes, *Geophysical Research Letters*, *15*(6), 621–624.

McFarland, F. S., J. J. Lienkaemper, and S. J. Caskey (2009), Data from theodolite measurements of creep rates on San Francisco Bay region faults, California, 1979-2012, *USGS Numbered Series 2009-1119*, U.S. Geological Survey, Reston, VA, doi: 10.3133/ofr20091119, code Number: 2009-1119 Code: Data from theodolite measurements of creep rates on San Francisco Bay region faults, California, 1979-2012 Publication Title: Data from theodolite measurements of creep rates on San Francisco Bay region faults, California, 1979-2012 Reporter: Data from theodolite measurements of creep rates on San Francisco Bay region faults, California, 1979-2012 Series: Open-File Report.

Mia, M. S., M. Abdelmeguid, and A. E. Elbanna (2022), Spatio-temporal clustering of seismicity enabled by off-fault plasticity, *Geophysical Research Letters*, *49*(8), e2021GL097,601.

Michel, S., J.-P. Avouac, N. Lapusta, and J. Jiang (2017), Pulse-like partial ruptures and high-frequency radiation at creeping-locked transition during megathrust earthquakes, *Geophysical Research Letters*, *44*(16), 8345–8351.

Mizuno, T., Y. Kuwahara, H. Ito, and K. Nishigami (2008), Spatial variations in fault-zone structure along the nojima fault, central japan, as inferred from borehole observations of fault-zone trapped waves, *Bulletin of the Seismological Society of America*, *98*(2), 558–570.

Mogi, K. (1962), Magnitude-frequency relation for elastic shocks accompanying fractures of various materials and some related problems in earthquakes, *Bull. Earthq. Res. Inst.*, *40*, 831–853.

Murray, J. R., S. E. Minson, and J. L. Svarc (2014), Slip rates and spatially variable creep on faults of the northern San Andreas system inferred through Bayesian inversion of Global Positioning System data, *Journal of Geophysical Research: Solid Earth*, *119*(7), 6023–6047, doi:https://doi.org/10.1002/2014JB010966, _eprint: https://agupubs.onlinelibrary.wiley.com/doi/pdf/10.1002/2014JB010966.

Nanjo, K. Z., N. Hirata, K. Obara, and K. Kasahara (2012), Decade-scale decrease inb value prior to the M9-class 2011 Tohoku and 2004 Sumatra quakes, *Geophysical Research Letters*, *39*(20), doi:10.1029/2012GL052997, _eprint: https://onlinelibrary.wiley.com/doi/pdf/10.1029/2012GL052997.

Nie, S., and S. Barbot (2021), Seismogenic and tremorgenic slow slip near the stability transition of frictional sliding, *Earth and Planetary Science Letters*, *569*, 117,037, doi: 10.1016/j.epsl.2021.117037.

Niu, F., P. G. Silver, T. M. Daley, X. Cheng, and E. L. Majer (2008), Preseismic velocity changes observed from active source monitoring at the Parkfield SAFOD drill site, *Nature*, *454*(7201), 204–208, doi:10.1038/nature07111, number: 7201 Publisher: Nature Publishing Group.

Noda, H., and T. Hori (2014), Under what circumstances does a seismogenic patch produce aseismic transients in the later interseismic period?, *Geophysical Research Letters*, *41*(21), 7477–7484.

Okubo, K., H. S. Bhat, E. Rougier, S. Marty, A. Schubnel, Z. Lei, E. E. Knight, and Y. Klinger (2019), Dynamics, radiation, and overall energy budget of earthquake rupture with coseismic off-fault damage, *Journal of Geophysical Research: Solid Earth*.

Olami, Z., H. J. S. Feder, and K. Christensen (1992), Self-organized criticality in a continuous, nonconservative cellular automaton modeling earthquakes, *Physical review letters*, *68*(8), 1244.

Olivier, G., F. Brenguier, R. Carey, P. Okubo, and C. Donaldson (2019), Decrease in Seismic Velocity Observed Prior to the 2018 Eruption of Kīlauea Volcano With Ambient Seismic Noise Interferometry, *Geophysical Research Letters*, *46*(7), 3734–3744, doi:10.1029/2018GL081609, _eprint: https://onlinelibrary.wiley.com/doi/pdf/10.1029/2018GL081609.

Ozawa, S. W., T. Hatano, and N. Kame (2019), Longer Migration and Spontaneous Decay of Aseismic Slip Pulse Caused by Fault Roughness, *Geophysical Research Letters*, *46*(2), 636–643, doi:10.1029/2018GL081465, _eprint: https://onlinelibrary.wiley.com/doi/pdf/10.1029/2018GL081465.

Page, M., and K. Felzer (2015), Southern san andreas fault seismicity is consistent with the gutenberg–richter magnitude–frequency distributionsouthern san andreas fault seismicity is consistent with the gutenberg–richter magnitude–frequency distribution, *Bulletin of the Seismological Society of America*, *105*(4), 2070, doi:10.1785/0120140340.

Parsons, T., E. L. Geist, R. Console, and R. Carluccio (2018), Characteristic earthquake magnitude frequency distributions on faults calculated from consensus data in california, *Journal of Geophysical Research: Solid Earth*, *123*(12), 10–761.

Pei, S., F. Niu, Y. Ben-Zion, Q. Sun, Y. Liu, X. Xue, J. Su, and Z. Shao (2019), Seismic velocity reduction and accelerated recovery due to earthquakes on the Longmenshan fault, *Nature Geoscience*, *12*(5), 387–392, doi:10.1038/s41561-019-0347-1, number: 5 Publisher: Nature Publishing Group.

Pelties, C., Y. Huang, and J.-P. Ampuero (2015), Pulse-like rupture induced by three-dimensional fault zone flower structures, *Pure and Applied Geophysics*, *172*(5), 1229–1241.

Peng, Z., and Y. Ben-Zion (2006a), Temporal changes of shallow seismic velocity around the karadere-düzce branch of the north anatolian fault and strong ground motion, *pure and applied geophysics*, *163*(2), 567–600, doi:10.1007/s00024-005-0034-6.

Peng, Z., and Y. Ben-Zion (2006b), Temporal Changes of Shallow Seismic Velocity Around the Karadere-Düzce Branch of the North Anatolian Fault and Strong Ground Motion, *pure and applied geophysics*, *163*(2), 567–600, doi:10.1007/s00024-005-0034-6.

Perfettini, H., J. Schmittbuhl, and A. Cochard (2003), Shear and normal load perturbations on a two-dimensional continuous fault: 2. dynamic triggering, *Journal of Geophysical Research: Solid Earth*, *108*(B9).

Perrin, C., I. Manighetti, J.-P. Ampuero, F. Cappa, and Y. Gaudemer (2016), Location of largest earthquake slip and fast rupture controlled by along-strike change in fault structural maturity due to fault growth, *Journal of Geophysical Research: Solid Earth*, *121*(5), 3666–3685, doi:10.1002/2015JB012671.

Poli, P. (2017), Creep and slip: Seismic precursors to the Nuugaatsiaq landslide (Greenland), *Geophysical Research Letters*, *44*(17), 8832–8836, doi:10.1002/2017GL075039, _eprint: https://onlinelibrary.wiley.com/doi/pdf/10.1002/2017GL075039.

Rice, J. R. (1993), Spatio-temporal complexity of slip on a fault, *Journal of Geophysical Research: Solid Earth*, *98*(B6), 9885–9907.

Rice, J. R., and Y. Ben-Zion (1996), Slip complexity in earthquake fault models, *Proceedings of the National Academy of Sciences*, *93*(9), 3811–3818.

Ripperger, J., J.-P. Ampuero, P. M. Mai, and D. Giardini (2007), Earthquake source characteristics from dynamic rupture with constrained stochastic fault stress, *Journal of Geophysical Research: Solid Earth*, *112*(B4), doi:10.1029/2006JB004515, _eprint: https://onlinelibrary.wiley.com/doi/pdf/10.1029/2006JB004515.

Rivera, L., and H. Kanamori (2002), Spatial heterogeneity of tectonic stress and friction in the crust, *Geophysical Research Letters*, *29*(6), 12–1.

Rivet, D., L. De Barros, Y. Guglielmi, F. Cappa, R. Castilla, and P. Henry (2016), Seismic velocity changes associated with aseismic deformations of a fault stimulated by fluid injection, *Geophysical Research Letters*, *43*(18), 9563–9572, doi:10.1002/2016GL070410, _eprint: https://onlinelibrary.wiley.com/doi/pdf/10.1002/2016GL070410.

Roux, P., and Y. Ben-Zion (2014), Monitoring fault zone environments with correlations of earthquake waveforms, *Geophysical Journal International*, *196*(2), 1073–1081, publisher: Oxford University Press.

Rubin, A., and J.-P. Ampuero (2005), Earthquake nucleation on (aging) rate and state faults, *Journal of Geophysical Research: Solid Earth*, *110*(B11).

Rubinstein, J. L., and G. C. Beroza (2005), Depth constraints on nonlinear strong ground motion from the 2004 parkfield earthquake, *Geophysical Research Letters*, *32*(14).

Rubinstein, J. L., W. L. Ellsworth, K. H. Chen, and N. Uchida (2012), Fixed recurrence and slip models better predict earthquake behavior than the time- and slip-predictable models: 1. Repeating earthquakes, *Journal of Geophysical Research: Solid Earth*, *117*(B2), doi:10.1029/2011JB008724, _eprint: https://onlinelibrary.wiley.com/doi/pdf/10.1029/2011JB008724.

Ruge, J. W., and K. Stüben (1987), Algebraic multigrid, in *Multigrid methods*, pp. 73–130, SIAM.

Ruina, A. (1983), Slip instability and state variable friction laws, *Journal of Geophysical Research: Solid Earth*, *88*(B12), 10,359–10,370, doi:10.1029/JB088iB12p10359.

Rundle, J. B. (1989), A physical model for earthquakes: 3. thermodynamical approach and its relation to nonclassical theories of nucleation, *Journal of Geophysical Research: Solid Earth*, *94*(B3), 2839–2855, doi:10.1029/JB094iB03p02839.

Rundle, J. B., and D. D. Jackson (1977), Numerical simulation of earthquake sequences, *Bulletin of the Seismological Society of America*, *67*(5), 1363–1377.

Rybicki, K., and T. Yamashita (2002), On faulting in inhomogeneous media, *Geophysical research letters*, *29*(10).

Scholz, C. (1968), The frequency-magnitude relation of microfracturing in rock and its relation to earthquakes, *Bulletin of the seismological society of America*, *58*(1), 399–415.

Scholz, C. H. (1998), Earthquakes and friction laws, *Nature*, *391*(6662), 37.

Schwartz, D. P., and K. J. Coppersmith (1984), Fault behavior and characteristic earthquakes: Examples from the wasatch and san andreas fault zones, *Journal of Geophysical Research: Solid Earth*, *89*(B7), 5681–5698, doi:10.1029/JB089iB07p05681.

Scuderi, M. M., C. Marone, E. Tinti, G. Di Stefano, and C. Collettini (2016), Precursory changes in seismic velocity for the spectrum of earthquake failure modes, *Nature Geoscience*, *9*(9), 695–700, doi:10.1038/ngeo2775, bandiera_abtest: a Cg_type: Nature Research Journals Number: 9 Primary_atype: Research Publisher: Nature Publishing Group Subject_term: Natural hazards;Seismology;Tectonics Subject_term_id: natural-hazards;seismology;tectonics.

Seitz, G., R. Weldon II, and G. P. Biasi (1997), The pitman canyon paleoseismic record: A re-evaluation of southern san andreas fault segmentation, *Journal of Geodynamics*, *24*(1-4), 129–138.

Shaw, B. E. (1995), Frictional weakening and slip complexity in earthquake faults, *Journal of Geophysical Research: Solid Earth*, *100*(B9), 18,239–18,251.

Shimazaki, K., and T. Nakata (1980), Time-predictable recurrence model for large earthquakes, *Geophysical Research Letters*, *7*(4), 279–282, doi:10.1029/GL007i004p00279, _eprint: https://onlinelibrary.wiley.com/doi/pdf/10.1029/GL007i004p00279.

Sibson, R. (1977), Fault rocks and fault mechanisms, *Journal of the Geological Society*, *133*(3), 191–213.

Smith, D. E., and T. H. Heaton (2011), Models of stochastic, spatially varying stress in the crust compatible with focal-mechanism data, and how stress inversions can be biased toward the stress rate, *Bulletin of the Seismological Society of America*, *101*(3), 1396–1421.

Snieder, R., C. Sens-Schönfelder, E. Ruigrok, and K. Shiomi (2016), Seismic shear waves as foucault pendulum, *Geophysical Research Letters*, *43*(6), 2576–2581.

Stanchits, S., S. Vinciguerra, and G. Dresen (2006), Ultrasonic velocities, acoustic emission characteristics and crack damage of basalt and granite, *pure and applied geophysics*, *163*(5), 975–994, doi:10.1007/s00024-006-0059-5.

Stanchits, S. A., D. A. Lockner, and A. V. Ponomarev (2003), Anisotropic Changes in P-Wave Velocity and Attenuation during Deformation and Fluid Infiltration of Granite, *Bulletin of the Seismological Society of America*, *93*(4), 1803–1822, doi:10.1785/0120020101.

Taira, T., P. G. Silver, F. Niu, and R. M. Nadeau (2009), Remote triggering of fault-strength changes on the San Andreas fault at Parkfield, *Nature*, *461*(7264), 636–639, doi:10.1038/nature08395, number: 7264 Publisher: Nature Publishing Group.

Tal, Y., and B. H. Hager (2018), Dynamic mortar finite element method for modeling of shear rupture on frictional rough surfaces, *Computational Mechanics*, *61*(6), 699–716, doi:10.1007/s00466-017-1475-3.

Tal, Y., B. H. Hager, and J. P. Ampuero (2018), The Effects of Fault Roughness on the Earthquake Nucleation Process, *Journal of Geophysical Research: Solid Earth*, *123*(1), 437–456, doi:10.1002/2017JB014746, _eprint: https://onlinelibrary.wiley.com/doi/pdf/10.1002/2017JB014746.

Tatebe, O. (1993), The multigrid preconditioned conjugate gradient method.

Thakur, P., and Y. Huang (2021), Influence of fault zone maturity on fully dynamic earthquake cycles, *Geophysical Research Letters*, *48*(17), e2021GL094,679.

Thakur, P., Y. Huang, and Y. Kaneko (2020), Effects of Low-Velocity Fault Damage Zones on Long-Term Earthquake Behaviors on Mature Strike-Slip Faults, *Journal of Geophysical Research: Solid Earth*, *125*(8), doi:10.1029/2020JB019587.

Thomas, M. Y., and H. S. Bhat (2018), Dynamic evolution of off-fault medium during an earthquake: a micromechanics based model, *Geophysical Journal International*, *214*(2), 1267–1280, doi:10.1093/gji/ggy129.

Thomas, M. Y., N. Lapusta, H. Noda, and J.-P. Avouac (2014), Quasi-dynamic versus fully dynamic simulations of earthquakes and aseismic slip with and without enhanced coseismic weakening, *Journal of Geophysical Research: Solid Earth*, *119*(3), 1986–2004.

Thurber, C., S. Roecker, K. Roberts, M. Gold, L. Powell, and K. Rittger (2003a), Earthquake locations and three-dimensional fault zone structure along the creeping section of the san andreas fault near parkfield, ca: Preparing for safod, *Geophysical Research Letters*, *30*(3).

Thurber, C., S. Roecker, K. Roberts, M. Gold, L. Powell, and K. Rittger (2003b), Earthquake locations and three-dimensional fault zone structure along the creeping section of the San Andreas fault near Parkfield, CA: Preparing for SAFOD, *Geophysical Research Letters*, *30*(3), doi:10.1029/2002GL016004, _eprint: https://onlinelibrary.wiley.com/doi/pdf/10.1029/2002GL016004.

Toké, N. A., J. R. Arrowsmith, J. J. Young, and C. J. Crosby (2006), Paleoseismic and postseismic observations of surface slip along the parkfield segment of the san andreas fault, *Bulletin of the Seismological Society of America*, *96*(4B), S221–S238.

Tong, X., D. T. Sandwell, and B. Smith-Konter (2013), High-resolution interseismic velocity data along the San Andreas Fault from GPS and InSAR, *Journal of Geophysical Research: Solid Earth*, *118*(1), 369–389, doi:https://doi.org/10.1029/2012JB009442, _eprint: https://agupubs.onlinelibrary.wiley.com/doi/pdf/10.1029/2012JB009442.

Townend, J., and M. D. Zoback (2000), How faulting keeps the crust strong, *Geology*, *28*(5), 399–402.

Tsai, V. C., and G. Hirth (2020), Elastic impact consequences for high-frequency earthquake ground motion, *Geophysical Research Letters*, *47*(5), e2019GL086,302.

Tschoegl, L., R. Below, and D. Guha-Sapir (2006), *An analytical review of selected data sets on natural disasters and impacts*, Centre for Research on the Epidemiology of Disasters Louvain.

Unsworth, M. J., P. E. Malin, G. D. Egbert, and J. R. Booker (1997), Internal structure of the san andreas fault at parkfield, california, *Geology*, *25*(4), 359–362.

Vidale, J. E., and Y.-G. Li (2003a), Damage to the shallow landers fault from the nearby hector mine earthquake, *Nature*, *421*(6922), 524–526.

Vidale, J. E., and Y.-G. Li (2003b), Damage to the shallow Landers fault from the nearby Hector Mine earthquake, *Nature*, *421*(6922), 524–526, doi:10.1038/nature01354, number: 6922 Publisher: Nature Publishing Group.

Waldhauser, F., and W. L. Ellsworth (2002), Fault structure and mechanics of the hayward fault, california, from double-difference earthquake locations, *Journal of Geophysical Research: Solid Earth*, *107*(B3), ESE–3.

Wang, K., and S. L. Bilek (2014), Invited review paper: Fault creep caused by subduction of rough seafloor relief, *Tectonophysics*, *610*, 1–24.

Weng, H., H. Yang, Z. Zhang, and X. Chen (2016), Earthquake rupture extents and co-seismic slips promoted by damaged fault zones, *Journal of Geophysical Research: Solid Earth*, *121*(6), 4446–4457.

Wesnousky, S. G. (1994), The gutenberg-richter or characteristic earthquake distribution, which is it?, *Bulletin of the Seismological Society of America*, *84*(6), 1940.

Whitcomb, J. H., J. D. Garmany, and D. L. Anderson (1973), Earthquake Prediction: Variation of Seismic Velocities before the San Francisco Earthquake, *Science*, *180*(4086), 632–635, doi:10.1126/science.180.4086.632, publisher: American Association for the Advancement of Science.

Wu, C., Z. Peng, and Y. Ben-Zion (2009), Non-linearity and temporal changes of fault zone site response associated with strong ground motion, *Geophysical Journal International*, *176*(1), 265–278, doi:10.1111/j.1365-246X.2008.04005.x.

Wu, J., J. A. Hole, and J. A. Snoke (2010), Fault zone structure at depth from differential dispersion of seismic guided waves: evidence for a deep waveguide on the san andreas fault, *Geophysical Journal International*, *182*(1), 343–354.

Yang, H. (2015), Recent advances in imaging crustal fault zones: A review, *Earthquake Science*, *28*(2), 151–162.

Yang, H., L. Zhu, and E. S. Cochran (2011), Seismic structures of the Calico fault zone inferred from local earthquake travel time modelling, *Geophysical Journal International*, *186*(2), 760–770, doi:10.1111/j.1365-246X.2011.05055.x.

Zhao, P., and Z. Peng (2009), Depth extent of damage zones around the central calaveras fault from waveform analysis of repeating earthquakes, *Geophysical Journal International*, *179*(3), 1817–1830.